



# Modelling of Welding with Various Constitutive Models for Steel

**Graeme John Oliver**

March 1994

Thesis submitted for the Degree of MSc.  
Department of Applied Mathematics  
University of Cape Town

The University of Cape Town has been given  
the right to reproduce this thesis in whole  
or in part. Copyright is held by the author.

The copyright of this thesis vests in the author. No quotation from it or information derived from it is to be published without full acknowledgement of the source. The thesis is to be used for private study or non-commercial research purposes only.

Published by the University of Cape Town (UCT) in terms of the non-exclusive license granted to UCT by the author.

## Summary

This dissertation is an attempt at the quality analysis of constitutive modelling of welding as a coupled thermo-mechanical or thermo-mechanical-metallurgical problem. Three types of inelastic theories of continua: unified viscoplasticity based on dislocation density theory, unified viscoplasticity based on potential theory, and transformation induced plasticity have been chosen for quantitative investigation. Material models proposed by Anand, Estrin and Mecking, Estrin, Robinson, and Leblond et.al. have been implemented into the finite element program ABAQUS. Specific subroutines have been written specifically for each constitutive equation. The material model implementation is based on the implicit solution of stress-strain relations and the derivation of associated constitutive tangent moduli necessary for the Nonlinear Finite Element solution procedures. Material model comparisons are based on numerical results obtained for the welding of thick plates; that is the bench mark problem considered in this thesis.

## Acknowledgements

This work was done under supervision of Dr. Jacek Ronda (Dr.Sc.) Whom I would like to thank for creating the kind of environment in which I like to work.

I would like to thank the FRD/UCT Center for Research into Computational and Applied Mechanics (CERECAM) for funding and for the use of their computational facilities. In this regard I would like to express my gratitude to Prof. J.B. Martin, Prof. B.D. Reddy, Dr. G.P. Mitchell and Mike Eastman.

I would also like to further thank Prof. Reddy for his assistance and encouragement without which I would not have undertaken any postgraduate study.

I would also like to acknowledge some assistance from my friends and colleagues in the Department of Applied Mathematics: Nicola Meinert for the work she did with me in the preparation of her honours project and Kevin Colville for the mutual assistance during periods of preparation of papers.

Thanks also to Prof. R Tait's mechanical engineering group for their welding experiments which provided some useful insights.

The private communications of Prof. Yuri Estrin of the University of Western Australia is also much appreciated. I also wish to thank Prof L. Anand of the Massachusetts Institute of Technology for taking the time to supply me with a requested paper.

Finally I would like to thank my family for their support.

# Contents

<b>1</b>	<b>Introduction</b>	<b>9</b>
1.1	History of Weld Modelling . . . . .	9
1.1.1	Historical Remarks on Computational Weld Mechanics . . . . .	9
1.1.2	Tasks in the Modelling of Welding . . . . .	10
1.2	Problem description . . . . .	11
<b>2</b>	<b>Mathematical Model of Welding</b>	<b>14</b>
2.1	Lagrangian Description . . . . .	14
2.2	Balance Laws for Thermo-Mechanical Process . . . . .	15
2.3	Finite Element Approximation . . . . .	19
2.3.1	FE Approximation of Equation of Virtual Work . . . . .	20
2.3.2	FE Approximation of Balance of Internal Energy . . . . .	21
2.4	Implementation of Material Models . . . . .	22
2.5	Solution of Finite Element Equations . . . . .	24
<b>3</b>	<b>Materials with Scalar Parameters</b>	<b>26</b>
3.1	General Solution Procedure . . . . .	26
3.2	Anand's Model . . . . .	28
3.2.1	Time-Integration of Constitutive Equations . . . . .	28
3.2.2	Derivatives for Internal Newton-Raphson Scheme . . . . .	29
3.2.3	Linearization of tangent modulus . . . . .	31
3.3	Estrin Model . . . . .	32
3.3.1	Equations for Material with Two Variables . . . . .	32
3.3.2	Time Integration Procedure for Constitutive Equations . . . . .	33
3.3.3	Derivatives for Newton-Raphson Method . . . . .	33
3.3.4	Consistent Tangent Modulus for Estrin's Model . . . . .	35
3.4	Contribution of Thermal Coupling due to Plastic Deformation . . . . .	35

<b>4</b>	<b>Potential Viscoplastic Models</b>	<b>37</b>
4.1	Robinson's Model . . . . .	37
4.1.1	Constitutive Equations . . . . .	37
4.1.2	Residual Equations for Robinson's Model . . . . .	39
4.1.3	Derivatives for Internal Newton-Raphson Method . . . . .	39
4.2	Contribution of Robinson's Model in FE Stiffness . . . . .	41
4.3	Thermal Coupling Contributions . . . . .	42
<b>5</b>	<b>Transformation Plasticity</b>	<b>44</b>
5.1	Model of Transformation Plasticity . . . . .	44
5.1.1	Residual Functions . . . . .	48
5.2	Contribution of Leblond's Model in Stiffness . . . . .	48
5.2.1	Derivatives for Internal Newton-Raphson Method . . . . .	49
5.2.2	Mixture Functions . . . . .	52
<b>6</b>	<b>Thermal and Mechanical Conditions</b>	<b>53</b>
6.1	Model of the Welding Arc . . . . .	53
6.2	Convection from the weld piece . . . . .	54
6.2.1	Convection from the upper surface . . . . .	55
6.2.2	Convection from the vertical surfaces . . . . .	55
6.3	Radiation from the weld piece . . . . .	55
6.4	Thermal contact conductance . . . . .	55
<b>7</b>	<b>Numerical Results</b>	<b>57</b>
7.1	Bench Mark Problem for Welding . . . . .	57
7.2	FE Discretization of Weld Joint . . . . .	57
7.3	Modelling of Boundary Conditions . . . . .	58
7.4	Temperatures . . . . .	58
7.5	Time integration studies of the constitutive models . . . . .	61
7.6	Results for the Thermo-Mechanical BVP . . . . .	72
<b>8</b>	<b>Conclusions</b>	<b>94</b>
<b>A</b>	<b>Values of Parameters Used in Models</b>	<b>96</b>
<b>B</b>	<b>Mathematical Derivations</b>	<b>98</b>

B.1	Relation between Deviatoric stress and Strain . . . . .	98
B.2	Relation between Equivalent Strain and Equivalent Stress . . . . .	99
<b>C</b>	<b>Matrix and Vector Representation of Tensors</b>	<b>100</b>

# List of Figures

2.1	The Lagrangian formulation . . . . .	15
3.1	Generalized uniaxial viscoplastic model . . . . .	27
4.1	Unified viscoplastic model for multiaxial loading . . . . .	38
5.1	Leblond's model solution scheme . . . . .	45
7.1	The mesh and mechanical boundary condition used to obtain results . . . . .	58
7.2	The model of the moving welding arc source . . . . .	59
7.3	The temperature dependent relation for the Grashof number on the upper surface . . . . .	59
7.4	The temperature dependent relations for the convection and radiation from the upper Surface . . . . .	60
7.5	The temperature dependent relations for the convection and radiation from the vertical surfaces . . . . .	60
7.6	The temperature field after (a) one second , (b) two seconds of welding . . . . .	62
7.7	The temperature field after (a) three seconds , (b) four seconds of welding . . . . .	63
7.8	The temperature field after (a) five seconds , (b) six seconds of welding . . . . .	64
7.9	The temperature field after (a) seven seconds , (b) eight seconds of welding . . . . .	65
7.10	The temperature field after (a) nine seconds, (b) ten seconds of welding . . . . .	66
7.11	Stress ( $T_{11}$ )-strain ( $L_{11}$ ) relation for Anand's model produced for 4 cycles of loading . . . . .	67
7.12	Stress ( $T_{11}$ )-strain ( $L_{11}$ ) relation for Estrin's model produced for 4 cycles of loading . . . . .	67
7.13	Stress ( $T_{11}$ )-strain ( $L_{11}$ ) relation for Robinson's model produced for 4 cycles of loading . . . . .	68
7.14	Stress ( $T_{11}$ )-strain ( $L_{11}$ ) showing thermal sensitivity over the range 300° to 1000° for Anand's model . . . . .	68

7.15	Stress ( $T_{11}$ )-strain ( $L_{11}$ ) showing thermal sensitivity over the range 300° to 1000° for Estrin's model . . . . .	69
7.16	Stress ( $T_{11}$ )-strain ( $L_{11}$ ) showing thermal sensitivity over the range 300° to 1000° for Robinson's model . . . . .	70
7.17	Stress ( $T_{11}$ )-strain ( $L_{11}$ ) showing the response to jumps in strain rate for Anand's model . . . . .	70
7.18	Stress ( $T_{11}$ )-strain ( $L_{11}$ ) showing the response to jumps in strain rate for Estrin's model . . . . .	71
7.19	Stress ( $T_{11}$ )-strain ( $L_{11}$ ) showing the response to jumps in strain rate for Robinson's model . . . . .	71
7.20	Permanent deformation for (a) Anand's, (b) Estrin's and (c) Robinson's model	73
7.21	Graph of residual a) strain b) stress components for Anand's model along weld line . . . . .	74
7.22	Graph of residual a) strain b) stress components for Estrin's model along weld line . . . . .	75
7.23	Graph of residual a) strain b) stress components for Robinson's model along weld line . . . . .	77
7.24	Residual stress contour plot for stress component $T_{11}$ for (a) Anand's , (b) Estrin's, (c) Robinson's model . . . . .	78
7.25	Residual stress contour plot for stress component $T_{22}$ for (a) Anand's , (b) Estrin's, (c) Robinson's model . . . . .	79
7.26	Residual stress contour plot for stress component $T_{33}$ for (a) Anand's , (b) Estrin's, (c) Robinson's model . . . . .	80
7.27	Residual stress contour plot for stress component $T_{12}$ for (a) Anand's , (b) Estrin's, (c) Robinson's model . . . . .	81
7.28	Residual stress contour plot for stress component $T_{13}$ for (a) Anand's , (b) Estrin's, (c) Robinson's model . . . . .	82
7.29	Residual stress contour plot for stress component $T_{23}$ for (a) Anand's , (b) Estrin's, (c) Robinson's model . . . . .	83
7.30	Residual strain contour plot for strain component $L_{11}$ for (a) Anand's , (b) Estrin's, (c) Robinson's model . . . . .	84
7.31	Residual strain contour plot for strain component $L_{22}$ for (a) Anand's , (b) Estrin's, (c) Robinson's model . . . . .	85
7.32	Residual strain contour plot for strain component $L_{33}$ for (a) Anand's , (b) Estrin's, (c) Robinson's model . . . . .	86
7.33	Residual strain contour plot for strain component $L_{12}$ for (a) Anand's , (b) Estrin's, (c) Robinson's model . . . . .	87

7.34	Residual strain contour plot for strain component $L_{13}$ for (a) Anand's , (b) Estrin's, (c) Robinson's model . . . . .	88
7.35	Residual strain contour plot for strain component $L_{23}$ for (a) Anand's , (b) Estrin's, (c) Robinson's model . . . . .	89
7.36	Residual value of Robinson's model backstress component (a) $Z_{11}$ , (b) $Z_{22}$ and (c) $Z_{33}$ . . . . .	90
7.37	Residual value of Robinson's model backstress component (d) $Z_{12}$ , (e) $Z_{13}$ and (f) $Z_{23}$ . . . . .	91
7.38	Residual value of (a) Anand's model internal variable (b) Estrin's model internal variable . . . . .	92
7.39	Von Mises equivalent stress contour plot for stress for (a) Anand's , (b) Estrin's, (c) Robinson's model . . . . .	93

## Some Notation

- **bold** is used primarily to indicate second rank (or order) tensors
- a hat placed over a bold symbol denotes a fourth rank tensor for example

$$\hat{\mathbf{C}} \equiv C_{ijkl}$$

is a fourth rank tensor

- $\mathbf{1} \equiv \delta_{ij}$

the second rank tensor identity

- $\hat{\mathbf{I}}$

the fourth rank tensor identity

- $\otimes$

outer product of two tensors which in this paper denotes the product of two second rank tensors to form a fourth rank tensor for example

$$\mathbf{A} \otimes \mathbf{B} = \hat{\mathbf{C}}$$

- $:$

the inner product or contraction of tensors

- a second order tensor contracted with a second order tensor results in a scalar

$$\mathbf{A} : \mathbf{B} = c$$

- a fourth order tensor product with a second order tensor results in a second order tensor

$$\hat{\mathbf{A}} : \mathbf{B} = \mathbf{C}$$

- a fourth order tensor product with a fourth order tensor results in a fourth order tensor

$$\hat{\mathbf{A}} : \hat{\mathbf{B}} = \hat{\mathbf{C}}$$

- $\mathbf{L} \equiv L_{ij}$  is the total strain tensor
- $\mathbf{E} \equiv E_{ij}$  is the deviatoric strain tensor
- $\mathbf{T} \equiv T_{ij}$  is the total stress tensor
- $\mathbf{S} \equiv S_{ij}$  is the deviatoric stress tensor
- $\bar{\mathbf{E}}$  is the volume averaged deviatoric strain tensor
- $\bar{\mathbf{S}}$  is the volume averaged deviatoric stress tensor

# Chapter 1

## Introduction

### 1.1 History of Weld Modelling

#### 1.1.1 Historical Remarks on Computational Weld Mechanics

Welding is a very complex thermo-mechanical process which involves four disciplines: continuum mechanics, heat transfer, materials sciences and production engineering. The mathematical modelling of welding requires simplifications and experimental verifications related to metallurgical and fracture toughness tests of weld joints. At the beginning of studies in the 1940s the research on mechanical aspects of welding was concentrated on the experimental approach. Some attempts to determine residual stresses and dilatations in a weldment have been done by Vinokurov [64] and Okerblom [46] for a very idealized mathematical model of welding mechanics. The heat transfer phenomena in the weldment has been initially modelled as a steady state heat transfer problem and solved by Rosenthal [56] using Fourier analysis. The current strategy for modelling of welding was formulated and refined in the 1970s with works by Hibbit and Marcal [21], Ueda [60], Freidman [16], Masubuchi [44] and Andersson [1]. Welding was simplified and formulated for:

- the two-dimensional problem in plane strain or plane stress or axisymmetric conditions,
- elastic-plastic material with temperature dependent properties,
- Lagrangian description of motion,
- the heat flux transferred from the weld arc to a body modelled as a prescribed heat flux,
- thermal stresses evaluated above some bounding temperatures.

In the 1980s, the welding analysis was developed by considering new phenomena associated with the weld model:

- residual stresses in welding large plates including the effects of tack welds (Karlsson [29]),
- distributed heat flux from the weld (Goldak et al [19]),
- viscoplastic effects of weld (Argyris [3]),
- three-dimensional coupled thermo-mechanical analysis of a weld (Goldak et al [18]),
- three-dimensional transient analysis of a girth weld of pipe with thermo-mechanical coupling (Karlsson [30]),
- three-dimensional analysis of the girth weld of pipe by using of shell elements (Lindgren and Karlsson [38]),
- addition of filler metal (Ohji et al [48]).

Multi-pass welds have been analyzed by Ueda [61], Rybicki [57] and Leung [37]. The modelling of this process consists of lumping together of several passes to reduce the cost of separate analysis. In several cases only the last pass is analyzed.

The coupling between the arc and weld bath is strong and it has been investigated by several researchers who attempted to solve a balance law of internal energy or the Boltzmann equation coupled with the fluid mechanics of the welding bath. Christensen et al [11] has studied the geometry and size of the fusion zone. Since that time there have been other empirical and semi-empirical attempts by Shinoda [58] at predicting fusion zone shape. Other attempts by Pardo and Weckman [47] (1989) have developed a numerical method to study the influence of weld parameters on fusion zone. The progress towards prediction of the flow inside a molten pool has been done by Kou et al [32] and Matsunawa et al [45]. The latent heat effects have been included into thermal analysis of welding by Ronda [52], [53] and Goldak [19].

The effect of the weld material microstructure transformation on the residual stress field has been investigated by several researchers and has been called transformation plasticity. The most complex analysis of transformation plasticity has been done by Inoue and Raniecki [26] following Lomakin [39], [40] papers. Inoue and Wang [27] developed this analysis for the Perzyna type viscoplastic constitutive relation.

Several other strategies has been tried for the prediction of the microstructure of weld. One such a method is proposed by Leblond et al [33], [34]. Another shown by Goldak et al [19] is based on the paper by Henwood [20].

### 1.1.2 Tasks in the Modelling of Welding

The thermal stresses in welding are evaluated by using the Finite Element Method. The early papers by Boley and Weiner [7], and Ziegler [65] attempted to undertake a thermodynamical

coupling of the temperature field and the stress and strain fields. The influence of thermo-mechanical coupling terms for many years has been considered as very small which is true when material phase transformations and inelastic dissipation effects are neglected. Hence, the analysis can be divided into the determination of temperature and the determination of stress and strain fields. The temperature distribution in a weldment is determined by heat input, initial temperature, welding technique, type and geometry of joint. The heat input is related to the heat flow in the weld arc. In most studies of welding processes the energy transfer from electrode to the weld is represented either by a surface heat source or by momentarily deposited heat. In general the temperature field should be taken as coupled with the mechanical field. The governing equation of heat follows the first law of thermodynamics and is called the balance of internal energy. The temperature field associated with a moving point heat source is used to approximate the temperature field in welding of thick plates.

The analysis of heat flow during welding is undertaken by the Finite Element Method [1] considering phase transformations and gives the temperature distribution in a welded joint.

The welding stress appears due to a non-uniform temperature field, inhomogeneous material properties, external restraints and volume changes during phase transformations. The thermal stress problem is also solved by FEM applied to a balance of the virtual work. The fields of temperature, stress and strain are coupled with the microstructure of the material [29] in a complex manner and the material microstructures would exhibit entirely different mechanical properties than the virgin material.

The microstructure depends on the chemical composition of the particular steel and on its thermal and mechanical history. The state of stress may affect the transformation behaviour of martensitic structures. This so-called transformation plasticity [35], [36] is a phenomenon in which a stressed body undergoes a phase transformation and exhibits permanent deformation which is finite, time-independent and proportional to the stress. This deformation appears even for stresses much lower than the yield strength.

Residual stresses generated by welding are reduced by Post Weld Heat Treatment (PWHT) when two processes are active: softening and thermal creeping. The first phenomenon can be included in thermal analysis by updating temperature dependent mechanical properties. The second is more complicated and requires rate-dependent constitutive models of weld.

The multi-pass weld modelling should include the effects of reheat cracking due to interactions between regions which soften faster or slower during heating than their neighbourhood. The ductility of a material depends on the thermal history and localization of a material failure may occur in softer regions.

## 1.2 Problem description

This paper encompasses aspects of analysis of the quality of constitutive modelling and the simulation of thermo-mechanical processes in solids. The applicability of different models

of a continuous medium for modelling of welding has been tested. Various theories for inelastic solids are reviewed and three of them: unified viscoplasticity based on dislocation density or flow potential, and transformation plasticity have been chosen for investigation. The unified theory of viscoplasticity based on dislocation density is represented by models proposed by Anand [2], Estrin and Mecking [13] and Estrin [14]. The Anand model consists of constitutive equations for rate dependent deformation of metals, which employ only a single scalar internal variable representing an isotropic resistance to plastic flow. The Estrin-Mecking isotropic viscoplastic model is microstructure-related and contains one internal parameter related to the total dislocation density. The improvement of this model, proposed by Estrin, is based on definitions of two internal variables related to the mobile and the relatively immobile dislocation density. The potential viscoplasticity theory, proposed by Robinson [4] incorporate the concept of flow potential and the definition of the tensor internal state variables representing the back stress. The evolution law of internal state variables is derived from the Bailey-Orowan theory of hardening and softening competing processes which proceed during material deformation. Transformation plasticity in steels which incorporates material phase transformations into calculation of a stress state, is proposed by Leblond et al [33], [34]. This concept of plasticity is attributed to the following two mechanisms: deformation of the body due to the formation of martensitic plates, and macroscopic plastic flow caused by the difference of volume between two coexisting phases.

All the above mentioned models have been implemented into the Finite Element Program ABAQUS by specifically writing subroutines. ABAQUS has two interface for such implementation: the UMAT (User MATerial) subroutine, and the UEL (User ELement) subroutine. The UMAT routine allows one to specify the constitutive relation for stress as a function of strain, that is suitable for the Anand, Estrin-Mecking, Estrin and Robinson models. The UEL subroutine allows one to define an element in a general way and is used for implementation of the Leblond et al model.

The comparison of residual stresses evaluated by the use of these four constitutive models representing three various theories for an inelastic solid is studied for a benchmark problem formulated for butt welded thick plates.

The Lagrangian formulation, with the second Piola-Kirchoff stress tensor conjugated with Green-Lagrange strain, is built into ABAQUS for the standard elements, and is used in a description of a thermo-mechanical problem of welding. This description of motion is thus the formulation used in the UMAT routines, which are applicable for the viscoplastic models. The Lagrangian formulation has been also used for the UEL routine, which implements the transformation plasticity.

The mechanical boundary conditions simulate clamping of welded plates. The thermal boundary conditions for heat input are appropriate for fusion welding in air such as gas-metal-arc welding. The molten pool can be seen to be a moving ellipsoid when the welding arc is modelled by a travelling Gaussian distribution. Heat outfluxes are given by empirical relations calculated from the Nusselt, Grashof and Prandtl numbers. Thermal contact

resistance is used to simulate the heat sink effect of a plate in contact with a flat support. The contours of residual strains, stresses and the Mises norm have been compared for different constitutive models and material parameters identified for carbon steel. Reliance on existing material parameters, however, limits the extent to which one can compare resultant magnitudes.

# Chapter 2

## Mathematical Model of Welding

### 2.1 Lagrangian Description

The Lagrangian description of a body motion is used in a formulation of welding as a thermo-mechanical problem for metals. The displacements in a weld joint are unknown and a finite element method is applied to find the configuration of a finite number of material points and corresponding stress states. In the Lagrangian analysis the initial position of the particle  $\mathbf{X} = (X_1^0, X_2^0, X_3^0)$  and the time  $t$  are taken as independent variables. They are called the Lagrangian or material variables. The motion, which carries a fixed material point through various spatial positions, may be expressed by the function of motion  $\mathbf{x} = \chi(\mathbf{X}, t)$ . This function expressed in terms of Lagrangian variables, describe the variation of physical parameters for a given particle during its wandering through the space. The Lagrangian analysis is used primarily when considering geometrically non-linear behaviour of elastic and inelastic structures since then the boundary conditions are usually referred to in the initial configuration. The vector joining the point  $X$  and its actual position in the space  $\mathbf{x} = (X_1^1, X_2^1, X_3^1)$  is the displacement vector given by  $\mathbf{u} = \mathbf{X} - \mathbf{x}$ . Fig.(2.1) shows the above statement of the motion description in the Lagrangian formulation which is valid for large displacements, large rotations and strains smaller than 2%. This occurs when an extension of the fibre of original length  $l_1$  at the initial configuration is small enough to assure strains below 2%. This requirement is fulfilled in the incremental analysis assuming a time increment small enough to keep the load and its increment in appropriate regimes.

The constitutive variables i.e. the stress and strain measures used in the Lagrangian formulation are the second Piola-Kirchhoff stress and the Green-Lagrange strain. These are conjugate in the sense of Hill's definition of energetically conjugated constitutive variables. The second Piola-Kirchhoff stress tensor  $\tilde{\mathbf{S}}$  is given in terms of the Cauchy stress  $\mathbf{T}$  by the formula:

$$\tilde{\mathbf{S}} = \frac{\rho^0}{\rho^t} \mathbf{F}^{-1} \mathbf{T} \{\mathbf{F}^{-1}\}^T \quad (2.1)$$

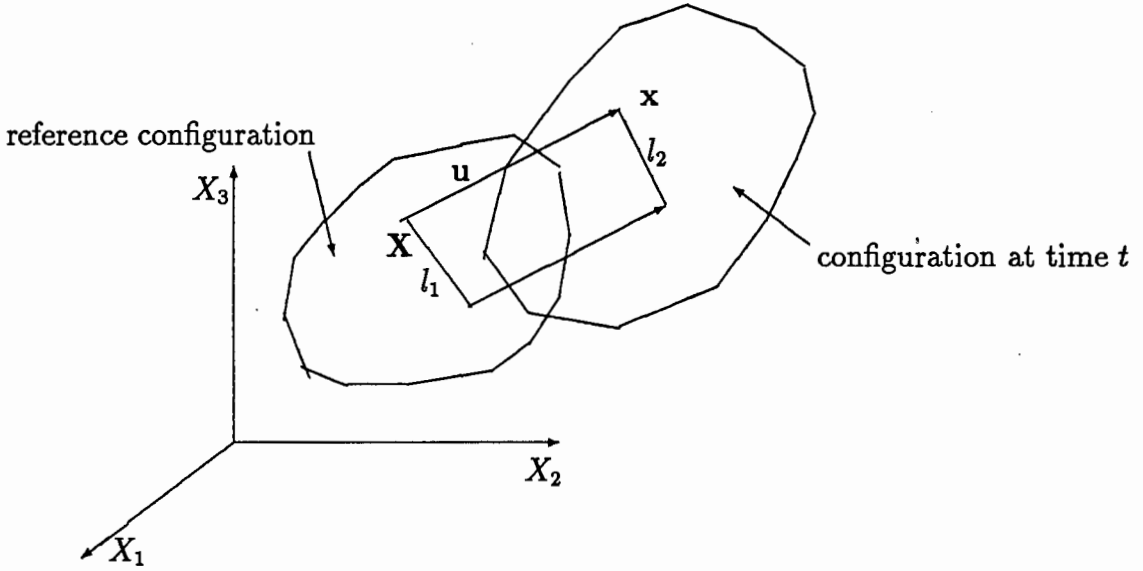


Figure 2.1: The Lagrangian formulation

where  $\rho^0, \rho^t$  are the reference and current densities, and the deformation gradient is

$$\mathbf{F} = \frac{\partial \mathbf{x}}{\partial \mathbf{X}}; F_{iK} = x_{i,K} = \frac{\partial x_i}{\partial X_K}; \quad (2.2)$$

where  $\mathbf{X}$  and  $\mathbf{x} = \mathbf{x}(\mathbf{X}, t)$  are the reference and current coordinates respectively. The Green-Lagrange strain conjugated with the second Piola-Kirchhoff stress is defined by:

$$\tilde{\mathbf{L}} = \frac{1}{2} (u_{I,J} + u_{J,I} + u_{K,I}u_{K,J}) \quad (2.3)$$

where the displacement gradient is

$$u_{I,J} = \frac{\partial u_I}{\partial X_J} \quad (2.4)$$

The large indices  $I, J, K$  refer to the reference configuration. The ',' is the usual abbreviated notation for differentiation with respect to coordinates.

The total Lagrangian formulation is built into the Finite Element Program ABAQUS for the standard material models and elements, and is also used in the UMAT and UEL routines which has been applied for the implementation of the viscoplastic and transformation plasticity models.

## 2.2 Balance Laws for Thermo-Mechanical Process

The mathematical model of welding consist of two principles expressing thermal and mechanical equilibrium, i.e. the balance of internal energy and the balance of momentum. These

principles have been derived to account for the coupling of thermal and mechanical effects for a thermo-inelastic body. The equilibrium equation for a solid is given by the following equations:

$$(S_{KL}x_{i,L})_{,K} - (b_i + r_i)\rho_0 = 0 \quad (2.5)$$

for the particle  $\mathbf{X} \in \Omega$ , and

$$S_{KL}x_{i,L}N_K = T_i \quad (2.6)$$

for the particle  $\mathbf{X} \in \partial\Omega$ , where  $b_i$  is the body force,  $r_i$  is the surface force,  $N_K$  is the outward normal to the body surface  $\partial\Omega$ ,  $T_i$  is the nominal stress vector. Assuming the actual coordinate system  $\{x_i\}$  which is collinear with the reference coordinate system  $\{X_I\}$  these equations can be rewritten in the forms

$$(S_{KI} + S_{KL}u_{i,L})_{,K} - (b_I + r_I)\rho_0 = 0 \quad (2.7)$$

$$(S_{KI} + S_{KL}u_{i,L})N_K = T_I \quad (2.8)$$

The balance law of internal energy for non-rigid conductor is expressed in the form

$$\rho\dot{e} + \text{div}\mathbf{q} = \mathbf{S} : \dot{\mathbf{L}} + {}_{\text{ext}}\mathbf{q} \cdot \mathbf{N} + \rho\mathcal{R} \quad (2.9)$$

where  $e$  is the energy density per unit mass and its rate is given by

$$\dot{e} = \frac{\partial e}{\partial t} + \mathbf{v} \cdot \nabla e, \quad (2.10)$$

$\nabla e$  is the gradient of  $e$ ,  $\mathbf{q}$  is the vector of heat flux transferred through the particle  $\mathbf{X} \in \Omega$ , and  ${}_{\text{ext}}\mathbf{q}$  is the heat flux supplied to welded body through the outer surface  $\partial\Omega$ . The velocity of the particle  $\mathbf{X} \in \Omega$  is  $\mathbf{v}$ , and  $\mathcal{R}$  is the energetic external radiation. The indicial form of Eq.(2.9) is

$$\rho\dot{e} + q_{I,I} = S_{IJ}\dot{L}_{IJ} + {}_{\text{ext}}q_J N_J + \rho\mathcal{R}. \quad (2.11)$$

Considering [52] and [63] the following substitutions can be done

$$\dot{e} = C_v \dot{\theta} \quad (2.12)$$

$$\mathbf{q} = \mathbf{k} \cdot \nabla \theta \quad (2.13)$$

$$\text{div}\mathbf{q} = \nabla \cdot \mathbf{q}$$

$$\nabla\{\mathbf{k} \cdot \nabla \theta\} = \{\mathbf{k} \cdot \nabla\} \nabla \theta + \{\nabla \theta \cdot \nabla\} \mathbf{k} + \nabla \theta \times \{\nabla \times \mathbf{k}\}$$

where  $c_v$  is the specific heat defined in relation to constant volume. The diagonal tensor of thermal conductivity  $\mathbf{k}$  is defined by

$$\mathbf{k} = \begin{bmatrix} k_{11} & 0 & 0 \\ 0 & k_{22} & 0 \\ 0 & 0 & k_{33} \end{bmatrix} \quad (2.14)$$

This matrix is usually considered to be isotropic although Pardo et al. [47], used anisotropic coefficients of conductivity to simulate droplet penetration. Such relations are given for  $k_{22}$  and  $k_{33}$  in the forms

$$\begin{aligned} k_{22} &= k_{mean} \left( 1 + 3 \exp \left( \frac{-r^2}{2\sigma_r^2} \right) \right) \\ k_{33} &= k_{mean} \left( 1 + 10 \exp \left( \frac{-r^2}{2\sigma_r^2} \right) \right) \\ k_{22} &= k_y \\ k_{33} &= k_z \end{aligned} \quad (2.15)$$

where  $k_{mean}$  is the mean conductivity,  $r$  is the horizontal distance from the weld center, and  $\sigma_r$  is the standard deviation of heat distribution measured in mm. The  $z$  direction is vertically perpendicular to the weld and the  $y$  direction is parallel to arc motion. This is an interesting approach but can only be implemented in a UEL subroutine and we have preferred not to use these relations.

The expression for  $\nabla\{\mathbf{k} \cdot \nabla\theta\}$  can be simplified assuming thermal homogeneity of inelastic conductor, that leads to  $k_{IJ}(\mathbf{X}) = const, \forall \mathbf{X} \in \Omega$ . Hence it can be expressed by

$$\nabla\{\mathbf{k} \cdot \nabla\theta\} = \{\mathbf{k} \cdot \nabla\} \nabla\theta \equiv \mathbf{k} \cdot \nabla^2\theta \quad (2.16)$$

or rewritten in the indicial form as

$$q_{I,I} = k_{IJ}\theta_{,JI} \quad (2.17)$$

where  $\nabla^2$  is the Laplacian operator.

The R.H.S. terms of Eq.(2.11) can be interpreted as follows:

- the rate of heat generation due to dissipation of mechanical energy

$$f_\theta^B = S_{IJ}\dot{L}_{IJ} \quad (2.18)$$

- the heat flux of welding arc and outfluxes due to convection and radiation

$$f_\theta^S = extq_J N_J + \rho\mathcal{R} \quad (2.19)$$

- concentrated heat fluxes

$$\sum_{\mathcal{J}} \mathcal{F}_\theta^{\mathcal{J}} \quad (2.20)$$

Substitution of Eqs.(2.12), (2.17), (2.18), (2.19), (2.20) to Eq.(2.11) results in the simple "heat equation" form of the balance of internal energy for inelastic conductor

$$c\dot{\theta} + k_{IJ}\theta_{,JI} = f_\theta^B + f_\theta^S + \sum_{\mathcal{J}} \mathcal{F}_\theta^{\mathcal{J}} \quad (2.21)$$

where  $c = \rho_0 C_v$ .

Balance laws for momentum and internal energy can be expressed in the functional form and then approximated by the Galerkin type Finite Element Method. A formulation of the functional forms of the balance laws consist of the following steps [25], [52]:

- Characterize two classes of functions: the trial solutions  $\mathcal{S}$  and the weighting functions  $\mathcal{V}$  (or variations), which are defined by

$$\mathcal{S} = \{u, \theta \mid u, \theta \in H^1\} \quad (2.22)$$

where  $u$  and  $\theta$  fulfills boundary conditions for the thermo-mechanical problem,

$$\mathcal{V} = \{v, \vartheta \mid v, \vartheta \in H^1\} \quad (2.23)$$

where  $u, \vartheta$  are equal zero at the boundary  $\partial\Omega$ , and  $H^1$  is the Hilbert space.

- Express the balance laws Eqs.(2.7), (2.21) as differential operators defined by

$$\mathcal{U}(\mathbf{u}) = (S_{KI} + S_{KL}u_{I,L})_{,K} - (b_I + r_I)\rho_0 \quad (2.24)$$

$$\Psi(\theta) = c\dot{\theta} + k_{IJ}\theta_{,JI} - f_{\theta}^B - f_{\theta}^S - \sum_{\mathcal{J}} \mathcal{F}_{\theta}^{\mathcal{J}} \quad (2.25)$$

- Take scalar products of these operators and weighting functions  $v$  and  $\vartheta$ , correspondingly,

$$\int_{V_0} (S_{KI} + S_{KL}u_{I,L})_{,K} v_I dV - \int_{V_0} b_I v_I dV - \int_{\partial V_0} r_I v_I d\mathcal{P} = 0 \quad (2.26)$$

$$\int_V (c\dot{\theta} + k_{IJ}\theta_{,JI}) \vartheta dV - \int_V f_{\theta}^B \vartheta dV - \int_{\partial V} f_{\theta}^S \vartheta d\mathcal{P} - \sum_{\mathcal{J}} \mathcal{F}_{\theta}^{\mathcal{J}} \vartheta |_{\mathcal{J}} = 0 \quad (2.27)$$

- Use the Green formula to decompose the first integral of Eq.(2.26)

$$\begin{aligned} \int_{V_0} (S_{KI} + S_{KL}u_{I,L})_{,K} v_I dV &= \int_{V_0} (S_{KI,K} + S_{KL,K}u_{I,L}) v_I dV + \\ &\int_{\partial V_0} S_{KL}u_{I,L} v_I d\mathcal{P} - \int_{V_0} S_{KL}u_{I,L} v_{I,K} dV \end{aligned} \quad (2.28)$$

where the second integral of R.H.S. vanishes because of the boundary conditions for the weighting function  $v \in \mathcal{V}$ .

- Use the Green formula to decompose the integral with the divergence of temperature in the heat equation

$$\int_V k_{IJ}\theta_{,JI} \vartheta dV = \int_{\partial V} k_{IJ}\theta_{,I} \vartheta d\mathcal{P} - \int_V k_{IJ}\theta_{,I} \vartheta_{,J} dV \quad (2.29)$$

- Combination of the above decompositions with Eq.(2.26) and Eq.(2.27) gives

$$\int_{V_0} S_{KLU_{I,L}v_{I,K}} dV - \int_{V_0} (S_{KI,K} + S_{KL,K}u_{I,L})v_I dV + \int_{V_0} b_I v_I dV + \int_{\partial V_0} r_I v_I d\mathcal{P} = 0 \quad (2.30)$$

$$\int_V k_{IJ} \theta_{,I} \vartheta_{,J} dV - \int_V c \dot{\theta} \vartheta dV + \int_V f_{\theta}^B \vartheta dV + \int_{\partial V} \hat{f}_{\theta}^S \vartheta d\mathcal{P} + \sum_{\mathcal{J}} \mathcal{F}_{\theta}^{\mathcal{J}} \vartheta |_{\mathcal{J}} = 0 \quad (2.31)$$

where

$$\int_{\partial V} \hat{f}_{\theta}^S \vartheta d\mathcal{P} = \int_{\partial V} f_{\theta}^S \vartheta d\mathcal{P} + \int_{\partial V} k_{IJ} \theta_{,I} \vartheta d\mathcal{P} \quad (2.32)$$

Stationary conditions for functionals Eq.(2.30) and Eq.(2.31) are the following variational equations obtained by using generalized derivatives:

$$\int_{V_0} S_{KLU_{I,L} \delta v_{I,K}} dV - \int_{V_0} (S_{KI,K} + S_{KL,K}u_{I,L}) \delta v_I dV + \int_{V_0} b_I \delta v_I dV + \int_{\partial V_0} r_I \delta v_I d\mathcal{P} = 0 \quad (2.33)$$

$$\int_V k_{IJ} \theta_{,I} \delta \vartheta_{,J} dV - \int_V c \dot{\theta} \delta \vartheta dV + \int_V f_{\theta}^B \delta \vartheta dV + \int_{\partial V} \hat{f}_{\theta}^S \delta \vartheta d\mathcal{P} + \sum_{\mathcal{J}} \mathcal{F}_{\theta}^{\mathcal{J}} \delta \vartheta |_{\mathcal{J}} = 0 \quad (2.34)$$

Solutions of these variational equations  $v$  and  $\vartheta$  are called the weak, or generalized, solutions. The equation Eq.(2.33) is called the equation of virtual work.

## 2.3 Finite Element Approximation

The Finite Element Method for the fully coupled thermo-mechanical problem is based on Galerkin's approximation of variational equations i.e. the principle of virtual work and the balance of internal energy. The FEM consists of the following steps [5], [25]:

- The first step in developing the method is to construct the finite-dimensional approximation of the collections of trial functions  $\mathcal{S}$  and the weighting functions  $\mathcal{V}$ , or variations, which are defined by

$$\mathcal{S}^h \subset \mathcal{S} \quad (2.35)$$

$$\text{if } u^h, \theta^h \in \mathcal{S}^h \text{ then } u^h, \theta^h \in \mathcal{S}$$

$$\mathcal{V}^h \subset \mathcal{V} \quad (2.36)$$

$$\text{if } v^h, \vartheta^h \in \mathcal{V}^h \text{ then } v^h, \vartheta^h \in \mathcal{V}$$

- Discretization of the domain  $\Omega = \{\mathbf{X} \in V; \in [t_i, t_f]\}$  by finite elements which are parameterised by characteristic length scales  $\{h_X, h_t\}$ ,

- Express  $v^h$  and  $\vartheta^h$  as linear combinations of given shape functions, or interpolation functions,
- Approximation of integrals in variational equations by sums,
- Formulation of a coupled system of linear algebraic equations, usually expressed in the matrix form and called the **Finite Element Equation**, for values of  $v^h$  and  $\vartheta^h$  at nodal points,
- Solution of the system of algebraic equations by the Newton-Raphson method.

### 2.3.1 FE Approximation of Equation of Virtual Work

The equation of virtual work Eq.(2.33) is solved by the Finite Element Method combined with linearization techniques for **Finite Element Equation**. The linearizations are applied after incremental decompositions for strain and stress given by

$$\tilde{\mathbf{L}}^{n+1} = \tilde{\mathbf{L}}^n + \tilde{\mathbf{L}}^0 \quad (2.37)$$

$$\tilde{\mathbf{S}}^{n+1} = \tilde{\mathbf{S}}^n + \tilde{\mathbf{S}}^0 \quad (2.38)$$

where  $\{\tilde{\mathbf{L}}, \tilde{\mathbf{S}}\}^{n+1}$  and  $\{\tilde{\mathbf{L}}, \tilde{\mathbf{S}}\}^n$  corresponds to the actual and the previous strain-stress state. The increments of strain and stress are  $\tilde{\mathbf{L}}^0, \tilde{\mathbf{S}}^0$ . The increment of the Green-Lagrange strain  $\tilde{\mathbf{L}}^0$  is further decomposed into its linear and nonlinear components:

$$\tilde{\mathbf{L}}^0 = \mathbf{L} + \mathbf{L}_\nu \quad (2.39)$$

where

$$\mathbf{L} = \frac{1}{2} (\Delta u_{I,J} + \Delta u_{J,I}) ; \mathbf{L}_\nu = \Delta u_{K,I} \Delta u_{K,J} \quad (2.40)$$

The **Finite Element Equation** [5], [25] for the Total Lagrangian Formulation at time  $(n+1)$  is obtained from Eq.(2.33) and is expressed by

$$\left( {}^t_0\mathbf{K}_L + {}^t_0\mathbf{K}_{NL} \right) \Delta \mathbf{u}^{(i)} = {}^{t+\Delta t}\mathbf{R}_u - {}^{t+\Delta t}_0\mathbf{F}^{(i-1)} \quad (2.41)$$

where  ${}^t_0\mathbf{K}_L$  and  ${}^t_0\mathbf{K}_{NL}$  is linear and nonlinear stiffness matrix,  $\Delta \mathbf{u}^{(i)}$  is the vector of displacement increment,  ${}^{t+\Delta t}\mathbf{R}_u$  is the vector of externally applied nodal point loads,  $\mathbf{F}$  is the vector of nodal point forces equivalent to the internal stresses. This equation is linear in respect of  $\Delta \mathbf{u}^{(i)}$  and the matrices in Eq.(2.41) are taken at the current and previous time steps and the current and previous iterations at the current time step. These matrices are evaluated at two time steps  $t$  and  $(t + \Delta t)$ , and for two iterations  $i$  and  $(i - 1)$ . The linear stiffness matrix is defined by

$${}^t_0\mathbf{K}_L = \int_{V_0} {}^t_0\mathbf{B}_L^T \hat{\mathbf{C}} {}^t_0\mathbf{B}_L dV_0 \quad (2.42)$$

The matrix  $\hat{\mathbf{C}}$  is the consistent or algorithmic tangent modulus which has to be defined for each material model as the  ${}^t_0[\frac{\partial \mathbf{T}}{\partial \mathbf{L}}]$  contribution to the global stiffness matrix, and  ${}^t_0\mathbf{B}_L$  is the linear strain displacement matrix. The nonlinear stiffness matrix is defined by

$${}^t_0\mathbf{K}_{NL} = \int_{V_0} {}^t_0\mathbf{B}_{NL}^T \hat{\mathbf{S}} {}^t_0\mathbf{B}_{NL} dV_0 \quad (2.43)$$

where  $\hat{\mathbf{S}}$  is the matrix representation of 2nd Piola-Kirchhoff stress, and  ${}^t_0\mathbf{B}_{NL}$  is the nonlinear strain-displacement matrix arising from  $\mathbf{L}_\nu$ . The linear and nonlinear stiffness matrices are not modified in iteration process at the step  $t + \Delta t$ . They are updated when the iteration process at  $t + \Delta t$  is completed. The vector of externally applied nodal point loads is given by

$${}^{t+\Delta t}\mathbf{R}_u = \int_{\partial V_0} \mathbf{H}_s^T {}^{t+\Delta t}\mathbf{r} d\mathcal{P} + \int_{V_0} \mathbf{H}^T {}^{t+\Delta t}\mathbf{b} dV_0 \quad (2.44)$$

where  $\mathbf{H}_s$  is the surface interpolation matrix, and  $\mathbf{H}$  is the volume interpolation matrix. These matrices are formed from the interpolating polynomial during the process of Gaussian integration. The matrix  $\mathbf{H}_s$  is evaluated for two of the 3-coordinates at Gauss points and one at the given surface. With  ${}^{t+\Delta t}\mathbf{r} = \{r_J\}$  and  ${}^{t+\Delta t}\mathbf{b} = \{b_J\}$  described in Eq.(2.33). The vector of nodal point forces equivalent to the stresses at time  ${}^{t+\Delta t}$  is defined as

$${}^{t+\Delta t}\mathbf{F}^{(i-1)} = \int_{V_0} {}^t_0\mathbf{B}_L {}^{t+\Delta t}\tilde{\mathbf{S}}^{(i-1)} dV_0 \quad (2.45)$$

### 2.3.2 FE Approximation of Balance of Internal Energy

The variational equation of internal energy balance Eq.(2.34) is solved by the Galerkin type Finite Element Method. The appropriate **Finite Element Equation** for the fully coupled thermo-mechanical problem is given by:

$${}^t_0\mathbf{C} {}^{t+\Delta t}\dot{\theta}^{(i)} + \left( {}^t_0\mathbf{K}^k + {}^t_0\mathbf{K}^c + {}^t_0\mathbf{K}^r \right) \Delta\theta^{(i)} = {}^{t+\Delta t}\mathbf{F}_\theta^c{}^{(i-1)} + {}^{t+\Delta t}\mathbf{F}_\theta^r{}^{(i-1)} + {}^{t+\Delta t}\mathbf{F}_\theta^k{}^{(i-1)} - {}^{t+\Delta t}\mathbf{F}_\Theta^{(i-1)} \quad (2.46)$$

where  ${}^t_0\mathbf{K}^k$  is the stiffness matrix corresponding to conduction,  ${}^t_0\mathbf{K}^c$  is the stiffness related to convection phenomena,  ${}^t_0\mathbf{K}^r$  is the stiffness resulting from radiation effects. The right hand side vectors of nodal thermal loads  ${}^{t+\Delta t}\mathbf{F}_\theta^c{}^{(i-1)}$ ,  ${}^{t+\Delta t}\mathbf{F}_\theta^r{}^{(i-1)}$ ,  ${}^{t+\Delta t}\mathbf{F}_\theta^k{}^{(i-1)}$  correspond to the thermal boundary conditions and to the internal heat flux  ${}^{t+\Delta t}\mathbf{F}_\Theta^{(i-1)}$  through the body surface  $\partial V$ . This heat flux is caused by the temperature distribution  $\theta^{(i-1)}$  in  $V \subset \Omega$ .

The combined **Global Finite Element Equation** for thermo-mechanical problem is

$$\begin{bmatrix} \mathbf{0} & \mathbf{0} \\ \mathbf{0} & {}^t_0\mathbf{C} \end{bmatrix} \begin{bmatrix} \mathbf{0} \\ {}^{t+\Delta t}\dot{\theta} \end{bmatrix}^{(i)} + \begin{bmatrix} {}^t_0\mathbf{K}_u & {}^t_0\mathbf{K}_{u\theta} \\ {}^t_0\mathbf{K}_{\theta u} & {}^t_0\mathbf{K}_\theta \end{bmatrix} \begin{bmatrix} \Delta\mathbf{u} \\ \Delta\theta \end{bmatrix}^{(i)} = \begin{bmatrix} {}^{t+\Delta t}\mathbf{R}_u \\ {}^{t+\Delta t}\mathbf{R}_\Theta \end{bmatrix} - \begin{bmatrix} {}^{t+\Delta t}\mathbf{F}_u \\ {}^{t+\Delta t}\mathbf{F}_\Theta \end{bmatrix}^{(i-1)} \quad (2.47)$$

where  ${}^t_0\mathbf{K}_u$  is the stiffness corresponding to mechanical effects,  ${}^t_0\mathbf{K}_{u\theta}$  is the matrix which transforms thermal energy into mechanical and matrix  ${}^t_0\mathbf{K}_{\theta u}$  transform mechanical energy

into thermal, the thermal stiffness  ${}^t_0\mathbf{K}_\theta$  is a sum of  ${}^t_0\mathbf{K}^k$ ,  ${}^t_0\mathbf{K}^c$  and  ${}^t_0\mathbf{K}^r$ . The right hand vectors of Eq.(2.47) are defined by

$${}^t_0+\Delta t\mathbf{F}_u^{(i-1)} = {}^t_0+\Delta t\mathbf{F}^{(i-1)}; \quad (2.48)$$

$${}^t_0+\Delta t\mathbf{R}_\Theta = {}^t_0+\Delta t[\mathbf{F}_\theta^k + \mathbf{F}_\theta^c + \mathbf{F}_\theta^r] \quad (2.49)$$

The stiffness matrices  ${}^t_0\mathbf{K}_u$ ,  ${}^t_0\mathbf{K}_\theta$ ,  ${}^t_0\mathbf{K}_{u\theta}$  and  ${}^t_0\mathbf{K}_{\theta u}$  defined by appropriate integrals with kernels expressed by a combination of unknowns  $\mathbf{u}$ ,  $\theta$ , shape functions and strain-displacement matrices [52], [53] can be also viewed from the perspective of the Newton-Raphson solution process as the derivatives of vectors  $\mathbf{F}_u$ ,  $\mathbf{F}_\Theta$  with respect to the state variable  $\mathbf{u}$  and  $\theta$ . Hence, they can be expressed as follows:

$$\begin{aligned} {}^t_0\mathbf{K}_u &= {}^t_0\mathbf{F}_{u,u} \\ {}^t_0\mathbf{K}_\theta &= {}^t_0\mathbf{F}_{\Theta,\theta} \\ {}^t_0\mathbf{K}_{u\theta} &= {}^t_0\mathbf{F}_{u,\theta} \\ {}^t_0\mathbf{K}_{\theta u} &= {}^t_0\mathbf{F}_{\Theta,u} \end{aligned} \quad (2.50)$$

where ',' indicates differentiation. Approximating the temperature rate by using the backward Euler scheme in Eq.(2.46)

$$\left(\frac{1}{\Delta t}{}^t_0\mathbf{C} + {}^t_0\mathbf{K}^k + {}^t_0\mathbf{K}^c + {}^t_0\mathbf{K}^r\right) \Delta\theta^{(i)} = {}^t_0+\Delta t\mathbf{R}_\Theta - {}^t_0+\Delta t\mathbf{F}_\Theta^{(i-1)} \quad (2.51)$$

and combining with equation Eq.(2.47), the finite element equation for the thermo-mechanical system can be rewritten in a more compact form

$$\begin{bmatrix} {}^t_0\mathbf{K}_u & {}^t_0\mathbf{K}_{u\theta} \\ {}^t_0\mathbf{K}_{\theta u} & \frac{1}{\Delta t}{}^t_0\mathbf{C} + {}^t_0\mathbf{K}_\theta \end{bmatrix} \begin{bmatrix} \Delta\mathbf{u} \\ \Delta\theta \end{bmatrix}^{(i)} = \begin{bmatrix} {}^t_0+\Delta t\mathbf{R}_u \\ {}^t_0+\Delta t\mathbf{R}_\Theta \end{bmatrix} - \begin{bmatrix} {}^t_0+\Delta t\mathbf{F}_u \\ {}^t_0+\Delta t\mathbf{F}_\Theta \end{bmatrix}^{(i-1)} \quad (2.52)$$

## 2.4 Implementation of Material Models

The installation of new constitutive theories into an ABAQUS UMAT routine consists of using the value of strain increment given by the global solution to solve for the current value of the stress tensor,  $\mathbf{T}$ , which contributes in Eq.(2.45) and Eq.(2.43) as well as providing the values which are interpolated for output in the contour plots. In the case of the class of viscoplastic constitutive theories considered in this paper this is achieved by the time integration of evolution equations and implicit solution techniques for the stress and internal variables associated with the specific model.

In addition the operator  $\hat{\mathbf{C}}$  as in Eq.(2.42), the **Consistent Tangent Modulus**, has to be supplied as well as terms associated with the coupling between temperature and stress.

In order to implement the consistent tangent modulus in a finite element program a  $6 \times 6$  matrix in conventional 3-D analysis needs to be define. This is under the assumption that the 2nd-rank tensors normally expressed as  $3 \times 3$  matrices are represented as  $6 \times 1$  vectors

and that 4-th rank tensors are represented as  $6 \times 6$  matrices. This structure is presented in the appendix. The intermediate and the final matrices which are supplied to ABAQUS are defined below.

The following constant matrices used in the evaluation of the **Consistent Tangent Modulus** are formed:

- the diagonal unit matrix of the fourth rank

$$\hat{\mathbf{I}} = \begin{bmatrix} 1 & 0 & 0 & 0 & 0 & 0 \\ 0 & 1 & 0 & 0 & 0 & 0 \\ 0 & 0 & 1 & 0 & 0 & 0 \\ 0 & 0 & 0 & 1 & 0 & 0 \\ 0 & 0 & 0 & 0 & 1 & 0 \\ 0 & 0 & 0 & 0 & 0 & 1 \end{bmatrix} \quad (2.53)$$

- the outer product of the second rank identity

$$\mathbf{1} \otimes \mathbf{1} = \begin{bmatrix} 1 & 1 & 1 & 0 & 0 & 0 \\ 1 & 1 & 1 & 0 & 0 & 0 \\ 1 & 1 & 1 & 0 & 0 & 0 \\ 0 & 0 & 0 & 0 & 0 & 0 \\ 0 & 0 & 0 & 0 & 0 & 0 \\ 0 & 0 & 0 & 0 & 0 & 0 \end{bmatrix} \quad \mathbf{1} = \begin{bmatrix} 1 \\ 1 \\ 1 \\ 0 \\ 0 \\ 0 \end{bmatrix} \quad (2.54)$$

- the deviatoric identity of the fourth rank

$$\hat{\mathbf{I}}_{dev} = \hat{\mathbf{I}} - \frac{1}{3} \mathbf{1} \otimes \mathbf{1}$$

$$\hat{\mathbf{I}}_{dev} = \begin{bmatrix} 1 & 0 & 0 & 0 & 0 & 0 \\ 0 & 1 & 0 & 0 & 0 & 0 \\ 0 & 0 & 1 & 0 & 0 & 0 \\ 0 & 0 & 0 & 1 & 0 & 0 \\ 0 & 0 & 0 & 0 & 1 & 0 \\ 0 & 0 & 0 & 0 & 0 & 1 \end{bmatrix} - \frac{1}{3} \begin{bmatrix} 1 & 1 & 1 & 0 & 0 & 0 \\ 1 & 1 & 1 & 0 & 0 & 0 \\ 1 & 1 & 1 & 0 & 0 & 0 \\ 0 & 0 & 0 & 0 & 0 & 0 \\ 0 & 0 & 0 & 0 & 0 & 0 \\ 0 & 0 & 0 & 0 & 0 & 0 \end{bmatrix} \quad (2.55)$$

Intermediate matrices  $\hat{\mathbf{M}}_i$ ,  $i = 1, 2, 3$  and the final matrix  $\hat{\mathbf{M}}_4$  which result from the consistent linearization process are determined for the deviatoric stress  $\mathbf{S}$  and tensorial or scalar internal variables  $\mathbf{Z}_i$  of a material model. These matrices are defined as follows

- the sum of terms resulting from the differentiation of the deviatoric strain increment and the plastic strain increment with respect to stress.

$$\hat{\mathbf{M}}_1 \equiv \frac{1}{2\mu} \hat{\mathbf{I}} + \Delta t \frac{\partial \dot{\mathbf{E}}}{\partial \mathbf{S}} \quad (2.56)$$

where  $\frac{\partial \hat{\mathbf{E}}}{\partial \mathbf{S}}$  is the derivative of strain, with respect to the second rank tensor  $\mathbf{S}$  resulting in a fourth rank tensor which is be represented by a  $6 \times 6$  matrix defined for each constitutive model.

- the product of the intermediate matrix  $\hat{\mathbf{M}}_1$  with the deviatoric identity to account for the chain rule product with  $\frac{\partial \mathbf{S}}{\partial \mathbf{T}}$ ,

$$\hat{\mathbf{M}}_2 = \hat{\mathbf{M}}_1 : \hat{\mathbf{I}}_{dev} \quad (2.57)$$

- the sum of the matrix representing elastic compression and  $\hat{\mathbf{M}}_2$

$$\hat{\mathbf{M}}_3 \equiv \frac{\partial \mathbf{L}}{\partial \mathbf{T}} = \hat{\mathbf{M}}_2 + \frac{1}{3\kappa} \mathbf{1} \otimes \mathbf{1} \quad (2.58)$$

- the inverse matrix  $[\hat{\mathbf{M}}_3]^{-1}$ ,

$$\hat{\mathbf{M}}_4 \equiv [\hat{\mathbf{M}}_3]^{-1} = \frac{\partial \mathbf{T}}{\partial \mathbf{L}} \quad (2.59)$$

The matrix  $\hat{\mathbf{M}}_4$  is approximated by  $\frac{\Delta \mathbf{T}}{\Delta \mathbf{L}}$  supplied to ABAQUS as the required operator termed either the **Algorithmic Tangent Modulus** or the **Consistent Tangent Modulus** in reference to the fact that the modulus derives from a linearisation of an expansion about a strain increment for the stress given by the algorithm used to implement the constitutive model.

## 2.5 Solution of Finite Element Equations

The nonlinear Finite Element system of equations given by Eq.(2.52) is solved iteratively by the Newton-Raphson scheme. The system Eq.(2.52) can be rewritten in the form

$$[\mathcal{K}][\mathcal{U}] = [\mathcal{R}] - [\mathcal{F}] \quad (2.60)$$

where

$$[\mathcal{K}] = \begin{bmatrix} {}^t_0 \mathbf{K}_u & {}^t_0 \mathbf{K}_{u\theta} \\ {}^t_0 \mathbf{K}_{\theta u} & \frac{1}{\Delta t} {}^t_0 \mathbf{C} + {}^t_0 \mathbf{K}_\theta \end{bmatrix} \quad (2.61)$$

$$[\mathcal{U}] = \begin{bmatrix} \Delta \mathbf{u} \\ \Delta \theta \end{bmatrix}^{(i)} \quad (2.62)$$

$$[\mathcal{F}] = \begin{bmatrix} {}^{t+\Delta t}_0 \mathbf{F}_u \\ {}^{t+\Delta t}_0 \mathbf{F}_\theta \end{bmatrix}^{(i-1)} \quad (2.63)$$

$$[\mathcal{R}] = \begin{bmatrix} t+\Delta t \mathbf{R}_u \\ t+\Delta t \mathbf{R}_\Theta \end{bmatrix} \quad (2.64)$$

The L.H.S. can be defined as the linear function of  $[\mathcal{U}]$

$$f[\mathcal{U}] = [\mathcal{K}][\mathcal{U}] \quad (2.65)$$

The Newton-Raphson method provides the approximation  $[\mathcal{U}]^{i+1}$  of the root  $[\mathcal{U}]^*$  of the equation

$$f[\mathcal{U}] = 0 \quad (2.66)$$

computed from the approximation  $[\mathcal{U}]^i$  using the equation

$$[\mathcal{U}]^{i+1} = [\mathcal{U}]^i - \frac{f[\mathcal{U}]^i}{\left. \frac{\partial f[\mathcal{U}]}{\partial \mathcal{U}} \right|_{\mathcal{U}^i}} \quad (2.67)$$

Replacing  $[\mathcal{K}][\mathcal{U}]$  by  $([\mathcal{R}] - [\mathcal{F}])$  and substituting  $\left. \frac{\partial f[\mathcal{U}]}{\partial \mathcal{U}} \right|_{\mathcal{U}^i} = [\mathcal{K}]$  in equation Eq.(2.67) implies that

$$[\mathcal{U}]^{i+1} = [\mathcal{U}]^i - \frac{[\mathcal{K}][\mathcal{U}]^i}{[\mathcal{K}]} = [\mathcal{U}]^i - [\mathcal{K}]^{-1}([\mathcal{R}] - [\mathcal{F}]^i) \quad (2.68)$$

The recombination of the last relation leads to the form

$$[\mathcal{K}]([\mathcal{U}]^{i+1} - [\mathcal{U}]^i) = [\mathcal{F}]^i - [\mathcal{R}] \quad (2.69)$$

from where the convergency of the method can be evaluated. The matrix  $[\mathcal{U}]^{i+1}$  converges to the solution  $[\mathcal{U}]^*$  when  $([\mathcal{U}]^{i+1} - [\mathcal{U}]^i)$  converges to zero that happens when the vector of nodal thermal and mechanical loads  $[\mathcal{R}]$  balances the vector of nodal stress vectors and heat fluxes  $[\mathcal{F}]^i$  i.e.  $[\mathcal{F}]^i - [\mathcal{R}] = \mathbf{0}$ .

# Chapter 3

## Materials with Scalar Parameters

The stresses given in the previous section are a function of the calculated strain, and in general of some other unknown parameters. This relationship is defined for each material by a mathematical model which either from phenomenological or theoretical principles attempts to define a stress-strain relation. In this section we consider models which consist of evolution equations for internal variables and inelastic strain. The stress state is determined from elastic part of strain when the energy is instantaneously released in plastic deformation.

### 3.1 General Solution Procedure

We consider unified viscoplastic models without an explicitly defined yield surface. These unified models assume plasticity at all levels of strain as opposed to the elastic-plastic and elastic-viscoplastic models which assume that plastic flow is initiated at some stress state. In metals the  $J_2$  plasticity theory is used in which the second invariant of deviatoric stress or the Mises stress is used to assess a critical stress state when a permanent deformation appears. It is assumed that only the deviatoric components contribute to plasticity and the hydrostatic component i.e. compressibility is assumed to always be elastic. The second invariant of stress defines the yield surface which expands in the stress space outwards in the case of hardening or shrinks in the case of softening. Temperature has a softening effect on the yield surface. Active loading, neutral loading, and unloading criteria for elastic-plastic and elastic-viscoplastic models are not applicable for the Anand, Estrin-Mecking and Estrin models where an unloading criteria is not explicitly defined. The case of unloading results in the measure of the increment of plastic strain becoming negligible rather than being set to zero. Instead of loading-unloading criteria in viscoplastic models with internal parameters arising from dislocation theory we have a set of evolution equations which define an evolution of stress-strain state. We have a differential equation for the plastic strain rate and usually one or more evolution equations for an internal variable or variables which deals with the hardening phenomena. The possibility of strain softening is dealt with by including a term which alters the sign of the hardening term in the softening instance.

1. Begin
2. Calculate Elastic Predictor:  $*\mathbf{T}^{n+1} = \mathbf{T}^n + \hat{\mathbf{C}} : \Delta \mathbf{L}^{n+1}$
3. Calculate Elastic Deviator  $*\mathbf{S}^{n+1} = *\mathbf{T}^{n+1} - \frac{1}{3} \text{tr} *\mathbf{T}^{n+1} \mathbf{1}$
- 4 Initialize:  $\mathbf{S}^{n+1} = *\mathbf{S}^{n+1}$ ,  $z_i^{n+1} = z_i^n$ , ( $i = 1..p$ )
5. Form Residual Functions:
 
$$F(\mathbf{S}, z_1, \dots, z_p) = \mathbf{S}^{n+1} - *\mathbf{S}^{n+1} + 3\mu\Delta t f(s, z_1, \dots, z_p) \frac{\mathbf{S}}{\|\mathbf{S}\|_M}$$

$$G_i(s, z_1, \dots, z_p) = z_i^{n+1} - z_i^n - \Delta t g_i(s, z_1, \dots, z_p), (i = 1..p)$$
6. Solve residual equations in 5 for  $\mathbf{S}^{n+1}$  and  $z_i^{n+1}$  by N-R scheme
7. Update solution  $\mathbf{S}^{i+1} = \mathbf{S}^i + \Delta \mathbf{S}^{i+1}$ 

$$z_k^{i+1} = z_k^i + \Delta z_k^{i+1}$$
8. Check For Convergence:
 

IF  $F(\mathbf{S}, z_1, \dots, z_p) > \text{TOL}$   
 OR  $G_k(\mathbf{S}, z_1, \dots, z_p), (k = 1..p) > \text{TOL}$   
 THEN goto 7
9. Update total stress tensor  $\mathbf{T}^{n+1} = \mathbf{S}^{n+1} + \frac{1}{3} \text{tr} *\mathbf{T}^{n+1} \mathbf{1}$
10. Update  $\hat{\mathbf{C}} \equiv \frac{\partial \mathbf{T}}{\partial \mathbf{L}}$  contribution to global stiffness matrix  
 derived from linearization of algorithm
11. End

Figure 3.1: Generalized uniaxial viscoplastic model

This class of viscoplastic models is based on concept of a constitutive equation for the plastic strain rate:

$$\dot{\epsilon}^p = f(s, z_1, \dots, z_k) \quad (3.1)$$

which is related to the Mises stress  $s$  and  $k$  scalar internal variables  $z_1, \dots, z_n$  determined by the following set of evolution equations for the internal variables:

$$\dot{z}_i = g_i(s, z_1, \dots, z_k), i = 1..k \quad (3.2)$$

The generalisation to multiaxial loading is in terms of the Levy-Mises equation [41]

$$\dot{\mathbf{E}}^p = \frac{3}{2} f(s, z_1, \dots, z_k) \frac{\mathbf{S}}{\|\mathbf{S}\|_M} \quad (3.3)$$

where  $s = \|\mathbf{S}\|_M$  is the Mises equivalent stress and it is equal to  $(\frac{3}{2})^{1/2} \|\mathbf{S}\|$  with the natural norm being defined by  $\|\mathbf{S}\| = (\mathbf{S} : \mathbf{S})^{1/2}$ . This norm is associated with the natural inner product induced by the trace of the product of two tensors i.e. full contraction. The plastic part of the strain tensor is thus given by Eq.(3.3).

Values of stress deviator and internal variables  $\mathbf{S}, z_1..z_k$  define the solution of the stress-strain relationship rather than stress states which lie on a yield surface. Values  $\mathbf{S}, z_1..z_k$  are

evaluated by formulating residual equations, satisfied at any time step of the integration process. We have:

$$F(\mathbf{S}, z_1, \dots, z_k) = \mathbf{S}^{n+1} - {}^* \mathbf{S}^{n+1} + 2\mu\Delta t \dot{\mathbf{E}}^p \quad (3.4)$$

and

$$G_i(s, z_1, \dots, z_k) = z_i^{n+1} - z_i^n - \Delta t g(s, z_1, \dots, z_k) \quad (3.5)$$

where  ${}^* \mathbf{S}^{n+1}$  is the elastic predicted stress  ${}^* \mathbf{S}^{n+1} = \mathbf{S}^n + \hat{\mathbf{I}}_{dev} : \hat{\mathbf{C}} : \Delta \mathbf{L}^{n+1}$  and the superscripts  $n, n + 1$  refer to the current and previous time steps respectively. The backward Euler algorithm has been used for the integration of these equations. Initial values of stress and internal variables in this iterative process are evaluated for the purely elastic strain increment. The complete procedure is presented in figure Eq.(3.1).

## 3.2 Anand's Model

The Anand model [2],[9] consists of approximate constitutive equations for the rate-dependent deformation of metals at elevated temperatures. Suggested constitutive equations employ only a single scalar internal variable which represents an isotropic resistance to plastic flow. The material constants appearing in the viscoplastic part of the constitutive equations were determined from results of continuous isothermal tension test, at a number of constant strain rates. In a tested temperature range the steel had an austenite structure. This model, which is originally of practical interest for analyzing of casting and low rate hot-working processes, is also useful for welding simulation.

### 3.2.1 Time-Integration of Constitutive Equations

The Anand constitutive equation for the plastic strain is given by [9]

$$\dot{\varepsilon}^p = A \exp\left(-\frac{Q}{R\theta}\right) \left[ \sinh\left(\frac{\xi \|\mathbf{S}\|_M}{z_1}\right) \right]^{\frac{1}{m}} \quad (3.6)$$

The evolution equation for the internal variable, formally termed the deformation resistance, is given by [9]

$$\begin{aligned} \dot{z}_1 &= h_0 \left[1 - \frac{z_1}{z^*}\right]^a \dot{\varepsilon}^p & (z_1 \leq z^*) \\ \dot{z}_1 &= -h_0 \left[\frac{z_1}{z^*} - 1\right]^a \dot{\varepsilon}^p & (z_1 > z^*) \end{aligned} \quad (3.7)$$

with

$$z^* = \bar{z} \left[ \frac{\dot{\varepsilon}^p}{A} \exp\left(\frac{Q}{R\theta}\right) \right]^n \quad (3.8)$$

where  $A, Q, \xi, m, z_0, h_0, a, \bar{z}, n$  being constants in Anand's model.  $R$  is the gas constant originally Boltzman's constant was used but this introduces Avogadro's number as a factor leading to constants which are very large. The Mises norm of stress is defined by

$$\|\mathbf{S}\|_M = \sqrt{3/2(\mathbf{S} : \mathbf{S})}^{\frac{1}{2}} \quad (3.9)$$

The residual functions for the simultaneous solution of the time integrated equations are given by

$$\mathbf{F}(\mathbf{S}, z_1) = \mathbf{S} - \mathbf{S}^* + 3\Delta t \mu \dot{\epsilon}^p \frac{\mathbf{S}}{\|\mathbf{S}\|_M} \quad (3.10)$$

and

$$G_1(\mathbf{S}, z_1) = z_1^{n+1} - z_1^n - \Delta t \dot{z}_1 \quad (3.11)$$

The Newton-Raphson method coupled with a Gauss elimination scheme with partial pivoting is used to solve residual equations and find  $\mathbf{S}, z_1$  simultaneously :

$$\hat{\mathbf{A}} (\mathbf{x}^{n+1} - \mathbf{x}^n) = -\mathbf{b} \quad (3.12)$$

$$\mathbf{x}^{n+1} = \begin{pmatrix} \mathbf{S} \\ z_1 \end{pmatrix}^{n+1}, \quad \mathbf{x}^n = \begin{pmatrix} \mathbf{S} \\ z_1 \end{pmatrix}^n, \quad \mathbf{b} = \begin{pmatrix} \mathbf{F} \\ G_1 \end{pmatrix}^n \quad (3.13)$$

$$\hat{\mathbf{A}} = \left[ \begin{array}{c|c} \frac{\partial \mathbf{F}}{\partial \mathbf{S}} & \frac{\partial \mathbf{F}}{\partial z_1} \\ \hline \frac{\partial G_1}{\partial \mathbf{S}} & \frac{\partial G_1}{\partial z_1} \end{array} \right] \quad (3.14)$$

Iteration proceeds by solving for  $(\mathbf{x}^{n+1} - \mathbf{x}^n)$  in Eq.(3.12) and updating the solution until the residual functions are approximately equal to zero within specified tolerances.

### 3.2.2 Derivatives for Internal Newton-Raphson Scheme

The N-R procedure for finding  $\mathbf{S}, z_1$  i.e. the solutions of residual equations requires the derivatives of the residual functions  $\mathbf{F}$  and  $G_1$  to be explicitly defined. The derivatives of the residual function  $\mathbf{F}(\mathbf{S}, z_1)$  is given by

$$\frac{\partial \mathbf{F}}{\partial \mathbf{S}} = \hat{\mathbf{I}} + 3\mu \Delta t \frac{\partial}{\partial \mathbf{S}} \left( \dot{\epsilon}^p \frac{\mathbf{S}}{\|\mathbf{S}\|_M} \right) \quad (3.15)$$

and

$$\begin{aligned}\frac{\partial}{\partial \mathbf{S}} \left( \dot{\varepsilon}^p \frac{\mathbf{S}}{\|\mathbf{S}\|_M} \right) &= \frac{\partial \dot{\varepsilon}^p}{\partial \mathbf{S}} \otimes \frac{\mathbf{S}}{\|\mathbf{S}\|_M} + \dot{\varepsilon}^p \frac{\partial}{\partial \mathbf{S}} \left( \frac{\mathbf{S}}{\|\mathbf{S}\|_M} \right) \\ &= \frac{\partial \dot{\varepsilon}^p}{\partial \mathbf{S}} \otimes \frac{\mathbf{S}}{\|\mathbf{S}\|_M} + \dot{\varepsilon}^p \left[ \frac{\hat{\mathbf{I}}}{\|\mathbf{S}\|_M} - \frac{3 \mathbf{S} \otimes \mathbf{S}}{2 \|\mathbf{S}\|_M^3} \right]\end{aligned}\quad (3.16)$$

where the derivative of plastic strain rate with respect to deviatoric stress being given by

$$\begin{aligned}\frac{\partial \dot{\varepsilon}^p}{\partial \mathbf{S}} &= \frac{A}{m} \exp \left( -\frac{Q}{R\theta} \right) \left[ \sinh \left( \frac{\xi \|\mathbf{S}\|_M}{z_1} \right) \right]^{\frac{1}{m}-1} \cosh \left( \frac{\xi \|\mathbf{S}\|_M}{z_1} \right) \frac{\xi}{z_1} \frac{\partial \|\mathbf{S}\|_M}{\partial \mathbf{S}} \\ &= \frac{A}{m} \exp \left( -\frac{Q}{R\theta} \right) \left[ \sinh \left( \frac{\xi \|\mathbf{S}\|_M}{z_1} \right) \right]^{\frac{1}{m}-1} \cosh \left( \frac{\xi \|\mathbf{S}\|_M}{z_1} \right) \frac{\xi}{z_1} \frac{3}{2} \frac{\mathbf{S}}{\|\mathbf{S}\|_M}\end{aligned}\quad (3.17)$$

The derivative of  $\mathbf{F}(\mathbf{S}, z_1)$  with respect to the internal variable is given by

$$\frac{\partial \mathbf{F}}{\partial z_1} = \Delta t 3\mu \frac{\partial \dot{\varepsilon}^p}{\partial z_1} \frac{\mathbf{S}}{\|\mathbf{S}\|_M} \quad (3.18)$$

$$\frac{\partial \dot{\varepsilon}^p}{\partial z_1} = \frac{A}{m} \exp \left( -\frac{Q}{R\theta} \right) \left[ \sinh \left( \frac{\xi \|\mathbf{S}\|_M}{z_1} \right) \right]^{\frac{1}{m}-1} \cosh \left( \frac{\xi \|\mathbf{S}\|_M}{z_1} \right) \left( -\xi \|\mathbf{S}\|_M z_1^{-2} \right) \quad (3.19)$$

The derivatives of the residual function  $G_1(\mathbf{S}, z_1)$  for the internal variable with respect to stress is given by

$$\begin{aligned}\frac{\partial G_1}{\partial \mathbf{S}} &= -\Delta t \left[ h_0 a \left( 1 - \frac{z_1}{z^*} \right)^{a-1} z_1 (z^*)^{-2} \dot{\varepsilon}^p \frac{\partial z^*}{\partial \mathbf{S}} + h_0 \left( 1 - \frac{z_1}{z^*} \right)^a \frac{\partial \dot{\varepsilon}^p}{\partial \mathbf{S}} \right] \quad (z_1 \leq z^*) \\ &= -\Delta t \left[ -h_0 a \left( \frac{z_1}{z^*} - 1 \right)^{a-1} \frac{(-z_1)}{(z^*)^2} \dot{\varepsilon}^p \frac{\partial z^*}{\partial \mathbf{S}} - h_0 \left( \frac{z_1}{z^*} - 1 \right)^a \frac{\partial \dot{\varepsilon}^p}{\partial \mathbf{S}} \right] \quad (z_1 > z^*)\end{aligned}\quad (3.20)$$

and that with respect to the internal variable is defined by

$$\frac{\partial G_1}{\partial z_1} = 1 - \Delta t \frac{\partial \dot{z}_1}{\partial z_1} \quad (3.21)$$

$$\begin{aligned}\frac{\partial \dot{z}_1}{\partial z_1} &= a h_0 \left( 1 - \frac{z_1}{z^*} \right)^{a-1} z_1 (z^*)^{-2} \frac{\partial z^*}{\partial z_1} \dot{\varepsilon}^p + h_0 \left( 1 - \frac{z_1}{z^*} \right)^a \frac{\partial \dot{\varepsilon}^p}{\partial z_1} \quad (z_1 \leq z^*) \\ &= -a h_0 \left( \frac{z_1}{z^*} - 1 \right)^{a-1} z_1 (z^*)^{-2} \frac{\partial z^*}{\partial z_1} \dot{\varepsilon}^p - h_0 \left( \frac{z_1}{z^*} - 1 \right)^a \frac{\partial \dot{\varepsilon}^p}{\partial z_1} \quad (z_1 > z^*)\end{aligned}\quad (3.22)$$

The derivatives of  $z^*$  in respect of  $\mathbf{S}$  and  $z_1$  are as follows:

$$\frac{\partial z^*}{\partial \mathbf{S}} = \frac{\bar{z}n}{A} \exp \left( \frac{Q}{R\theta} \right) \left[ \frac{\dot{\varepsilon}^p}{A} \exp \left( \frac{Q}{R\theta} \right) \right]^{n-1} \frac{\partial \dot{\varepsilon}^p}{\partial \mathbf{S}} \quad (3.23)$$

$$\frac{\partial z^*}{\partial z_1} = \frac{\bar{z}n}{A} \exp \left( \frac{Q}{R\theta} \right) \left[ \frac{\dot{\varepsilon}^p}{A} \exp \left( \frac{Q}{R\theta} \right) \right]^{n-1} \frac{\partial \dot{\varepsilon}^p}{\partial z_1} \quad (3.24)$$

### 3.2.3 Linearization of tangent modulus

The solution of the finite element equation Eq.(2.41) requires the matrix  $\hat{\mathbf{C}}$ , given by Eq.(2.42), for each time increment which has to be found for the equilibrium stress. Such equilibrium stress  $\mathbf{S}$  is determined by the algorithm described in the previous section.

The matrix  $\hat{\mathbf{C}}$  is termed the consistent tangent modulus [28], [59], and is obtained by linearization of the algorithm for evaluation of stress increment for a given strain increment. The residual function for strain is

$$\psi^{n+1} = (\mathbf{L}_{n+1} - \mathbf{L}_n) - \frac{1}{3\kappa} \text{tr} \Delta \mathbf{T}_{n+1} \mathbf{1} - \frac{1}{2\mu} (\mathbf{S}_{n+1} - \mathbf{S}_n) - \frac{3}{2} \Delta t \dot{\epsilon}^p \frac{\mathbf{S}}{\|\mathbf{S}\|_M} \quad (3.25)$$

The Taylor series expansion of the function  $\psi^{n+1}$  up to linear terms is

$$\psi^{n+1} = \psi^n + \frac{\partial \psi}{\partial \mathbf{L}} : \Delta \mathbf{L} + \frac{\partial \psi}{\partial \mathbf{T}} : \Delta \mathbf{T} \quad (3.26)$$

since  $\psi^n$  and  $\psi^{n+1}$  tend to zero for the final approximation of  $\mathbf{S}_{n+1}$  and  $z_1$  we may write

$$\frac{\partial \psi}{\partial \mathbf{L}} : \Delta \mathbf{L} + \frac{\partial \psi}{\partial \mathbf{T}} : \Delta \mathbf{T} = \mathbf{0} \quad (3.27)$$

Thus the consistently linearised tangent modulus CTM can be obtained from

$$\hat{\mathbf{C}} \equiv \frac{\partial \mathbf{T}}{\partial \mathbf{L}} \approx - \frac{\partial \psi}{\partial \mathbf{T}}^{-1} : \frac{\partial \psi}{\partial \mathbf{L}} \quad (3.28)$$

The general derivation of the CTM applied to Anand's model requires the derivatives of the residual function  $\psi^{n+1}$  defined by Eq.(3.25) with respect to strain  $\mathbf{L}$ ,

$$\frac{\partial \psi}{\partial \mathbf{L}_{n+1}} = \hat{\mathbf{I}} \quad (3.29)$$

and stress,  $\mathbf{T}$ ,

$$\frac{\partial \psi}{\partial \mathbf{T}} = -\frac{1}{3\kappa} \mathbf{1} \otimes \mathbf{1} - \frac{1}{2\mu} \hat{\mathbf{I}}_{dev} - \frac{3}{2} \Delta t \left[ \frac{\partial \dot{\epsilon}^p}{\partial \mathbf{S}_{n+1}} \otimes \frac{\mathbf{S}}{\|\mathbf{S}\|_M} + \dot{\epsilon}^p \left( \frac{\mathbf{I}}{\|\mathbf{S}\|_M} - \frac{3 \mathbf{S} \otimes \mathbf{S}}{2 \|\mathbf{S}\|_M^3} \right) \right] \hat{\mathbf{I}}_{dev} \quad (3.30)$$

Thus the consistent tangent modulus  $\hat{\mathbf{C}}$  for Anand's model is given by

$$\hat{\mathbf{C}} = - \left\{ -\frac{1}{3\kappa} \mathbf{1} \otimes \mathbf{1} - \frac{1}{2\mu} \hat{\mathbf{I}}_{dev} - \frac{3}{2} \Delta t \left[ \frac{\partial \dot{\epsilon}^p}{\partial \mathbf{S}} \otimes \frac{\mathbf{S}}{\|\mathbf{S}\|_M} + \dot{\epsilon}^p \left( \frac{\mathbf{I}}{\|\mathbf{S}\|_M} - \frac{3 \mathbf{S} \otimes \mathbf{S}}{2 \|\mathbf{S}\|_M^3} \right) \right] : \hat{\mathbf{I}}_{dev} \right\}^{-1} \quad (3.31)$$

and derivative  $\frac{\partial \dot{\epsilon}^p}{\partial \mathbf{S}}$  defined by Eq.(3.17).

The correctness of the CTM can be judged by using a pilot program which has the strain increments as input and stress as output. The stress increments calculated by the non-linear UMAT subroutine and that evaluated by the CTM on the basis of the stress state should be approximately the same for any given strain increment. The UMAT algorithm gives the exact estimation of stress whereas multiplying strain increment by the CTM gives the linear approximation to the stress increment. In practice the closeness will also vary according to the dominance of terms associated with elastic and plastic contributions. This allows one to find the source of any errors in the evaluation of the CTM. A similar debugging process is possible for the Newton scheme for the solution of the non-linear equations.

### 3.3 Estrin Model

Estrin proposed two constitutive models, firstly with one internal variable [13] and recently with two internal parameters [14]. The isotropic elastic-viscoplastic constitutive model is microstructure-related and contains one internal or structure parameter related to the total dislocation density. Microstructural features, such as grain size or spacing of unshearable second-phase particle effects are incorporated in the constitutive equations. A significant feature of the one-parameter model is a distinction between the flow kinetics and the structure evolution kinetics. The flow kinetics represents the material response to mechanical loading at a fixed structure and is governed by dislocation glide only. The structure evolution kinetics is given by an evolution equation for the total dislocation density which rate of variation is related to the shear strain and depends on the current structural state. The one-internal variable model is not flexible enough to account for rapid changes of deformation paths when a finer differentiation between the dislocation types is desirable e.g. in cyclic deformation cases. Thus two internal variables related to the mobile and the relatively immobile, forest dislocation density have been proposed. The proposed evolution equations for two internal variables account for dislocation multiplication and annihilation processes.

#### 3.3.1 Equations for Material with Two Variables

The Estrin constitutive equation [13] originally determines the plastic strain as a function of the uniaxial stress which may be generalized using Mises equivalent stress in keeping with the assumption that plasticity is a function only of the deviatoric component of stress as the same has been done for metals in a frame of the  $J_2$  type plasticity theory,

$$\dot{\epsilon}^p = \xi \left( \frac{\|\mathbf{S}\|_M}{\sigma_0} \right)^m z_1 z_2^{-\frac{m}{2}} \quad (3.32)$$

The evolution equations for the two internal variables  $z_1, z_2$  which represent non-dimensional dislocation densities [14] are given by

$$\dot{z}_1 = \left( -C - C_1 z_2^{-\frac{1}{2}} - C_3 z_1 + C_4 \frac{z_2}{z_1} \right) q \dot{\epsilon}^p \quad (3.33)$$

$$\dot{z}_2 = \left( C + C_1 z_2^{\frac{1}{2}} - C_2 z_2 + C_3 z_1 \right) \dot{\epsilon}^p \quad (3.34)$$

where  $C_1, C_2, C_3, C_4, \xi, \sigma_0, q, m, n$  are constants in the model and

$$C_2 = C_{20} \left( \frac{\dot{\epsilon}^p}{\dot{\epsilon}_0} \right)^{-\frac{1}{n}} \quad (3.35)$$

with  $\dot{\epsilon}_0$  assumed constant.

### 3.3.2 Time Integration Procedure for Constitutive Equations

The deviatoric stress tensor  $\mathbf{S}$  and the two internal variables  $z_1, z_2$  of the Estrin's model are determined by means of Newton-Raphson scheme applied to the following system of residual functions

$$\mathbf{F}(\mathbf{S}, z_1, z_2) = \mathbf{S} - \mathbf{S}^* + 2\mu\Delta t\dot{\mathbf{E}}^p = \mathbf{S} - \mathbf{S}^* + 3\mu\Delta t\dot{\varepsilon}^p \frac{\mathbf{S}}{\|\mathbf{S}\|_M} \quad (3.36)$$

$$G_1(\mathbf{S}, z_1, z_2) = z_1^{n+1} - z_1^n - \Delta t\dot{z}_1 \quad (3.37)$$

$$G_2(\mathbf{S}, z_1, z_2) = z_2^{n+1} - z_2^n - \Delta t\dot{z}_2 \quad (3.38)$$

where the shear modulus is  $\mu$ . The last term of the residual Eq.(3.36)

$$\frac{3}{2}\dot{\varepsilon}^p \frac{\mathbf{S}}{\|\mathbf{S}\|_M} = \dot{\mathbf{E}}^p \quad (3.39)$$

is derived from the Levy-Mises flow law. The following system has been solved by the same procedure as applied previously to the Anand's model

$$\hat{\mathbf{A}} (\mathbf{x}^{n+1} - \mathbf{x}^n) = -\mathbf{b} \quad (3.40)$$

where the vectors and the matrix is given by

$$\mathbf{x}^{n+1} = \begin{pmatrix} \mathbf{S} \\ z_1 \\ z_2 \end{pmatrix}^{n+1}, \quad \mathbf{b} = \begin{pmatrix} \mathbf{F} \\ G_1 \\ G_2 \end{pmatrix}^n \quad (3.41)$$

$$\hat{\mathbf{A}} = \begin{bmatrix} \frac{\partial \mathbf{F}}{\partial \mathbf{S}} & \frac{\partial \mathbf{F}}{\partial z_1} & \frac{\partial \mathbf{F}}{\partial z_2} \\ \frac{\partial G_1}{\partial \mathbf{S}} & \frac{\partial G_1}{\partial z_1} & \frac{\partial G_1}{\partial z_2} \\ \frac{\partial G_2}{\partial \mathbf{S}} & \frac{\partial G_2}{\partial z_1} & \frac{\partial G_2}{\partial z_2} \end{bmatrix} \quad (3.42)$$

### 3.3.3 Derivatives for Newton-Raphson Method

Derivatives of residual functions  $\mathbf{F}, G_1, G_2$  which form the matrix  $\hat{\mathbf{A}}$  are necessary for Newton-Raphson methods, and they are defined in this section.

The derivatives in the first row are the following:

$$\frac{\partial \mathbf{F}}{\partial \mathbf{S}} = \hat{\mathbf{I}} + \Delta t 2\mu \frac{\partial \dot{\mathbf{E}}^p}{\partial \mathbf{S}} \quad (3.43)$$

$$\frac{\partial \mathbf{F}}{\partial z_1} = 3\mu\Delta t \frac{\partial \dot{\epsilon}^p}{\partial z_1} \frac{\mathbf{S}}{\|\mathbf{S}\|_M} \quad , \quad \frac{\partial \mathbf{F}}{\partial z_2} = 3\mu\Delta t \frac{\partial \dot{\epsilon}^p}{\partial z_2} \frac{\mathbf{S}}{\|\mathbf{S}\|_M} \quad (3.44)$$

Where the tensor derivative is

$$\frac{\partial \dot{\mathbf{E}}^p}{\partial \mathbf{S}} = \frac{3}{2} \left[ \frac{\partial \dot{\epsilon}^p}{\partial \mathbf{S}} \otimes \frac{\mathbf{S}}{\|\mathbf{S}\|_M} + \dot{\epsilon}^p \frac{\partial}{\partial \mathbf{S}} \frac{\mathbf{S}}{\|\mathbf{S}\|_M} \right] \quad (3.45)$$

with the derivative of the plastic strain rate for Estrin's model with respect to  $\mathbf{S}$  given by

$$\frac{\partial \dot{\epsilon}^p}{\partial \mathbf{S}} = \frac{\xi m}{\sigma_0} \left( \frac{\|\mathbf{S}\|_M}{\sigma_0} \right)^{m-1} \frac{3}{2} \frac{\mathbf{S}}{\|\mathbf{S}\|_M} z_1 z_2^{-\frac{m}{2}} \quad (3.46)$$

The scalar derivatives required in Eq.(3.44) are

$$\frac{\partial \dot{\epsilon}^p}{\partial z_1} = \xi \left( \frac{\|\mathbf{S}\|_M}{\sigma_0} \right)^m z_2^{-\frac{m}{2}} \quad (3.47)$$

$$\frac{\partial \dot{\epsilon}^p}{\partial z_2} = \xi \left( \frac{\|\mathbf{S}\|_M}{\sigma_0} \right)^m z_1 \left( \frac{-m}{2} \right) z_2^{-\frac{m}{2}-1} \quad (3.48)$$

The derivatives of the internal variables in respect of stress are

$$\frac{\partial \dot{z}_1}{\partial \mathbf{S}} = \left( -C - C_1 z_2^{-\frac{1}{2}} - C_3 z_1 + C_4 \frac{z_2}{z_1} \right) q \frac{\partial \dot{\epsilon}^p}{\partial \mathbf{S}} \quad (3.49)$$

$$\frac{\partial \dot{z}_2}{\partial \mathbf{S}} = \left( C + C_1 z_2^{\frac{1}{2}} - C_2 z_2 + C_3 z_1 \right) \frac{\partial \dot{\epsilon}^p}{\partial \mathbf{S}} + \left( -\frac{\partial C_2}{\partial \mathbf{S}} z_2 \right) \dot{\epsilon}^p \quad (3.50)$$

The derivative of Estrin's model function  $C_2$  which is dependent on strain rate is

$$\frac{\partial C_2}{\partial \mathbf{S}} = -\frac{1}{n} C_{20} \left( \frac{\dot{\epsilon}^p}{\dot{\epsilon}_0} \right)^{-\frac{1}{n}-1} \frac{1}{\dot{\epsilon}_0} \frac{\partial \dot{\epsilon}^p}{\partial \mathbf{S}} \quad (3.51)$$

The derivatives of the scalar residual functions  $G_1$  and  $G_2$  with respect to the internal variables are

$$\frac{\partial G_1}{\partial z_1} = 1 - \Delta t \frac{\partial \dot{z}_1}{\partial z_1} \quad , \quad \frac{\partial G_1}{\partial z_2} = -\Delta t \frac{\partial \dot{z}_1}{\partial z_2} \quad (3.52)$$

and

$$\frac{\partial G_2}{\partial z_1} = -\Delta t \frac{\partial \dot{z}_2}{\partial z_1} \quad , \quad \frac{\partial G_2}{\partial z_2} = 1 - \Delta t \frac{\partial \dot{z}_2}{\partial z_2} \quad (3.53)$$

where derivatives of rates of internal variables are

$$\frac{\partial \dot{z}_1}{\partial z_1} = \left( -C_3 - C_4 z_2 z_1^{-2} \right) q \dot{\epsilon}^p + \left( -C - C_1 z_2^{-\frac{1}{2}} - C_3 z_1 + C_4 \frac{z_2}{z_1} \right) q \frac{\partial \dot{\epsilon}^p}{\partial z_1} \quad (3.54)$$

$$\frac{\partial \dot{z}_1}{\partial z_2} = \left( \frac{1}{2} C_1 z_2^{-\frac{3}{2}} + \frac{C_4}{z_1} \right) q \dot{\epsilon}^p + \left( -C - C_1 z_2^{-\frac{1}{2}} - C_3 z_1 + C_4 \frac{z_2}{z_1} \right) q \frac{\partial \dot{\epsilon}^p}{\partial z_2} \quad (3.55)$$

$$\frac{\partial \dot{z}_2}{\partial z_1} = C_3 \dot{\epsilon}^p + \left( C + C_1 z_2^{\frac{1}{2}} - C_2 z_2 + C_3 z_1 \right) \frac{\partial \dot{\epsilon}^p}{\partial z_1} \quad (3.56)$$

$$\frac{\partial \dot{z}_2}{\partial z_2} = \left( \frac{1}{2} C_1 z_2^{-\frac{1}{2}} - C_2 \right) \dot{\epsilon}^p + \left( C + C_1 z_2^{\frac{1}{2}} - C_2 z_2 + C_3 z_1 \right) \frac{\partial \dot{\epsilon}^p}{\partial z_2} \quad (3.57)$$

### 3.3.4 Consistent Tangent Modulus for Estrin's Model

As for Anand's model we derive an expression for the consistent tangent modulus which is the contribution of Estrin's model to the global stiffness matrix. The expression is derived from the same residual function as the one used previously.

$$\Psi \equiv \underbrace{(\mathbf{L}_{n+1} - \mathbf{L}_n)}_{\Delta \text{total strain}} - \underbrace{\frac{1}{2\mu}(\mathbf{S}_{n+1} - \mathbf{S}_n)}_{\Delta \text{elastic-deviatoric}} - \underbrace{\frac{1}{3\kappa} \text{tr} \Delta \mathbf{T} \mathbf{1}}_{\Delta \text{compression}} - \underbrace{\Delta t \dot{\mathbf{E}}^p}_{\Delta \text{inelastic}} = 0 \quad (3.58)$$

The inelastic contribution in Eq.(3.58) here refers to the internal variable for viscoplastic strain in Estrin's model. The CTM is thus given by

$$\hat{\mathbf{C}} = - \left\{ -\frac{1}{3\kappa} \mathbf{1} \otimes \mathbf{1} - \frac{1}{2\mu} \hat{\mathbf{I}}_{dev} - \frac{3}{2} \Delta t \left[ \frac{\partial \dot{\mathbf{E}}^p}{\partial \mathbf{S}} \otimes \frac{\mathbf{S}}{\|\mathbf{S}\|_M} + \dot{\mathbf{E}}^p \left( \frac{\mathbf{I}}{\|\mathbf{S}\|_M} - \frac{3 \mathbf{S} \otimes \mathbf{S}}{2 \|\mathbf{S}\|_M^3} \right) \right] : \hat{\mathbf{I}}_{dev} \right\}^{-1} \quad (3.59)$$

and derivative  $\frac{\partial \dot{\mathbf{E}}^p}{\partial \mathbf{S}}$  is defined by equation Eq.(3.46).

## 3.4 Contribution of Thermal Coupling due to Plastic Deformation

A fully coupled temperature-displacement analysis requires not only the consideration of the coupling between temperature and displacement via the thermal strains considered in the previous sections, but also the other direction of coupling where the temperature is affected by displacement via the dissipation of inelastic energy. The terms resulting from this coupling are considered in this section. The non-linear solution process, utilizing the Newton-Raphson method to solve the systems of finite element equations, also requires the consideration of contributions of the aforementioned terms to the stiffness matrix.

During plastic deformation a portion of the energy is dissipated as heat. The rate of heat generated due to the dissipation of plastic strain energy is given by

$$\dot{F}_\theta^p = f_{IH} (\mathbf{T} : \dot{\mathbf{E}}^p) \quad (3.60)$$

$f_{IH}$  is the fraction of plastic strain energy converted to heat.

The required contributions to the stiffness matrix are:  $\frac{\partial F_\theta^p}{\partial \mathbf{L}}$  and  $\frac{\partial F_\theta^p}{\partial \theta}$

$$\frac{\partial F_\theta^p}{\partial \mathbf{L}} = f_{IH} \left( \frac{\partial \mathbf{T}}{\partial \mathbf{L}} : \dot{\mathbf{E}}^p + \frac{\partial \dot{\mathbf{E}}^p}{\partial \mathbf{L}} : \mathbf{T} \right) \quad (3.61)$$

with  $\dot{\mathbf{E}}^p$  given by

$$\dot{\mathbf{E}}^p \equiv \frac{3}{2} f(\|\mathbf{S}\|_M, z_1, \dots, z_k) \frac{\mathbf{S}}{\|\mathbf{S}\|_M}$$

for the class of viscoplastic model dealt with in this chapter and which simplifies to

$$\frac{\partial F_{\theta}^p}{\partial \mathbf{L}} = f_{IH} (\hat{\mathbf{C}} : \dot{\mathbf{E}}^p) \quad (3.62)$$

The additional derivative contribution is given by

$$\frac{\partial F_{\theta}^p}{\partial \theta} = f_{IH} \left( \frac{\partial \mathbf{T}}{\partial \theta} : \dot{\mathbf{E}}^p + \frac{\partial \dot{\mathbf{E}}^p}{\partial \theta} : \mathbf{T} \right) \quad (3.63)$$

$$\frac{\partial \Delta \mathbf{T}}{\partial \Delta \theta} \approx - \left\{ \left[ \frac{\partial \psi}{\partial \mathbf{T}} \right]_{n+1}^{(i)} \right\}^{-1} : \left[ \frac{\partial \psi}{\partial \theta} \right]_{n+1}^{(i)} \quad (3.64)$$

with

$$\frac{\partial \psi}{\partial \theta} = - \frac{\partial}{\partial \theta} \left( \frac{1}{3\kappa} \right) \text{tr} \Delta \mathbf{T} \mathbf{1} - \frac{\partial}{\partial \theta} \left( \frac{1}{2\mu} \right) [\mathbf{S}_{n+1} - \mathbf{S}_n] - \Delta t \frac{\partial \dot{\mathbf{E}}^p}{\partial \theta} \quad (3.65)$$

we require the derivatives, with respect to temperature, of the Lamé parameters, which depend on the thermal interpolation functions used for the material constants, and of the derivative of the plastic strain rate,  $\dot{\mathbf{E}}^p$ . This derivative is given, for the models considered here, by

$$\frac{\partial \dot{\mathbf{E}}^p}{\partial \theta} = \frac{3}{2} \frac{\mathbf{S}}{\|\mathbf{S}\|_{\mathbf{M}}} \frac{\partial}{\partial \theta} f(s, z_1, \dots, z_k, \theta) \quad (3.66)$$

The scalar function  $f(\dots)$  for the strain rate varies for each model and moreover depends on material constants used in these models. These may or may not be considered as functions of temperature under certain circumstances. The derivative varies accordingly but is straightforward to compute once the specific forms are fixed in terms of thermal dependence. For example for, for the material constant used for Estrin's model in this paper the derivative of this function is zero but is non-zero in the general formulation for this model.

# Chapter 4

## Potential Viscoplastic Models

### 4.1 Robinson's Model

Robinson's model is based on the concept of flow potential. The flow and evolution of internal variables are derived from this flow potential. The material behaviour is elastic for all the stress states within the yield surface, and it is viscoplastic for all the stress states outside the yield surface. The total strain rate is written as the sum of elastic and inelastic components. The material is assumed to be isotropic and Hookean for evaluation of elastic strain rate. The evolution law of internal state variables is based on the Bailey-Orowan theory which states that the high temperature deformation of materials takes place under influence of two competing mechanisms i.e. hardening process associated with accumulated deformation and recovery or softening process proceeding with time. These two mechanisms balance each other in steady-state conditions.

#### 4.1.1 Constitutive Equations

The constitutive equation for the plastic strain rate is a flow law of the following form:

$$\dot{\mathbf{E}}^p = \begin{cases} \frac{1}{2\bar{\mu}} f(\Upsilon) \boldsymbol{\Sigma} & \Upsilon > 0 \text{ and } \mathbf{S} : \boldsymbol{\Sigma} > 0 \\ 0 & \Upsilon \leq 0 \text{ or } \Upsilon > 0 \text{ and } \mathbf{S} : \boldsymbol{\Sigma} \leq 0 \end{cases} \quad (4.1)$$

where effective stress is  $\boldsymbol{\Sigma} = \mathbf{S} - \mathbf{Z}$ ,  $\mathbf{S}$  is the deviatoric stress and  $\mathbf{Z}$  is the tensor of internal state variable. The scalar flow function is given by

$$f(\Upsilon) = \frac{(\Upsilon)^n}{(J_2)^{\frac{1}{2}}} \quad (4.2)$$

The specific form of  $\Upsilon$  is

$$\Upsilon = \frac{J_2}{K_R^2} - 1 \quad (4.3)$$

1. *Begin*
2. *Form Deviatoric Strain Increment :*  $\Delta \mathbf{E} = \Delta \mathbf{L} - \frac{1}{3} \text{tr} \Delta \mathbf{L}$
3. *Calculate Elastic Predictor:*  ${}^* \mathbf{S}^{n+1} = \mathbf{S}^n + 2\mu \Delta \mathbf{E}^{n+1}$
4. *Initialize:*  $\mathbf{S}^{n+1} = {}^* \mathbf{S}^{n+1}, \mathbf{Z}^{n+1} = \mathbf{Z}^n$
5. *Form residual functions:*  
 $\mathbf{F}(\mathbf{S}, \mathbf{Z}) = \mathbf{S}^{n+1} - {}^* \mathbf{S}^{n+1} + 2\mu \Delta t \mathbf{f}(\mathbf{S}, \mathbf{Z})$   
 $\mathbf{G}(\mathbf{S}, \mathbf{Z}) = \mathbf{Z}^{n+1} - \mathbf{Z}^n - \Delta t \mathbf{g}(\mathbf{S}, \mathbf{Z})$
6. *Solve residual equations in 5. for  $\mathbf{S}^{n+1}$  and  $\mathbf{Z}^{n+1}$  by N-R*
7. *Update solution*
8. *Check For Convergence:*  
 IF  $\mathbf{F}(\mathbf{S}, \mathbf{Z}) > \text{TOL}$   
 OR  $\mathbf{G}(\mathbf{S}, \mathbf{Z}) > \text{TOL}$   
 THEN goto 7
9. *Update total stress tensor*  
 $\mathbf{T}^{n+1} = \mathbf{S}^{n+1} + \frac{1}{3} \mathbf{1} \text{tr } {}^* \mathbf{T}^{n+1}$
10. *Update  $\hat{\mathbf{C}} \equiv \frac{\partial \mathbf{T}}{\partial \mathbf{L}}$  for contribution to global stiffness matrix*
11. *End*

Figure 4.1: Unified viscoplastic model for multiaxial loading

The evolution of the internal variable is governed by an equation which accounts for two competing phenomena i.e. hardening,  $h(\mathbf{Z})$  and recovery or softening  $r(\mathbf{Z})$ .

$$\dot{\mathbf{Z}} = h(\mathbf{Z}) \dot{\mathbf{E}}^p - r(\mathbf{Z}) \mathbf{Z} \quad (4.4)$$

Where hardening is determined by the equation

$$h(\mathbf{Z}) = \begin{cases} \frac{2\mu_R H_R}{G_R^\beta} & \text{if } G_R > G_0 \text{ and } \mathbf{S} : \mathbf{Z} > 0 \\ \frac{2\mu_R H_R}{G_0^\beta} & \text{if } G_R \leq G_0 \text{ or } \mathbf{S} : \mathbf{Z} \leq 0 \end{cases} \quad (4.5)$$

The softening or recovery function is defined by

$$r(\mathbf{Z}) = \begin{cases} R G_R^{m-\beta} & \text{if } G_R > G_0 \text{ and } \mathbf{S} : \mathbf{Z} > 0 \\ R G_0^{m-\beta} & \text{if } G_R \leq G_0 \text{ or } \mathbf{S} : \mathbf{Z} \leq 0 \end{cases} \quad (4.6)$$

where the criterial number  $G_R$  is given by

$$G_R = \frac{\mathbf{Z} : \mathbf{Z}}{2K_R^2}$$

Effects of temperature are incorporated in the Robinson's model through the temperature-dependent constants  $\bar{\mu}$  and  $R$  using the following relations:

$$\bar{\mu} = \mu_R \exp(-\theta_1) ,$$

$$\theta_1 = (23.8\theta - 2635) \left( \frac{1}{811} - \frac{1}{\theta} \right)$$

$$R = 9.0 \times 10^{-8} \exp(\theta_2) \text{ and}$$

$$\theta_2 = 4 \times 10^4 \left( \frac{1}{811} - \frac{1}{\theta} \right)$$

The parameters  $\beta$ ,  $G_0$ ,  $H$ ,  $K_R$ ,  $m$ ,  $\mu_R$  and  $n$  are temperature independent constants. The only material parameters available in the literature are applicable for 2.25  $C_r$ -1 *Mo* steel. The scalar state variable  $K_R$  denotes the scalar Bingham stress or threshold stress. As soon as the second invariant of stress state  $J_2$  goes below  $K_R$ , the inelastic strain rate vanishes. The inequalities in the above equations define boundaries across which the growth and flow laws change form discontinuously.

### 4.1.2 Residual Equations for Robinson's Model

The residual equations used for evaluation of the stress and internal variable tensors are given by:

$$\mathbf{F} = \mathbf{S}^{n+1} - \mathbf{S}^* + 2\mu\Delta t \frac{1}{\bar{\mu}} \mathbf{f}(\mathbf{S}, \mathbf{Z}) \quad (4.7)$$

$$\mathbf{G} = \mathbf{Z}^{n+1} - \mathbf{Z}^n - \Delta t \mathbf{g}(\mathbf{S}, \mathbf{Z}) \quad (4.8)$$

where  $\mathbf{S}^*$  is the stress predicted for the Hookean elastic material, and functions  $\mathbf{f}(\mathbf{S}, \mathbf{Z})$ , and  $\mathbf{g}(\mathbf{S}, \mathbf{Z})$  are defined as the following:

$$\mathbf{f}(\mathbf{S}, \mathbf{Z}) = \frac{1}{2\bar{\mu}} \Upsilon \mathbf{n} \quad (4.9)$$

$$\mathbf{g}(\mathbf{S}, \mathbf{Z}) = h(\mathbf{Z})\mathbf{f}(\mathbf{S}, \mathbf{Z}) - r(\mathbf{Z})\mathbf{Z} \quad (4.10)$$

### 4.1.3 Derivatives for Internal Newton-Raphson Method

Derivatives of residual functions  $\mathbf{F}$  and  $\mathbf{G}$ , which are necessary for Newton-Raphson method, are derived in this section. Derivatives of  $\mathbf{F}$  and  $\mathbf{G}$  in respect of the deviatoric stress  $\mathbf{S}$  and internal state variable tensor  $\mathbf{Z}$  are the following:

$$\frac{\partial \mathbf{F}}{\partial \mathbf{S}} = \hat{\mathbf{I}} + 2\frac{\mu}{\bar{\mu}} \Delta t \frac{\partial \mathbf{f}(\mathbf{S}, \mathbf{Z})}{\partial \mathbf{S}} \quad (4.11)$$

$$\frac{\partial \mathbf{F}}{\partial \mathbf{Z}} = 2\frac{\mu}{\bar{\mu}} \Delta t \frac{\partial \mathbf{f}(\mathbf{S}, \mathbf{Z})}{\partial \mathbf{Z}} \quad (4.12)$$

$$\frac{\partial \mathbf{G}}{\partial \mathbf{S}} = -\Delta t \frac{\partial \mathbf{g}(\mathbf{S}, \mathbf{Z})}{\partial \mathbf{S}} \quad (4.13)$$

$$\frac{\partial \mathbf{G}}{\partial \mathbf{Z}} = \hat{\mathbf{I}} - \Delta t \frac{\partial \mathbf{g}(\mathbf{S}, \mathbf{Z})}{\partial \mathbf{Z}} \quad (4.14)$$

Internal derivatives of the function  $\mathbf{f}(\mathbf{S}, \mathbf{Z})$  are given by

$$\frac{\partial \mathbf{f}(\mathbf{S}, \mathbf{Z})}{\partial \mathbf{S}} = \frac{1}{2\bar{\mu}} \left[ \bar{F} \frac{\partial \mathbf{n}}{\partial \mathbf{S}} + \frac{\partial \bar{F}}{\partial \mathbf{S}} \otimes \mathbf{n} \right] \quad (4.15)$$

$$\frac{\partial \mathbf{f}}{\partial \mathbf{Z}} = -\frac{\partial \mathbf{f}}{\partial \mathbf{S}} \quad (4.16)$$

where

$$\frac{\partial \bar{F}}{\partial \mathbf{S}} = (0.5)^{-\frac{1}{2}n} \left( \frac{J_2}{K_R^2} - 1 \right)^{n-1} \frac{1}{K_R^2} \boldsymbol{\Sigma} \quad (4.17)$$

$$\frac{\partial \mathbf{n}}{\partial \mathbf{S}} = \frac{1}{\|\boldsymbol{\Sigma}\|} \left( \hat{\mathbf{I}} - \frac{\boldsymbol{\Sigma} \otimes \boldsymbol{\Sigma}}{\|\boldsymbol{\Sigma}\|^2} \right) \quad (4.18)$$

Internal derivatives of the function  $\mathbf{g}(\mathbf{S}, \mathbf{Z})$  are given by

$$\frac{\partial \mathbf{g}}{\partial \mathbf{S}} = h(\mathbf{Z}) \frac{\partial \mathbf{f}}{\partial \mathbf{S}} \quad (4.19)$$

$$\frac{\partial \mathbf{g}}{\partial \mathbf{Z}} = \left[ h(\mathbf{Z}) \frac{\partial \mathbf{f}(\mathbf{S}, \mathbf{Z})}{\partial \mathbf{Z}} + \frac{\partial h(\mathbf{Z})}{\partial \mathbf{Z}} \otimes \mathbf{f}(\mathbf{S}, \mathbf{Z}) \right] - \left[ r(\mathbf{Z}) \frac{\partial \mathbf{Z}}{\partial \mathbf{Z}} + \frac{\partial r(\mathbf{Z})}{\partial \mathbf{Z}} \otimes \mathbf{Z} \right] \quad (4.20)$$

where

$$\frac{\partial h}{\partial \mathbf{Z}} = -\mu_R H \beta G_r^{-\beta-1} \frac{1}{K_R} I_2^{-\frac{1}{2}} \mathbf{Z} \quad (4.21)$$

$$\frac{\partial r}{\partial \mathbf{Z}} = R \left[ -\frac{1}{2} G_r^{m-\beta} I_2^{-\frac{3}{2}} \mathbf{Z} + \frac{1}{2} (m - \beta) G_r^{m-\beta-1} I_2^{-1} \frac{1}{K_R} \mathbf{Z} \right] \quad (4.22)$$

and

$$\frac{\partial \mathbf{Z}}{\partial \mathbf{Z}} = \hat{\mathbf{I}}$$

## 4.2 Contribution of Robinson's Model in FE Stiffness

The contribution of the Robinson constitutive equation to the Finite Element stiffness matrix is defined as the derivative of the total stress increment  $\Delta \mathbf{T}$  in respect to an increment of the linear component the Green-Lagrange strain  $\Delta \mathbf{L}$ . The derivation of this contribution is based on a definition of a residual function for a strain increment and its Taylor series expansion. The strain increment residual function consisting of terms representing total, elastic-deviatoric, compression and inelastic strains is defined by

$$\Psi \equiv \underbrace{(\mathbf{L}_{n+1} - \mathbf{L}_n)}_{\Delta \text{total strain}} - \underbrace{\frac{1}{2\mu}(\mathbf{S}_{n+1} - \mathbf{S}_n)}_{\Delta \text{elastic-deviatoric}} - \underbrace{\frac{1}{3\kappa} \text{tr} \Delta \mathbf{T} \mathbf{1}}_{\Delta \text{compression}} - \underbrace{\Delta t \dot{\mathbf{E}}^p}_{\Delta \text{inelastic}} = 0 \quad (4.23)$$

where  $\Delta \text{compression}$  means the spherical part of the elastic strain increment.

The Taylor series expansion of the residual function Eq.(4.23) at time  $n + 1$  upto first order terms is

$$\Psi_{n+1}^{(i+1)} = \Psi_{n+1}^{(i)} + \left[ \frac{\partial \Psi}{\partial \mathbf{T}} : \Delta \mathbf{T} \right]_{n+1}^{(i)} + \left[ \frac{\partial \Psi}{\partial \mathbf{L}} : \Delta \mathbf{L} \right]_{n+1}^{(i)} \quad (4.24)$$

where the superscript  $(i)$  means an iteration number and the subscript  $n + 1$  refers to the time step. The terms  $\Psi_{n+1}^{(i+1)}$  and  $\Psi_{n+1}^{(i)}$  tend to zero at the end of the iteration in the solution of the constitutive equations so that the contribution of the Robinson constitutive equation to the Finite Element stiffness matrix is given by

$$\frac{\partial \Delta \mathbf{T}}{\partial \Delta \mathbf{L}} \approx - \left\{ \left[ \frac{\partial \Psi}{\partial \mathbf{T}} \right]_{n+1}^{(i)} \right\}^{-1} : \left[ \frac{\partial \Psi}{\partial \mathbf{L}} \right]_{n+1}^{(i)} \quad (4.25)$$

Substituting expressions for derivatives of the residual strain function  $\Psi$

$$\frac{\partial \Psi}{\partial \mathbf{L}} = \hat{\mathbf{I}} \quad (4.26)$$

$$\frac{\partial \Psi}{\partial \mathbf{T}} = -\frac{1}{2\mu} \hat{\mathbf{I}}_{dev} - \frac{1}{3\kappa} \mathbf{1} \otimes \mathbf{1} - \Delta t \frac{\partial \dot{\mathbf{E}}^p}{\partial \mathbf{S}} : \hat{\mathbf{I}}_{dev} \quad (4.27)$$

into Eq.(4.25) leads to the final form of the Robinson model contribution to FE stiffness

$$\frac{\partial \Delta \mathbf{T}}{\partial \Delta \mathbf{L}} \approx - \left[ -\frac{1}{2\mu} \hat{\mathbf{I}}_{dev} - \frac{1}{3\kappa} \mathbf{1} \otimes \mathbf{1} - \Delta t \frac{\partial \dot{\mathbf{E}}^p}{\partial \mathbf{S}} : \hat{\mathbf{I}}_{dev} \right]^{-1} \quad (4.28)$$

with

$$\frac{\partial \dot{\mathbf{E}}^p}{\partial \mathbf{S}} = \frac{\partial \mathbf{f}(\mathbf{S}, \mathbf{Z})}{\partial \mathbf{S}}$$

being given by Eq.(4.15).

### 4.3 Thermal Coupling Contributions

Full thermal coupling is implemented with the heat generation due to the dissipation of plastic strain energy being defined by

$$\dot{F}_\theta^p = 0.9 (\mathbf{T} : \dot{\mathbf{E}}^p) \quad (4.29)$$

where  $\dot{F}_\theta^p$  is the rate at which heat is generated per unit volume and 0.9 is the fraction of plastic strain energy converted to heat. The plastic strain rate term can be obtained directly from each viscoplastic model where it is implicitly the primary internal variable or internal variable tensor as in this model.

This term gives rise to a contribution to the tangent moduli terms associated with the full coupled thermo-mechanical process. In order to form this term ABAQUS inputs the derivative terms:  $\frac{\partial F_\theta^p}{\partial \mathbf{L}}$ ,  $\frac{\partial F_\theta^p}{\partial \theta}$  in the UMAT subroutine.

$$\frac{\partial F_\theta^p}{\partial \mathbf{L}} = 0.9 \left( \frac{\partial \mathbf{T}}{\partial \mathbf{L}} : \dot{\mathbf{E}}^p + \frac{\partial \dot{\mathbf{E}}^p}{\partial \mathbf{L}} : \mathbf{T} \right) \quad (4.30)$$

which simplifies to

$$\frac{\partial F_\theta^p}{\partial \mathbf{L}} = 0.9 (\hat{\mathbf{C}} : \dot{\mathbf{E}}^p) \quad (4.31)$$

The additional derivative contribution is given by

$$\frac{\partial F_\theta^p}{\partial \theta} = 0.9 \left( \frac{\partial \mathbf{T}}{\partial \theta} : \dot{\mathbf{E}}^p + \frac{\partial \dot{\mathbf{E}}^p}{\partial \theta} : \mathbf{T} \right) \quad (4.32)$$

The derivative of stress with respect to temperature used in the preceding equation is also required for the Newton Raphson solution as a contribution in Eq.(2.52). We arrive at this term by again considering the linearization of the Taylor series expansion of the residual function Eq.(4.23) we have.

$$\frac{\partial \Delta \mathbf{T}}{\partial \Delta \theta} \approx - \left\{ \left[ \frac{\partial \Psi}{\partial \mathbf{T}} \right]_{n+1}^{(i)} \right\}^{-1} : \left[ \frac{\partial \Psi}{\partial \theta} \right]_{n+1}^{(i)} \quad (4.33)$$

with

$$\frac{\partial \Psi}{\partial \theta} = -\frac{\partial}{\partial \theta} \left( \frac{1}{3\kappa} \right) \text{tr} \Delta \mathbf{T} \mathbf{1} - \frac{\partial}{\partial \theta} \left( \frac{1}{2\mu} \right) [\mathbf{S}_{n+1} - \mathbf{S}_n] - \Delta t \frac{\partial \dot{\mathbf{E}}^p}{\partial \theta} \quad (4.34)$$

where the derivatives of the lamé parameters  $\mu$ ,  $\kappa$  depend on the interpolation functions used for the temperature dependent data this is described in the results section. The derivative

of the plastic strain rate with respect to temperature is given by

$$\frac{\partial \dot{\mathbf{E}}^p}{\partial \theta} = -\frac{\Upsilon}{2\bar{\mu}^2} \Sigma \mu_R \exp(-\theta_1) (-1) \frac{\partial \theta_1}{\partial \theta} \quad (4.35)$$

where the derivative in the preceding equation is given by

$$\frac{\partial \theta_1}{\partial \theta} = 23.8 \left( \frac{1}{811} - \frac{1}{\theta} \right) + (23.8\theta - 2635) \theta^{-2} \quad (4.36)$$

# Chapter 5

## Transformation Plasticity

The effect of the stress on phase transformation in steel has been investigated both experimentally and theoretically for several years. The stress influences the location of the temperature interval for the final phase transformation from austenite to bainite or martensite. The amount of transformed material is also affected by the stress. The plastic deformation may occur during this transformation at the level of stress which is lower than the yield limits for the phases before transformation. Several researchers have investigated how this additional plastic strain called transformation plasticity phenomenon, affects the development of stresses during the material hardening. Two ways of modelling transformation plasticity have been proposed. The first one consists of a lowering of the yield stress for the temperature interval where phase changes occur. Such model was proposed by Inoue and Wang [27], Wang and Inoue [62]. The second approach is developed on the assumption that the plastic strain rate is proportional to the rate of martensite formation and the stress deviator, and the postulate that an additional plastic strain should be included in the constitutive equation. This type transformation plasticity has been proposed by Raniecki [49], Inoue and Raniecki [26], Fischer [15], and Leblond et al [33], [34]. The Leblond et al model has been chosen for implementation in ABAQUS FE program.

### 5.1 Model of Transformation Plasticity

The transformation plasticity incorporates material phase transformation into calculation of the stress state. The kinematics of phase transformation is determined by the volume fraction of phase denoted by  $z$  which assumes value  $0 \leq z \leq 1$ ,

In the model, proposed by Leblond [33], [35], strain and stress measures are averaged for a volume of an entire finite element.

The total strain-rate is expressed as the sum of the elastic, thermal and plastic strain rates:

$$\dot{\mathbf{E}}^t = \dot{\mathbf{E}}^e + \dot{\mathbf{E}}^{thm} + \dot{\mathbf{E}}^p \quad (5.1)$$

The macro-plastic strain rate  $\dot{\mathbf{E}}^p$  is composed of the transformation strain rate  $\dot{\mathbf{E}}^{tp}$  and the

<b>1. Elastic Predictor</b>	
1.1. <i>Begin</i>	
1.2. <i>Form entire element strain vector</i>	
1.2.1 <i>For each material point, <math>k</math>, form:</i>	
$\mathbf{B}_L \leftarrow (H_{,x} \leftarrow (J^{-1}, H_{,r}))$	
1.2.2 <i>Form: <math>\mathbf{L}_k = {}_k\mathbf{B}_L \mathbf{u}_k</math></i>	
1.2.3 <i>Form: <math>\mathbf{L}_e = [\mathbf{L}_1 \dots \mathbf{L}_k]^T</math></i>	
1.3 <i>Form element elastic predicted stress</i>	
$\mathbf{T}_e = [\mathbf{T}_1 \dots \mathbf{T}_k]^T$ , $\mathbf{T}_k = \mathbf{T}_k^{n-1} + \hat{\mathbf{C}} \Delta \mathbf{L}_k$	
1.4 <i>Form volume averaged deviatoric stress</i>	
$\langle \mathbf{S}^* \rangle = \frac{[w_1^q \mathbf{S}_1 + \dots + w_k^q \mathbf{S}_k]}{(\sum_{i=1..k} w_i^q)}$	
<b>2. Plastic Corrector</b>	
2.1. <i>Initialize Macroscopic Deviator</i>	$\mathbf{S} = \langle \mathbf{S}^* \rangle_v$
2.2. <i>Recover internal variables and initialize effective strains</i>	$(\mathbf{E}_1^{eff})^{n+1} = (\mathbf{E}_1^{eff})^n$ , $(\mathbf{E}_2^{eff})^{n+1} = (\mathbf{E}_2^{eff})^n$
2.3. <i>Form Equivalent Macro Stress and Equivalent Strain</i>	$\Sigma^{eq} = (3/2 \mathbf{S} : \mathbf{S})^{0.5}$ , $\mathbf{E}^{eq} = (2/3 \mathbf{E} : \mathbf{E})^{0.5}$
2.4. <i>Form: <math>\Sigma^y</math></i>	
2.5. <i>Form: <math>\mathbf{E}^p</math></i>	
$\Delta \mathbf{E}^p = \Delta t (\dot{\mathbf{E}}^p + \dot{\mathbf{E}}_\Sigma^{cp} + \dot{\mathbf{E}}_T^{cp})$	if $\Sigma^{eq} < \Sigma^y$
$\Delta \mathbf{E}^p = \Delta t (3/2) \dot{\mathbf{E}}^{eq} / \Sigma^{eq} \mathbf{S}$	if $\Sigma^{eq} = \Sigma^y$
2.6. <i>Form eight Residual Equations</i>	
$\mathbf{F} = \mathbf{S} - \langle \mathbf{S}^* \rangle_v + 2\mu \mathbf{E}^p$	
$\mathbf{G} = (\mathbf{E}_1^{eff})^{n+1} - (\mathbf{E}_1^{eff})^n - \Delta t \dot{\mathbf{E}}_1^{eff}$	
$\mathbf{H} = (\mathbf{E}_2^{eff})^{n+1} - (\mathbf{E}_2^{eff})^n - \Delta t \dot{\mathbf{E}}_2^{eff}$	
2.7. <i>Perform N-R step on the eight equations in 2.6.</i>	
2.8. <i>Update solution of macroscopic stress tensor and internal variables</i>	
2.9. <i>Check for convergence</i>	
IF $\mathbf{F}(\mathbf{S}, \mathbf{E}_1^{eff}, \mathbf{E}_2^{eff})$ or $\mathbf{G}(\mathbf{S}, \mathbf{E}_1^{eff}, \mathbf{E}_2^{eff})$	
or $\mathbf{H}(\mathbf{S}, \mathbf{E}_1^{eff}, \mathbf{E}_2^{eff}) > \text{TOL}$ GOTO 3	
2.10. <i>Calculate deviatoric stress by Eq.(5.20)</i>	
2.11. <i>Form <math>k</math> contributions to the global stiffness matrix</i>	

Figure 5.1: Leblond's model solution scheme

classical plastic strain rate  $\dot{\mathbf{E}}^{cp}$  i.e.

$$\dot{\mathbf{E}}^p = \dot{\mathbf{E}}^{tp} + \dot{\mathbf{E}}^{cp} \quad (5.2)$$

The second rate is expressed as the sum of the classical plastic strain rate induced thermally  $\dot{\mathbf{E}}_T^{cp}$  and the classical plastic strain rate induced by stress  $\dot{\mathbf{E}}_\Sigma^{cp}$ , therefore the plastic strain rate is given by:

$$\dot{\mathbf{E}}^p = \dot{\mathbf{E}}^{tp} + \dot{\mathbf{E}}_\Sigma^{cp} + \dot{\mathbf{E}}_T^{cp} \quad (5.3)$$

Finally the total strain-rate is expressed as the sum of five terms:

$$\dot{\mathbf{E}}^t = \dot{\mathbf{E}}^e + \dot{\mathbf{E}}^{thm} + \dot{\mathbf{E}}^{tp} + \dot{\mathbf{E}}_\Sigma^{cp} + \dot{\mathbf{E}}_T^{cp} \quad (5.4)$$

with components defined by the following constitutive equations:

$$\dot{\mathbf{E}}_i^e = \frac{1}{\mu_i} \dot{\mathbf{S}}, \quad i = 1, 2, \quad (5.5)$$

$$\dot{\mathbf{E}}_i^{thm} = \alpha_i \dot{\theta}, \quad i = 1, 2 \quad (5.6)$$

$$\dot{\mathbf{E}}^{tp} = \frac{-\Delta \epsilon_{1 \rightarrow 2}^{th}}{\sigma_1^y E_1^{eff}} S h \left( \frac{\Sigma^{eq}}{\Sigma^y} \right) \ln(z) \dot{z} \quad (5.7)$$

$$\dot{\mathbf{E}}_\Sigma^{cp} = \frac{3(1-z)g(z)}{2\sigma_1^y E_1^{eff} E} S \dot{\Sigma}^{eq} \quad (5.8)$$

$$\dot{\mathbf{E}}_T^{cp} = \frac{3(\alpha_1 - \alpha_2)}{\sigma_1^y E_1^{eff}} z \ln(z) S \dot{\theta} \quad (5.9)$$

where

$$\Delta \epsilon_{1 \rightarrow 2}^{th} = \mathbf{E}_2^{thm} - \mathbf{E}_1^{thm} \quad (5.10)$$

$$\Sigma^y = [1 - f(z)] \sigma_1^y E_1^{eff} + f(z) \sigma_2^y E_2^{eff} \quad (5.11)$$

$$\Sigma^{eq} = (3/2 \mathbf{S} : \mathbf{S})^{1/2}. \quad (5.12)$$

Here, the thermal expansion coefficient is denoted by  $\alpha_i$ , shear modulus is denoted by  $\mu_i$ , and  $i$  is taken for one of two phases  $i = 1, 2$ . The ultimate stress  $\Sigma^y$  is the maximal possible value of  $\Sigma^{eq}$  and  $\mathbf{S}$  is the macro-deviatoric stress defined by

$$\mathbf{S} = \langle \mathbf{S} \rangle_v = \frac{[w_1^g \mathbf{S}_1 + \dots + w_k^g \mathbf{S}_k]}{\left( \sum_{j=1, \dots, k} w_j^g \right)} \quad (5.13)$$

where  $w_j^g$  is the weight from the Gauss integration scheme. The functions  $f(z)$ ,  $g(z)$  are defined discretely by Leblond et al [33] and in order to incorporate them into the finite element code is necessary to fit curves to these functions. Yield limits of the two phases, at the particular time step, are denoted by  $\sigma_1^y, \sigma_2^y$ , and  $E$  is Young's modulus.

Expressions for the evaluation of  $E_1^{eff}$  and  $E_2^{eff}$  contribute to the relations for  $\dot{\mathbf{E}}^{tp}$ ,  $\dot{\mathbf{E}}_\Sigma^{cp}$ ,  $\dot{\mathbf{E}}_T^{cp}$

and  $\Sigma^y$ . The effective strain rates, used in calculating the macro-yield  $\Sigma^y$ , when  $\Sigma^y$  is more than  $\Sigma^{eq}$ , are defined by the following equations:

$$\dot{\epsilon}_1^{eff} = -\frac{z\Delta\epsilon_{1\rightarrow 2}^{th}}{1-z}h\left(\frac{\Sigma^{eq}}{\Sigma^y}\right)(\ln z)\dot{z} + \frac{g(z)}{E}\dot{\Sigma}^{eq} + \frac{2(\alpha_1 - \alpha_2)z \ln z}{1-z}\dot{\theta} \quad (5.14)$$

$$\dot{\epsilon}_2^{eff} = -\frac{\dot{z}}{z}E_2^{eff} + \vartheta\frac{\dot{z}}{z}E_1^{eff} \quad (5.15)$$

where  $\Delta\epsilon_{1\rightarrow 2}^{th}$  is given by Eq.(5.7), and  $K$  is a constant determined experimentally for various phases. The correction function  $h$  is defined by Leblond et al. in [33].

$$h\left(\frac{\Sigma^{eq}}{\Sigma^y}\right) = \begin{cases} 1 & \frac{\Sigma^{eq}}{\Sigma^y} \leq \frac{1}{2} \\ 1 + 3.5 \left(\frac{\Sigma^{eq}}{\Sigma^y} - \frac{1}{2}\right) & \frac{\Sigma^{eq}}{\Sigma^y} \geq \frac{1}{2} \end{cases} \quad (5.16)$$

The macro-plastic strain rate, in the case when  $\Sigma^y$  is equal to  $\Sigma^{eq}$ , is expressed by

$$\dot{E}^p = (3\dot{E}^{eq}/2\Sigma^{eq})S \quad (5.17)$$

$$\dot{\epsilon}_1^{eff} = \dot{E}^{eq} \quad (5.18)$$

$$\dot{\epsilon}_2^{eff} = \dot{E}^{eq} - \frac{\dot{z}}{z}E_2^{eff} + \vartheta\frac{\dot{z}}{z}E_1^{eff} \quad (5.19)$$

where  $\dot{E}^{eq} = (2/3\dot{E} : \dot{E})^{1/2}$ . The  $\vartheta$  factor reflects the material recovery phenomena.

The macro-deviatoric stress  $S$  averaged for a volume  $V$  may be converted to the deviatoric stress at each material point  $\mathbf{S}$  by using the relation

$$\mathbf{S} = (\sigma_p^y/\Sigma^y)S \quad (5.20)$$

where the yield limit  $\sigma_p^y$  is evaluated for each material point from an averaging formula  $\sigma_p^y = z\sigma_1^y + (1-z)\sigma_2^y$ , and  $\sigma_2^y$  is taken for the current material phase as the yield limit for pearlite, bainite or martensite.

The phase fraction is determined by the relation:

$$z = 1 - \sum_p y_p, \quad (5.21)$$

where  $y_p$  are defined for the isothermal kinetics of transformations by diffusion of carbon. This kinetics is modelled by the Johnson-Mehl-Avrami law [12] developed for continuous cooling

$$y_p = y_{max_p}[1 - \exp(-b_p t^{n_p})] \quad (5.22)$$

where  $y_p$  is the volume fraction of constituent  $p$  transformed into austenite,  $b_p$  and  $n_p$  are temperature dependent constants and  $t$  is the transformation time. These parameters are calculated using TTT diagrams for particular temperatures and for e.g. 10 % and 90 % fractions of the phase. The martensitic transformation is given by the Koisten-Marburger law [12].

$$y_s = [1 - \exp(-\alpha(M_s - \theta))] \bar{y}_a, \quad \bar{y}_a = 1 - y_{pearlite} - y_{bainite} - y_{ferrite}, \quad (5.23)$$

where  $M_s$  is the martensitic temperature, below which the diffusionless transformation to martensite takes place for rapid cooling. Here  $\alpha$  is calculated for the  $M_{50}$  and  $M_{90}$  i.e. the 50 % and 90 % martensitic temperatures.

### 5.1.1 Residual Functions

The eight residual equations used for evaluation of the macro-deviatoric stress  $S$  and the effective strain rates have the following forms:

$$\begin{aligned} F(S, E_1^{eff}, E_2^{eff}) &= S - \langle S^* \rangle_v + 2\mu\Delta t\dot{E}^p \\ G(S, E_1^{eff}, E_2^{eff}) &= (E_1^{eff})^{n+1} - (E_1^{eff})^n - \Delta t\dot{E}_1^{eff} \\ H(S, E_1^{eff}, E_2^{eff}) &= (E_2^{eff})^{n+1} - (E_2^{eff})^n - \Delta t\dot{E}_2^{eff} \end{aligned} \quad (5.24)$$

where the averaged deviatoric stress  $\langle S^* \rangle_v$  is defined by Eq.(5.13) and the plastic strain rate  $\dot{E}^p$  is given by Eq.(5.3) as a function of  $S, E_1^{eff}$  and  $E_2^{eff}$ . Functions  $G$  and  $H$  arise from using the backward Euler method to integrate  $\dot{E}_1^{eff}$  and  $\dot{E}_2^{eff}$  in respect of time. Values of effective strains are taken at  $(n + 1)$  and  $n$  time steps.

The solution of this system of residual functions is obtained as before by the Newton-Raphson method.

$$\hat{A} (\mathbf{x}^{n+1} - \mathbf{x}^n) = -\mathbf{b} \quad (5.25)$$

where the vectors and the matrix is now given by

$$\mathbf{x}^{n+1} = \begin{pmatrix} S \\ E_1^{eff} \\ E_2^{eff} \end{pmatrix}^{n+1}, \quad \mathbf{b} = \begin{pmatrix} F \\ G \\ H \end{pmatrix}^n \quad (5.26)$$

$$\hat{A} = \begin{bmatrix} \frac{\partial F}{\partial S} & \frac{\partial F}{\partial E_1^{eff}} & \frac{\partial F}{\partial E_2^{eff}} \\ \frac{\partial G}{\partial S} & \frac{\partial G}{\partial E_1^{eff}} & \frac{\partial G}{\partial E_1^{eff}} \\ \frac{\partial H}{\partial S} & \frac{\partial H}{\partial E_1^{eff}} & \frac{\partial H}{\partial E_2^{eff}} \end{bmatrix} \quad (5.27)$$

## 5.2 Contribution of Leblond's Model in Stiffness

The tangent modulus  $\frac{\partial T}{\partial L}$  for transformation plasticity is given by differentiation of the following expression for the total stress tensor

$$\mathbf{T} = \mathbf{T}^* - 2\mu\Delta t\dot{E}^p \quad (5.28)$$

where  $\mathbf{T}^*$  is the averaged stress predicted for the Hookean elastic material.

$$\frac{\partial \mathbf{T}}{\partial \mathbf{L}} = \frac{\partial}{\partial \mathbf{E}} \left( \mathbf{T}^* - 2\mu\Delta t \dot{\mathbf{E}}^p \right) \quad (5.29)$$

substituting for the macro-plastic strain rate from Eq.(5.3) and Eq.(5.17) we obtain

$$\frac{\partial \mathbf{T}}{\partial \mathbf{L}} = \begin{cases} \frac{\partial}{\partial \mathbf{L}} \left( \mathbf{T}^* - 2\mu\Delta t \left\{ \dot{\mathbf{E}}^{tp} + \dot{\mathbf{E}}_{\Sigma}^{cp} + \dot{\mathbf{E}}_T^{cp} \right\} \right) & \text{if } \Sigma^y > \Sigma^{eq} \\ \frac{\partial}{\partial \mathbf{L}} \left( \mathbf{T}^* - 3\mu\Delta t \left\{ \frac{\dot{\mathbf{E}}^{eq}}{\Sigma^{eq}} \mathbf{S} \right\} \right) & \text{if } \Sigma^y = \Sigma^{eq} \end{cases} \quad (5.30)$$

The derivatives of  $\mathbf{T}^*$  and  $\dot{\mathbf{E}}^p$  from Eq.(5.29) are the following:

$$\frac{\partial \mathbf{T}^*}{\partial \mathbf{L}} = \hat{\mathbf{C}} \quad (5.31)$$

and

$$\begin{aligned} \frac{\partial \dot{\mathbf{E}}^p}{\partial \mathbf{L}} &= \frac{\partial \dot{\mathbf{E}}^p}{\partial \mathbf{S}} \frac{\partial \mathbf{S}}{\partial \mathbf{S}} \frac{\partial \mathbf{S}}{\partial \mathbf{E}} \frac{\partial \mathbf{E}}{\partial \mathbf{L}} \\ &= \frac{\partial \dot{\mathbf{E}}^p}{\partial \mathbf{S}} \frac{\partial}{\partial \mathbf{S}} \left( \mathbf{S} \frac{\Sigma^y}{\sigma_p^y} \right) \frac{\partial}{\partial \mathbf{E}} 2\mu (\mathbf{E} - \mathbf{E}^p) \frac{\partial}{\partial \mathbf{L}} (\mathbf{L} : \hat{\mathbf{I}}_{dev}) \\ &= \frac{\partial \dot{\mathbf{E}}^p}{\partial \mathbf{S}} \frac{\Sigma^y}{\sigma_p^y} 2\mu \hat{\mathbf{I}} : \hat{\mathbf{I}} : \hat{\mathbf{I}}_{dev} \\ &= \frac{\partial \dot{\mathbf{E}}^p}{\partial \mathbf{S}} \frac{\Sigma^y}{\sigma_p^y} 2\mu \hat{\mathbf{I}}_{dev} \end{aligned} \quad (5.32)$$

where  $\hat{\mathbf{C}}$  is the Elastic Tangent Modulus.

### 5.2.1 Derivatives for Internal Newton-Raphson Method

Derivatives of the residual function,  $F$ , for the macro-deviator,  $\mathbf{S}$  and internal variables,  $\mathbf{E}_1^{eff}$  and  $\mathbf{E}_2^{eff}$

$$\frac{\partial F}{\partial \mathbf{S}} = \hat{\mathbf{I}} + 2\mu\Delta t \frac{\partial \dot{\mathbf{E}}^p}{\partial \mathbf{S}}, \quad (5.33)$$

$$\frac{\partial F}{\partial \mathbf{E}_1^{eff}} = 2\mu\Delta t \frac{\partial \dot{\mathbf{E}}^p}{\partial \mathbf{E}_1^{eff}}, \quad (5.34)$$

$$\frac{\partial F}{\partial \mathbf{E}_2^{eff}} = 2\mu\Delta t \frac{\partial \dot{\mathbf{E}}^p}{\partial \mathbf{E}_2^{eff}} \quad (5.35)$$

Derivatives of the residual function,  $G$ , for the macro-deviator,  $\mathbf{S}$ , and internal variables,  $\mathbf{E}_1^{eff}$  and  $\mathbf{E}_2^{eff}$  :

$$\frac{\partial G}{\partial \mathbf{S}} = \Delta t \frac{\partial \dot{\mathbf{E}}_1^{eff}}{\partial \mathbf{S}}, \quad (5.36)$$

$$\frac{\partial G}{\partial E_1^{eff}} = 1 - \Delta t \frac{\partial \dot{E}_1^{eff}}{\partial E_1^{eff}}, \quad (5.37)$$

$$\frac{\partial G}{\partial E_2^{eff}} = \Delta t \frac{\partial \dot{E}_1^{eff}}{\partial E_2^{eff}} \quad (5.38)$$

Derivatives of the residual function,  $H$ , for the macro-deviator,  $S$  and internal variables,  $E_1^{eff}$  and  $E_2^{eff}$  :

$$\frac{\partial H}{\partial S} = \Delta t \frac{\partial \dot{E}_2^{eff}}{\partial S}, \quad (5.39)$$

$$\frac{\partial H}{\partial E_1^{eff}} = \Delta t \frac{\partial \dot{E}_2^{eff}}{\partial E_1^{eff}}, \quad (5.40)$$

$$\frac{\partial H}{\partial E_2^{eff}} = 1 - \Delta t \frac{\partial \dot{E}_2^{eff}}{\partial E_2^{eff}} \quad (5.41)$$

The preceding relations used in the internal N-R scheme contain derivatives of the plastic strain rate components and internal variables with respect to the solution variables i.e. the macro deviatoric stress and the two scalar hardening variables. These are presented in the derivations which follow.

The derivatives of the components of the plastic strain rate,  $\dot{E}^p$ , in respect of macro-deviatoric stress  $S$  are

$$\frac{\partial \dot{E}^{tp}}{\partial S} = \frac{-\Delta \epsilon_{1 \rightarrow 2}^{th}}{\sigma_1^y E_1^{eff}} \ln(z) \dot{z} \left[ \hat{\mathbf{I}} h \left( \frac{\Sigma^{eq}}{\Sigma^y} \right) + \mathbf{S} \otimes \frac{\partial}{\partial S} h \left( \frac{\Sigma^{eq}}{\Sigma^y} \right) \right] \quad (5.42)$$

$$\frac{\partial \dot{E}_T^{cp}}{\partial S} = 3 \frac{\alpha_1 - \alpha_2}{\sigma_1^y E_1^{eff}} z \ln(z) \theta \hat{\mathbf{I}} \quad (5.43)$$

$$\frac{\partial E_\Sigma^{cp}}{\partial S} = 3 \frac{(1-z) g(z)}{2 \sigma_1^y E_1^{eff}} \frac{\partial (S \dot{\Sigma}^{eq})}{\partial S} \quad (5.44)$$

$$\frac{\partial (S \dot{\Sigma}^{eq})}{\partial S} = \hat{\mathbf{I}} \dot{\Sigma}^{eq} + \frac{3}{2} \frac{1}{\dot{\Sigma}^{eq}} \mathbf{S} \otimes \dot{S} \quad (5.45)$$

where the last relation has been obtained from

$$\begin{aligned} \frac{\partial (S \dot{\Sigma}^{eq})}{\partial S} &= \hat{\mathbf{I}} \dot{\Sigma}^{eq} + \mathbf{S} \otimes \frac{\partial}{\partial S} \left( \frac{3}{2} \dot{S} : \dot{S} \right)^{-\frac{1}{2}} \\ &= \hat{\mathbf{I}} \dot{\Sigma}^{eq} + \mathbf{S} \frac{1}{2} \left( \frac{3}{2} \dot{S} : \dot{S} \right)^{-\frac{1}{2}} \frac{3}{2} (\dot{S} : \hat{\mathbf{I}} + \hat{\mathbf{I}} : \dot{S}) \\ &= \hat{\mathbf{I}} \dot{\Sigma}^{eq} + \mathbf{S} \frac{3}{4} \frac{1}{\dot{\Sigma}^{eq}} 2 \dot{S} \\ &= \hat{\mathbf{I}} \dot{\Sigma}^{eq} + \frac{3}{2} \frac{1}{\dot{\Sigma}^{eq}} \mathbf{S} \otimes \dot{S} \end{aligned}$$

The derivative of the components of the macroscopic plastic strain rate,  $\dot{E}^{tp}$ ,  $\dot{E}_\Sigma^{cp}$  and  $\dot{E}_T^{cp}$ , with respect to the internal variable  $E_1^{eff}$  are given by

$$\begin{aligned}\frac{\partial \dot{E}^{tp}}{\partial E_1^{eff}} &= -\frac{3\Delta\epsilon_{1\rightarrow 2}^{th}}{\sigma_1^y} S \frac{\partial}{\partial E_1^{eff}} \left[ (E_1^{eff})^{-1} h \left( \frac{\Sigma^{eq}}{\Sigma^y} \right) \right] \\ &= -\frac{3\Delta\epsilon_{1\rightarrow 2}^{th}}{\sigma_1^y} S \left[ -(E_1^{eff})^{-2} h \left( \frac{\Sigma^{eq}}{\Sigma^y} \right) + (E_1^{eff})^{-1} \frac{\partial}{\partial E_1^{eff}} h \left( \frac{\Sigma^{eq}}{\Sigma^y} \right) \right]\end{aligned}\quad (5.46)$$

$$\frac{\partial \dot{E}_\Sigma^{cp}}{\partial E_1^{eff}} = \frac{-3(1-z)g(z)}{2\sigma_1^y(E_1^{eff})^2} S \dot{\Sigma}^{eq} \quad (5.47)$$

$$\frac{\partial \dot{E}_T^{cp}}{\partial E_1^{eff}} = \frac{-3(\alpha_1 - \alpha_2)}{\sigma_1^y(E_1^{eff})^2} z \ln(z) S \dot{\theta} \quad (5.48)$$

The derivative of the components of the macroscopic plastic strain rate,  $\dot{E}^{tp}$ ,  $\dot{E}_\Sigma^{cp}$  and  $\dot{E}_T^{cp}$ , with respect to the internal variable  $E_2^{eff}$  are given by

$$\frac{\partial \dot{E}^{tp}}{\partial E_2^{eff}} = \frac{3\Delta\epsilon_{1\rightarrow 2}^{th}}{\sigma_1^y E_1^{eff}} S \frac{\partial}{\partial E_2^{eff}} h \left( \frac{\Sigma^{eq}}{\Sigma^y} \right) \quad (5.49)$$

$$\frac{\partial \dot{E}_\Sigma^{cp}}{\partial E_2^{eff}} = 0 \quad (5.50)$$

$$\frac{\partial \dot{E}_T^{cp}}{\partial E_2^{eff}} = 0 \quad (5.51)$$

The derivatives of the scalar internal variable rates  $\dot{E}_1^{eff}$  and  $\dot{E}_2^{eff}$  are

$$\frac{\partial \dot{E}_1^{eff}}{\partial S} = -\frac{z\Delta\epsilon_{1\rightarrow 2}^{th}}{1-z} \frac{\partial}{\partial S} h \left( \frac{\Sigma^{eq}}{\Sigma^y} \right) \ln(z) \dot{z} + \frac{g(z)}{E} \frac{\partial \dot{\Sigma}^{eq}}{\partial S} \quad (5.52)$$

$$\frac{\partial \dot{E}_1^{eff}}{\partial E_1^{eff}} = \frac{-z\Delta\epsilon_{1\rightarrow 2}^{th}}{1-z} \ln(z) \dot{z} \frac{\partial}{\partial E_1^{eff}} h \left( \frac{\Sigma^{eq}}{\Sigma^y} \right) \quad (5.53)$$

$$\frac{\partial \dot{E}_1^{eff}}{\partial E_2^{eff}} = \frac{-z\Delta\epsilon_{1\rightarrow 2}^{th}}{1-z} \ln(z) \dot{z} \frac{\partial}{\partial E_2^{eff}} h \left( \frac{\Sigma^{eq}}{\Sigma^y} \right) \quad (5.54)$$

$$\frac{\partial \dot{E}_2^{eff}}{\partial S} = 0^T \quad (5.55)$$

$$\frac{\partial \dot{E}_2^{eff}}{\partial E_1^{eff}} = \vartheta \frac{\dot{z}}{z} \quad (5.56)$$

$$\frac{\partial \dot{E}_2^{eff}}{\partial E_2^{eff}} = -\frac{\dot{z}}{z} \quad (5.57)$$

The above derivations also lead to the derivatives of the function  $h\left(\frac{\Sigma^{eq}}{\Sigma^y}\right)$ :

$$\frac{\partial}{\partial S} h\left(\frac{\Sigma^{eq}}{\Sigma^y}\right) = \begin{cases} 0 & \frac{\Sigma^{eq}}{\Sigma^y} \leq \frac{1}{2} \\ 5.25 (d\Sigma^{eq} \Sigma^y)^{-1} S & \frac{\Sigma^{eq}}{\Sigma^y} \geq \frac{1}{2} \end{cases} \quad (5.58)$$

$$\frac{\partial}{\partial E_1^{eff}} h\left(\frac{\Sigma^{eq}}{\Sigma^y}\right) = \begin{cases} 0 & \frac{\Sigma^{eq}}{\Sigma^y} \leq \frac{1}{2} \\ 3.5 \Sigma^{eq} (-\Sigma^y)^{-2} [1 - f(z)] \sigma_1^y & \frac{\Sigma^{eq}}{\Sigma^y} \geq \frac{1}{2} \end{cases} \quad (5.59)$$

$$\frac{\partial}{\partial E_2^{eff}} h\left(\frac{\Sigma^{eq}}{\Sigma^y}\right) = \begin{cases} 0 & \frac{\Sigma^{eq}}{\Sigma^y} \leq \frac{1}{2} \\ 3.5 \Sigma^{eq} (-\Sigma^y)^{-2} f(z) \sigma_2^y & \frac{\Sigma^{eq}}{\Sigma^y} \geq \frac{1}{2} \end{cases} \quad (5.60)$$

### 5.2.2 Mixture Functions

The mixture functions  $f(z)$  and  $g(z)$  are defined discretely by Leblond [33] and in order to incorporate them into the finite element code it is necessary to fit curves to these functions. The following fits has been obtained by using STATGRAPHICS package for  $f(z)$  and  $g(z)$ :

$$f(z) = .2597(1 - \exp(-2.393z)) \quad (5.61)$$

$$g(z) = \begin{cases} 4.88 - 4.72z & 0 \leq z < 0.25 \\ \exp(1.89391 - 1.95557z) & 0.25 \leq z \leq 1 \end{cases} \quad (5.62)$$

# Chapter 6

## Thermal and Mechanical Conditions

There are various types of welding which broadly fall into two groups: fusion and solid state welding. Examples of solid state welding are friction, ultrasonic and explosive welding. The thermal boundary conditions for heat input which we will consider here concern only fusion welding. Although it is theoretically possible to model solid state welding to some extent, it is a very different process. Examples of fusion welding are gas tungsten arc welding (GTAW or TIG), shielded metal arc welding (SMA), gas metal arc welding (GMA or MIG) submerged arc welding (SMAW), Plasma-Arc welding, Electron beam, Laser beam welding and resistance welding (electrical spot).

The difference between these processes are essentially in whether a consumable electrode is used for fusion and what type, the size of heat affected zone (HAZ) and in the environment (gas, wet or dry) in which the process takes place. The extent to which we can model this process is primarily in the magnitude and distribution of the heat input over the metal surface and to the rate at which the center of the HAZ moves as also the heat exchange with the environment.

We have previously [52] modelled the boundary conditions associated with SMAW. We will here concern ourselves with the thermal boundary conditions associated with surface welding for the GMA process. We will also neglect the addition of material and assume the existence of material prior to the start of welding since although it is possible to add and remove elements in ABAQUS it leads to numerical problems in the solution process even when doing this gradually with the *amplitude* option. As an alternative we will in future work attempt to use multipoint constraints and equations which define relations between nodes to simulate the addition of filler material.

### 6.1 Model of the Welding Arc

The welding arc is modelled by a travelling Gaussian distribution:

$$F_{\theta}^{arc} = \frac{\phi\eta VI}{2\pi\sigma_{arc}^2} \exp(-r^2/2\sigma_{arc}^2) \quad (6.1)$$

where  $\sigma_{arc}$  is the standard deviation of this distribution representing the thermal 'impression' made by the weld electrode,  $\eta$  is the efficiency of the energy to heat relation,  $\phi$  is the net fraction of heat input and  $r$  is the horizontal radial distance from the weld center.

## 6.2 Convection from the weld piece

Convection from the weld piece is given by empirical relations [24] in terms of non-dimensional constants:  $N_f, G_f, P_f, R_f$  are the Nusselt, Grashof, Prandtl and Rayleigh numbers evaluated at the film temperature. The film temperature is given by

$$\theta_f = \frac{\theta_\infty + \theta_w}{2} \quad (6.2)$$

and the convection coefficient is given by

$$h_c = \bar{N}_f \frac{k_f}{l_c} \quad (6.3)$$

where  $k_f$  is the conductivity of the boundary layer

$$k_f = (9.75603 \times 10^{-3} + 5.71995 \times 10^{-5} \theta_f) / 1000 \text{ Watts/mm.} \quad (6.4)$$

and  $l_c$  is the characteristic length of the boundary layer The flux,  $F_\theta^c$ , due to convection is

$$F_\theta^c = h_c (\theta_f - \theta_\infty) \quad (6.5)$$

The specific value of the Nusselt number derives from a temperature dependent relation for the Prandtl number and relations for the Grashof number dependent on both the temperature and the orientation of surface from which convection takes place. The prandtl number is given by

$$\begin{aligned} P_f &= 1.13786 (\theta_f)^{-0.083107} & \theta_f &\leq 500 \\ P_f &= 0.651978 + 4.7895 \times 10^{-5} \theta & 500 < \theta_f &\leq 1200 \\ P_f &= 0.705 & \theta_f &> 1200 \end{aligned} \quad (6.6)$$

The other temperature dependent relations that are used in the relations which follow are the volumetric expansion coefficient,  $\beta$  and the viscosity,  $\nu$ .

$$\beta = \frac{1}{\theta_a} \quad (6.7)$$

where  $\theta_a$  is the absolute temperature.

$$\nu = 8.69754 \times 10^{-4} (\theta_f)^{1.71067} \quad (6.8)$$

The rayleigh number is defined as

$$R_f = G_f P_f \quad (6.9)$$

### 6.2.1 Convection from the upper surface

For the upper surface the Grashof number is given by

$$G_f = \frac{g\beta\theta_f l_c^3}{\nu^2} \quad (6.10)$$

where  $g$  is the acceleration due to gravity,  $\beta$  is the volumetric expansion coefficient,  $\nu$  is the viscosity of the film and  $l_c$  is the characteristic length which for the upper surface of the plate is the area divided by the perimeter.

The Nusselt number on the upper surface:

$$\begin{aligned} N_f &= 0.13(R_f)^{\frac{1}{3}} \quad R_f \leq 2 \times 10^8 \\ N_f &= 0.16(R_f)^{\frac{1}{3}} \quad R_f > 2 \times 10^8 \end{aligned} \quad (6.11)$$

### 6.2.2 Convection from the vertical surfaces

$$G_f = \frac{g\beta\theta_f l_c^3}{\nu^2} \quad (6.12)$$

$l_c$  is the characteristic length which for a vertical surface of the plate is the vertical height.

$$N_f = \left[ \frac{0.825 + 0.387(R_f)^{\frac{1}{4}}}{\left(1 + \frac{0.492}{Pr_f}\right)^{\frac{9}{25}}} \right]^{\frac{1}{2}} \quad (6.13)$$

## 6.3 Radiation from the weld piece

The radiation coefficient is given by

$$h_r = \sigma_s \epsilon_r (\theta^4 - \theta_{sink}^4) \quad (6.14)$$

where  $\sigma_s$  is the Stefan Boltzmann constant,  $\epsilon_r$  is the emmissivity of steel and  $\theta_{sink}$  is the sink temperature on which the constants are based. Hence the flux,  $F_\theta^r$ , due to radiation is given by

$$F_\theta^r = h_r (\theta - \theta_e) \quad (6.15)$$

## 6.4 Thermal contact conductance

The base of the weld piece is assumed to be in contact with a workbench which acts as a heat sink. Thermal contact relations [24] are used to estimate the heat flux from the weld piece through this contact. The flux  $F_\theta^{cc}$  is given by

$$F_\theta^{cc} = h_{cc} (\theta - \theta_c) \quad (6.16)$$

where  $h_{cc}$  is the thermal contact conductance coefficient for steel. This derives from the inverse relation for the thermal contact resistance defined as  $h_{cr} = \frac{1}{h_{cc}A}$  where  $A$  is the contact area.

The thermal contact resistance derives from an averaging of conductance from solid-to-solid spots of contact and conductance through entrapped gases in void spaces created by contact. The resistance derives from the low conductivity of the void spaces compared with the metal on metal contact. The roughness of the surface, temperature and pressure affects this coefficient. There is thus a fair amount of approximation involved in using this relation over a range of temperatures and surface conditions. The value used is that given for stainless steel 316 ([24],p.57) with air occupying the void spaces.

A necessary simplifying assumption is made here, that of the sink temperature  $\theta_c$  of the relatively massive work bench being constant.

A more complex approach would be to use a layer of special finite elements to solve for the contact between the weld piece and its support. This would give both the mechanical contact and thermal gap conductance based on contact pressure. A facility for doing this exists in ABAQUS and we have done some preliminary work in this regard [50]. This type of analysis can be included again in future work. Solving a thermo-mechanical contact problem poses additional numerical problems in the transient finite analysis used for the BVP. As it is the data available for this addition would not necessarily lead to a result which would justify the cost of its inclusion.

This particular thermal boundary condition does, however, deserve the most attention since it dominates the solution for a large part of the analysis for a typical boundary value problem (BVP).

# Chapter 7

## Numerical Results

### 7.1 Bench Mark Problem for Welding

We consider a boundary value problem which is of manageable size and which can be repeated for all three UMAT routines for the constitutive theories as our bench mark problem.

The bench mark problem considered in this thesis is that of the welding of a thick plate. Two steel plates are joined by electric arc welding. The base of the plate is firmly clamped to a workbench which acts as a heat sink. Due to symmetry only one half of the joint is considered i.e. one half plate.

### 7.2 FE Discretization of Weld Joint

The finite element mesh used to obtain these results was much more dense than ones used previously in obtaining results [54], [50]. The mesh contains 2880 8-node brick elements as opposed to the 800 elements used previously. This was made possible by the upgrading of equipment over the period of time in which this research was done.

The increase in element density was deemed necessary to ensure that the moving heat flux distribution was distributed over several elements, or more to the point, over several gauss points in the horizontal plane at any one time. Although no problems with stability were found during previous analysis with this type of mesh, such problems did arise when an irregular fillet weld was modelled with the mesh closely following the real deposits of a multipass weld.

The mesh used was regular with the highest element density along the weld line and with element density decreasing uniformly away from the weld line in two directions and constant in the plane in which the heat source is moving.

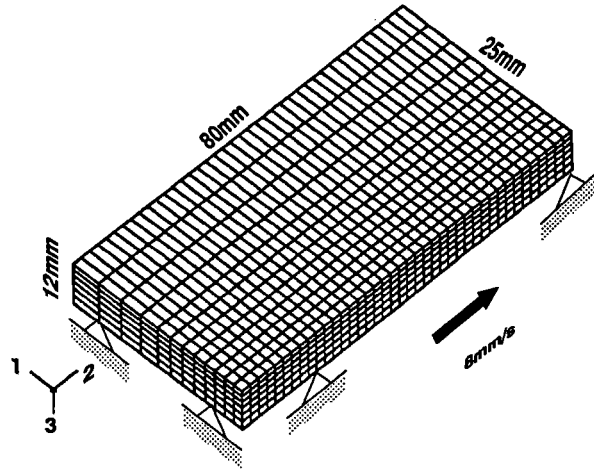


Figure 7.1: The mesh and mechanical boundary condition used to obtain results

### 7.3 Modelling of Boundary Conditions

The mechanical boundary conditions applied simulate the simple clamping of the base of the plate. The nodes at the base of the plate are restrained in all three degrees of freedom due to gravity and surface friction. More complex mechanical boundary conditions did cause numerical problems in the solution. The simple fixing of the base of the plate without constraints on plate sides makes easy to extract the purely material reaction from the total plate reaction that includes interaction of boundary conditions and internal stress. The coordinates 1,2,3 refer respectively to the x,y,z coordinates referred to elsewhere.

The thermal boundary conditions use the relations for convection and radiation as described in the chapter on thermal and mechanical boundary conditions. We apply radiation and convection as well as the thermal contact resistance relation applied to the base. The moving welding arc is used to arrive at the thermal fields. Results for the relations used in the BVP are shown below.

Figure(7.2) shows the distribution of the moving heat flux at a particular point along the weld line i.e. the middle of the welding pass at  $y=40\text{mm}$  (time = 5 seconds). The distribution is Gaussian in both the y-z plane and the x-z plane as defined.

### 7.4 Temperatures

Temperature field distributions for the BVP is shown at one second intervals showing the heat affected zone (HAZ) formed from the combined effects of the heat input due to the welding arc and the heat loss due to convection, radiation and thermal contact conductance.

The motion of the welding arc across the weld line can be seen for Figs.(7.6), (7.10) of temperature fields. The expected ellipsoid shape of the HAZ is clearly visible for the temperature

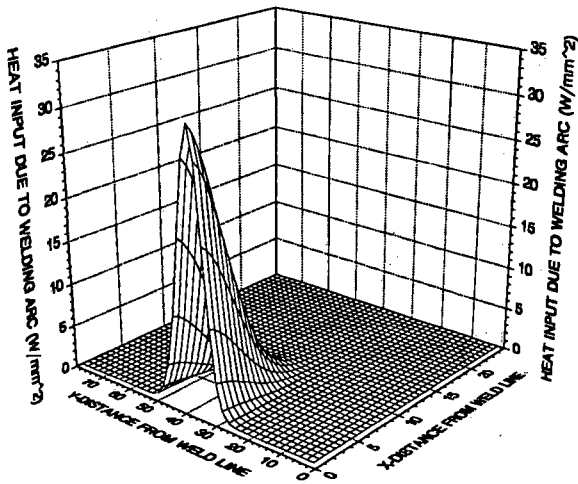


Figure 7.2: The model of the moving welding arc source

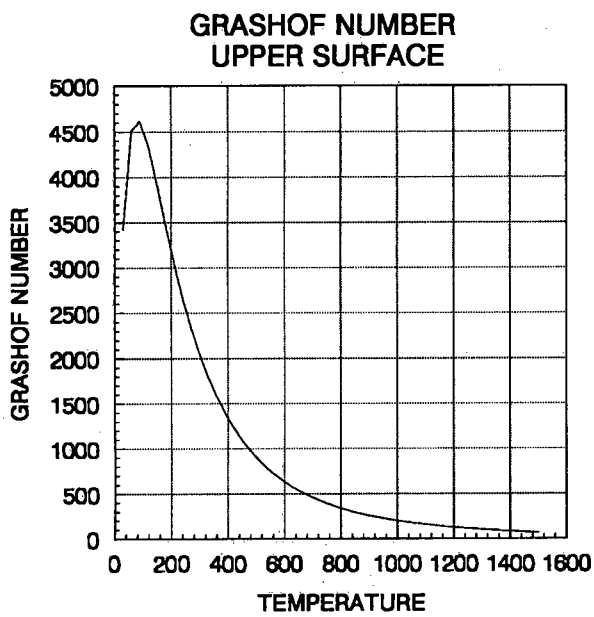


Figure 7.3: The temperature dependent relation for the Grashof number on the upper surface

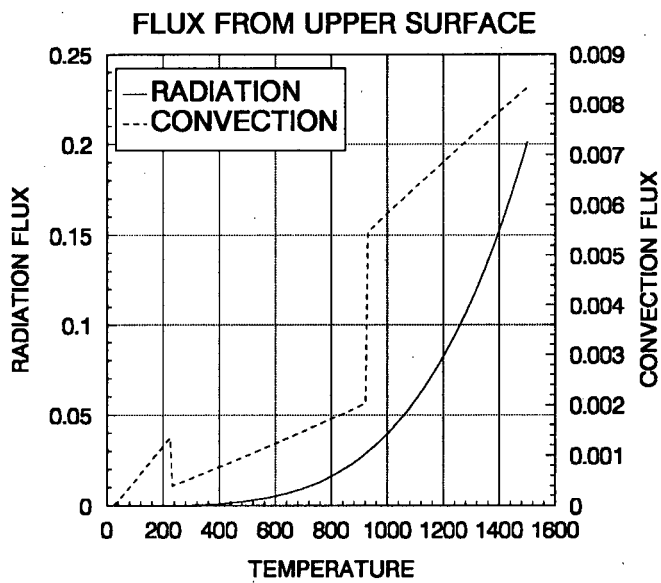


Figure 7.4: The temperature dependent relations for the convection and radiation from the upper Surface

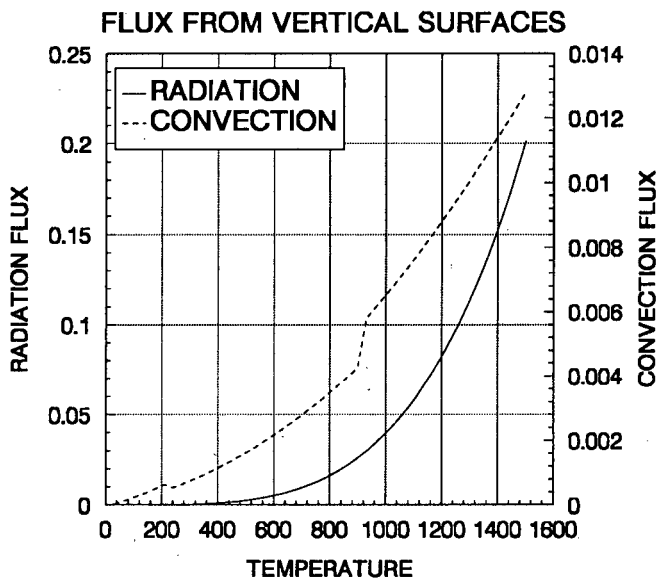


Figure 7.5: The temperature dependent relations for the convection and radiation from the vertical surfaces

fields far enough from the edges of the plate. The shape of the HAZ is not symmetrical on either side of 5 seconds since the weld does not cool down instantaneously. The rate of the disappearance of the HAZ as the welding arc moves on is comparable to experimental results conducted at the department of mechanical engineering by Prof. B. Tait.

## 7.5 Time Integration Studies of the Constitutive Models

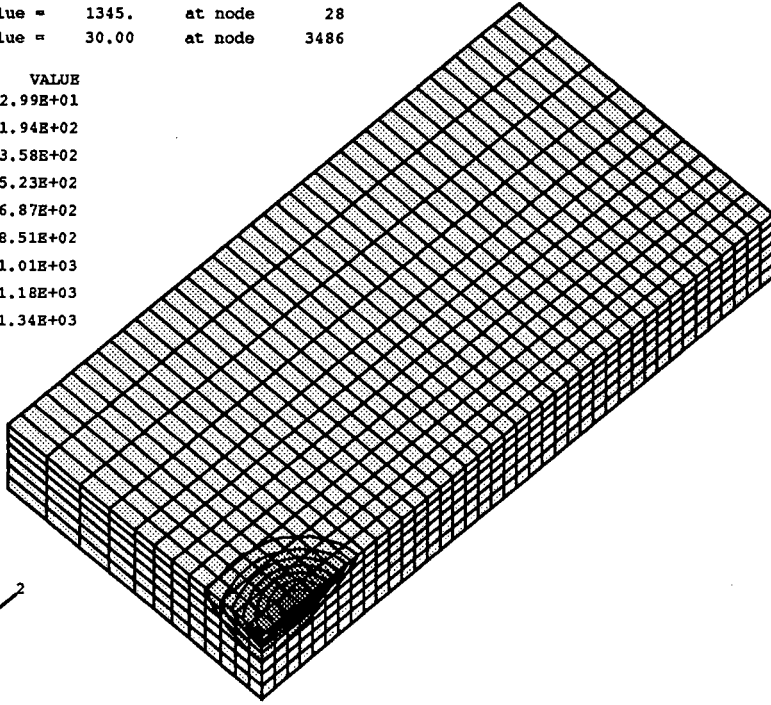
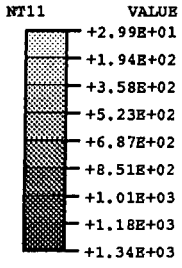
In this section we show the stress strain relations produced by the various constitutive models by prescribing strain increments at a material point as a loading history. The stress-strain relationship is thus for a single material point not a BVP.

This provides insights into the mechanisms at work within each model and the correctness of implementation of each model. Sensitivity to strain rate and temperature is also shown. The stress-strain relation produced for Anand's model is shown in Fig.(7.11). The strain history input into the algorithm Fig.(3.1) applied to Anand's model is that of starting at 0 strain and then increasing uniformly (no strain rate jumps) to a strain of 0.01 (expansion) then down to -0.01 (compression) strain for the strain component  $L_{11}$  while the strain components,  $L_{22}$ ,  $L_{33}$  are similarly incremented with the opposite sign to  $L_{11}$  and half the magnitude. This procedure simulates a tension-compression test in which the volume of the specimen remains constant.

The stress-strain loops for Anand's model are set of curves which start off in the elastic region proceed into the inelastic region and unload elastically. Pronounced work hardening occurs in this model in an isotropic fashion with no translation of stress-strain solution space as would occur in a model with kinematic hardening. The curves are thus typical for a hysteretic constitutive model.

The strain-strain loops produced for Estrin's model are as with Anand's model a set of curves which show elastic and inelastic sections in the curves with the the onset of inelastic behaviour occurring at increasingly higher levels of stress which indicates work hardening. This hardening occurs in an isotropic fashion as with Anand's model but is less pronounced. It should, however, be pointed out that the parameters for this model were identified for a softer steel than for Anand's model. Although it was possible for us to have parameters identified for this model by its originator we were unable to provide experimental results of a suitable strain rate and temperature dependent nature. The stress-strain loops shown for this model in figure Fig.(7.13) are typical of a model which exhibits kinematic hardening with a pronounced Bauschinger effect during unloading. The four cycles harden towards a single loop. The material for which parameters were indentified for this model was a hard pressure vessel steel. Fig.(7.14) shows the difference between stress-strain cycles for different temperatures. The curves are obtained at a material point by implementation of the algorithm for the model as discussed previously. The curves are labelled for four different temperatures in degrees Celsius in the accompanying legend. The model and parameters used are identified for hot-working and thus show a marked response to temperature. This response is

Maximum value = 1345. at node 28  
Minimum value = 30.00 at node 3486



Maximum value = 1453. at node 64  
Minimum value = 29.99 at node 3486

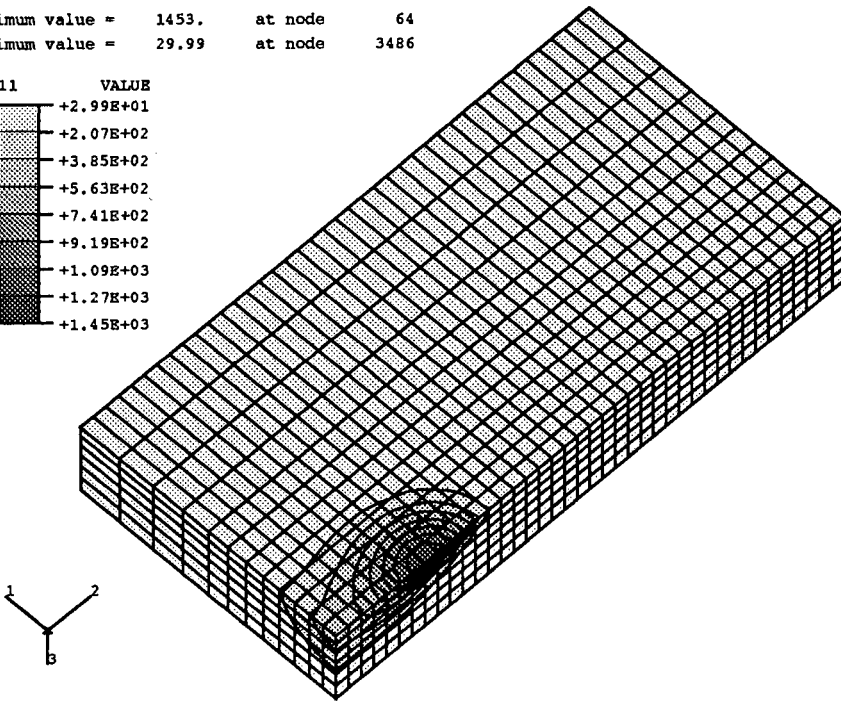
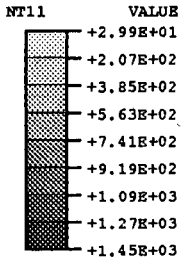
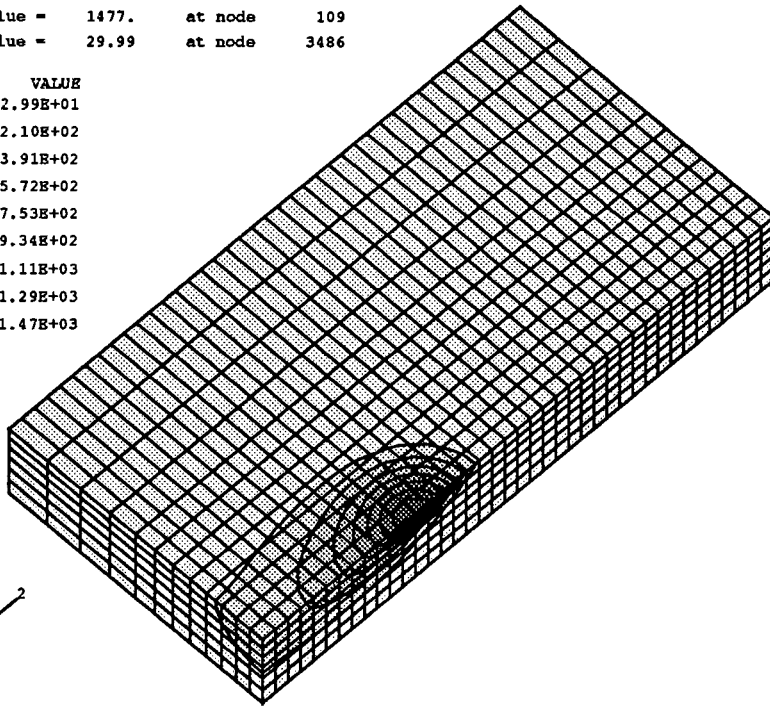
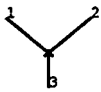
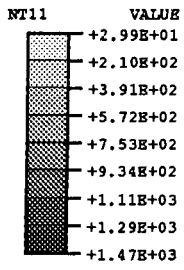


Figure 7.6: The temperature field after (a) one second , (b) two seconds of welding

Maximum value = 1477. at node 109  
Minimum value = 29.99 at node 3486



Maximum value = 1479. at node 136  
Minimum value = 29.99 at node 3486

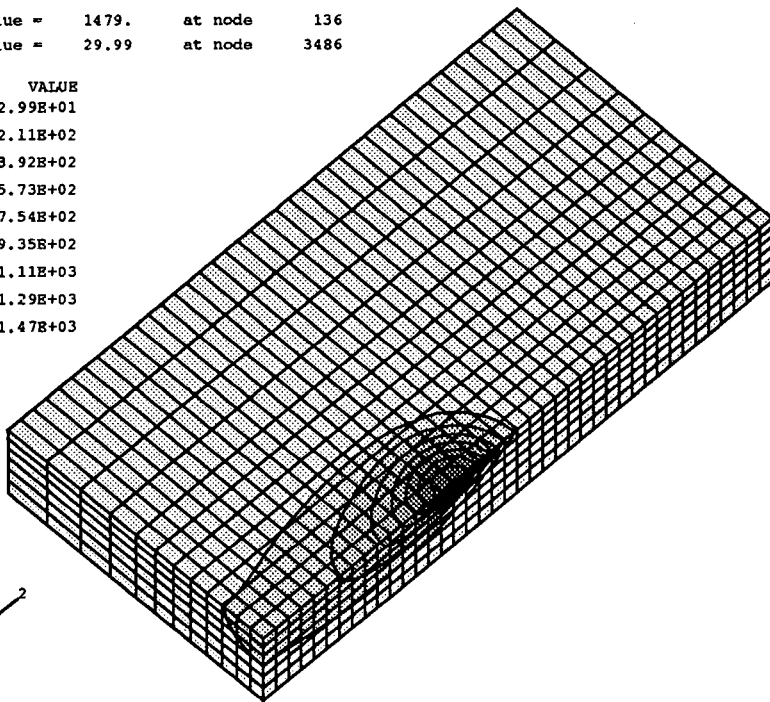
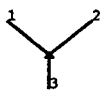
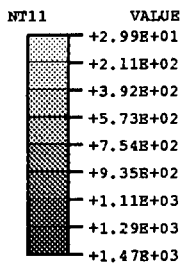
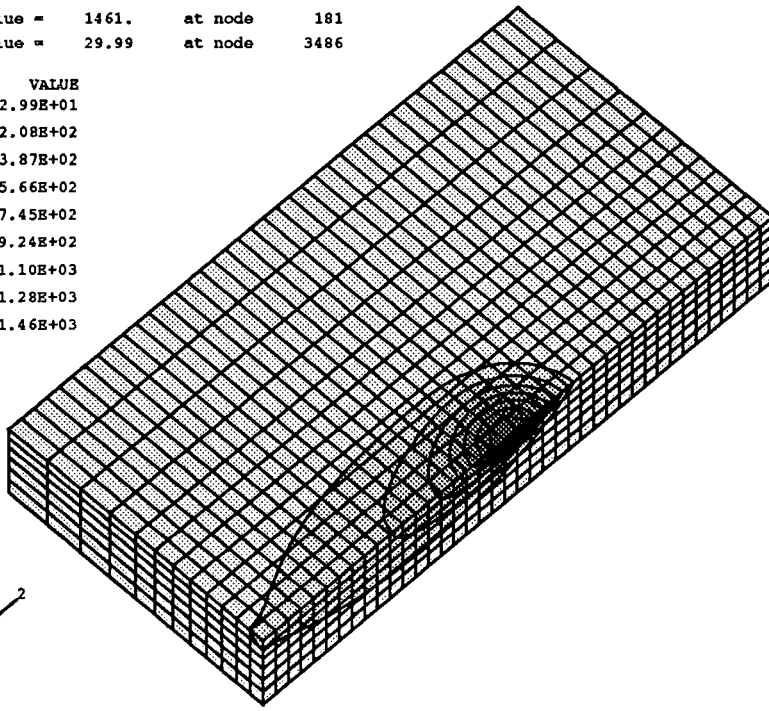
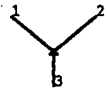
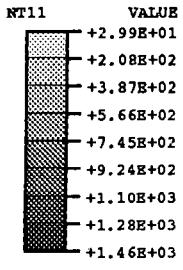


Figure 7.7: The temperature field after (a) three seconds , (b) four seconds of welding

Maximum value = 1461. at node 181  
Minimum value = 29.99 at node 3486



Maximum value = 1467. at node 1341  
Minimum value = 29.99 at node 3486

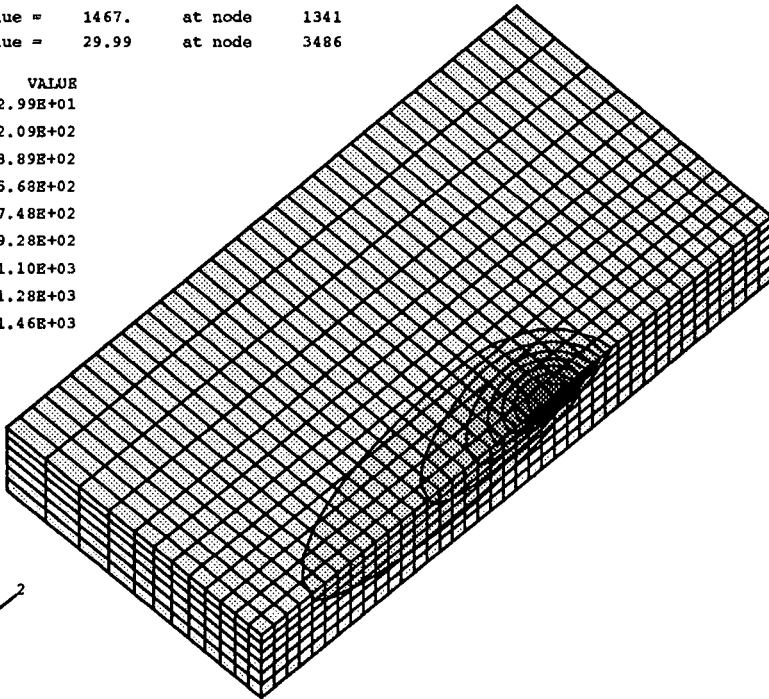
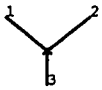
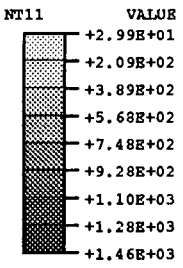
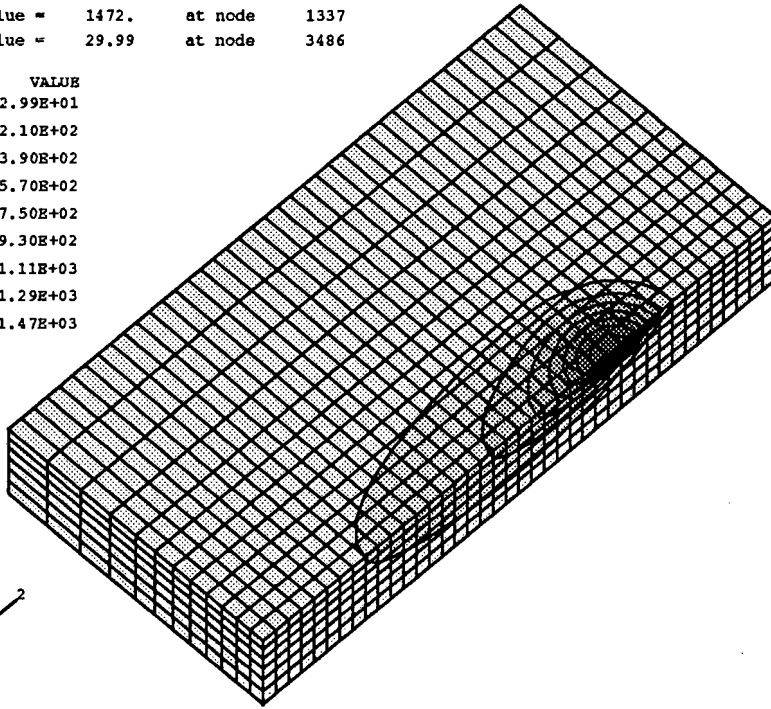
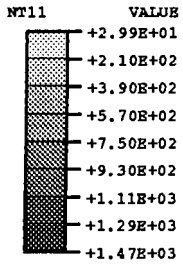


Figure 7.8: The temperature field after (a) five seconds , (b) six seconds of welding

Maximum value = 1472. at node 1337  
Minimum value = 29.99 at node 3486



Maximum value = 1467. at node 1334  
Minimum value = 29.99 at node 3486

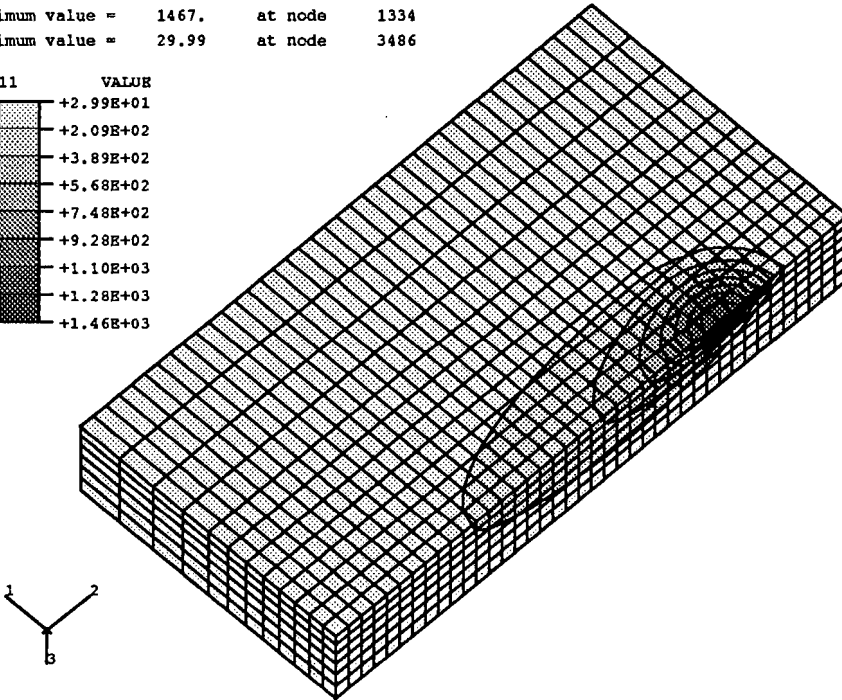
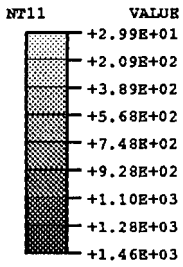
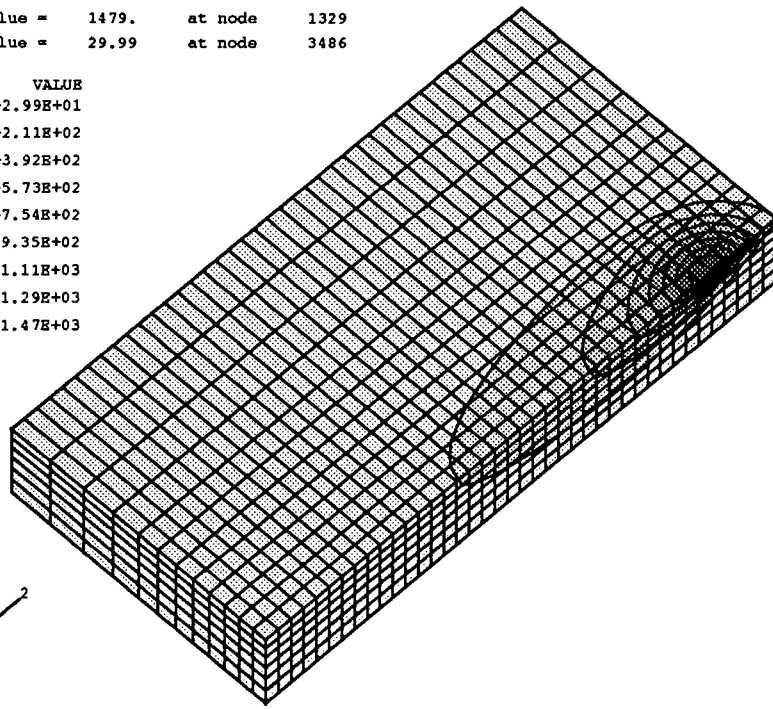
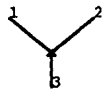
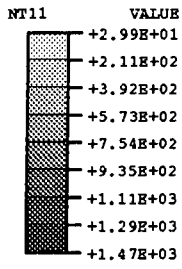


Figure 7.9: The temperature field after (a) seven seconds , (b) eight seconds of welding

Maximum value = 1479. at node 1329  
Minimum value = 29.99 at node 3486



Maximum value = 1589. at node 1324  
Minimum value = 30.00 at node 3486

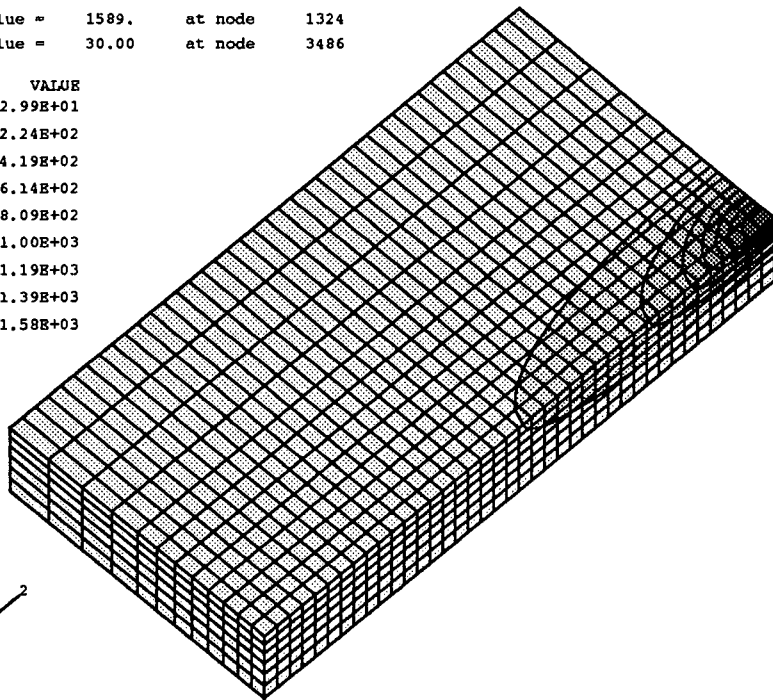
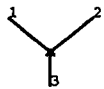
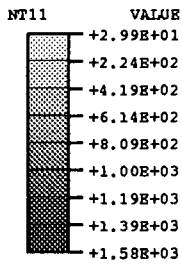


Figure 7.10: The temperature field after (a) nine seconds, (b) ten seconds of welding

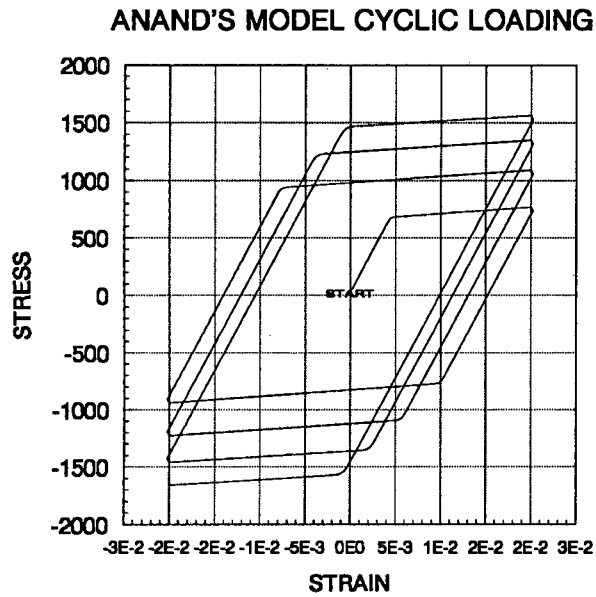


Figure 7.11: Stress ( $T_{11}$ )-strain ( $L_{11}$ ) relation for Anand's model produced for 4 cycles of loading

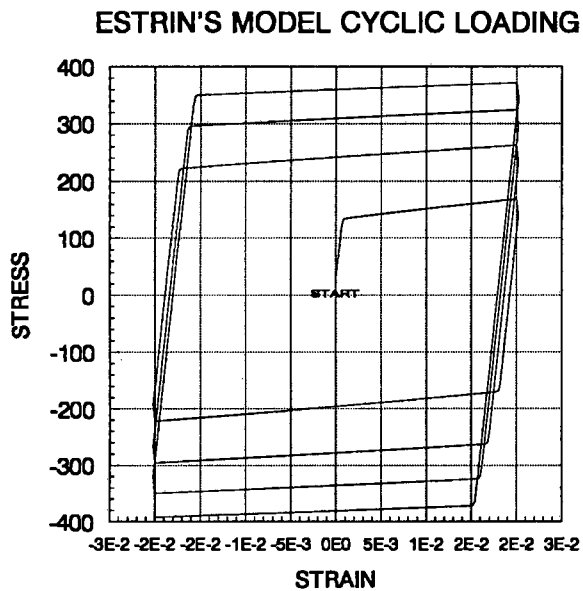


Figure 7.12: Stress ( $T_{11}$ )-strain ( $L_{11}$ ) relation for Estrin's model produced for 4 cycles of loading

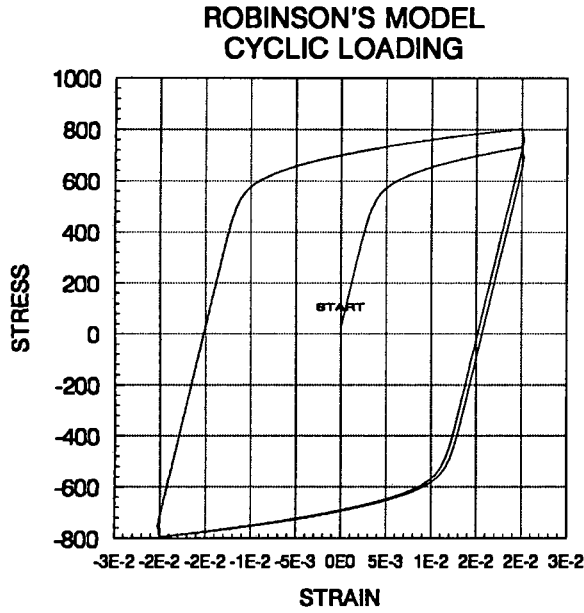


Figure 7.13: Stress ( $T_{11}$ )-strain ( $L_{11}$ ) relation for Robinson's model produced for 4 cycles of loading

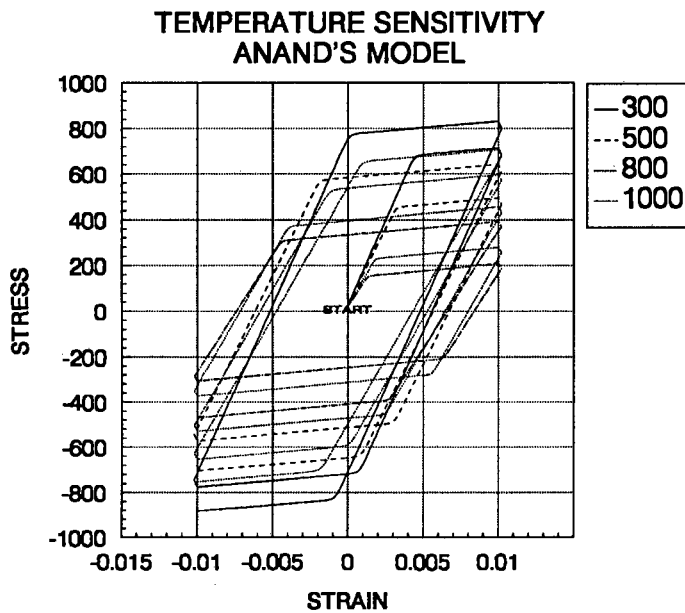


Figure 7.14: Stress ( $T_{11}$ )-strain ( $L_{11}$ ) showing thermal sensitivity over the range  $300^{\circ}$  to  $1000^{\circ}$  for Anand's model

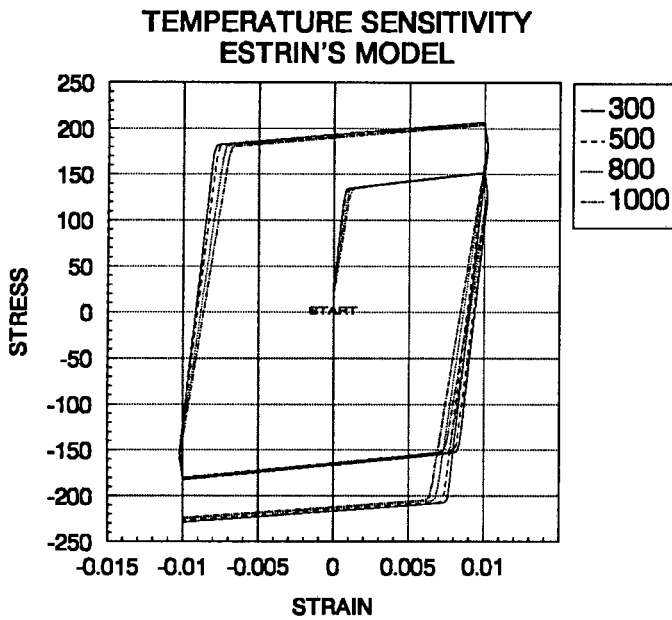


Figure 7.15: Stress ( $T_{11}$ )-strain ( $L_{11}$ ) showing thermal sensitivity over the range  $300^{\circ}$  to  $1000^{\circ}$  for Estrin's model

both in the elastic region where all the models have the same temperature dependent Lamé parameters and in the onset of inelastic behaviour.

Unlike Anand's model the parameters identified for Estrin's Model were identified for stress-strain curves which were independent of temperature as well as for a soft steel as mentioned previously. The parameters normally taken to be functions of temperature in this model (as identified for Al1100) were therefore treated as constants. Thus in Fig.(7.15) we see that the only sensitivity is in the slope of the elastic response. This due purely to the temperature dependent Lamé parameters. Robinson's model contains temperature dependent parameters rather than the model being directly a function of temperature as in the case of Anand's model. Fig.(7.16) thus shows a surprisingly large response to temperature changes. It should be noted that the curves obtained in this figure are at a higher strain rate than those in Fig.(7.13) hence the elastic loading and unloading parts of the curve are closer together as measured on the strain axis. The curves rotate in a clockwise direction with increasing temperature and also the onset of inelastic behaviour occurs at lower levels of stress as expected.

To produce the figure for Anand's model Fig.(7.17) and the figures for the other models which follow we kept the strain increments constant but decreased the time increments by a factor of ten when strain reached  $3 \times 10^{-3}$  and again when strain reached  $6 \times 10^{-3}$ . The result is that the stress jumps to a higher level than the previous slope of the line would indicate and in fact from then follows the curve for corresponding to the higher strain rate. The strain rate jump response for Robinson's model, shown in Fig.(7.19), and computed from the algorithm detailed in Fig.(4.1) is quite distinct at the temperature of  $800^{\circ}$  as shown. At lower temperatures the curves are more vertical than at this temperature and the response to strain rate is masked by the curvature associated with kinematic hardening.

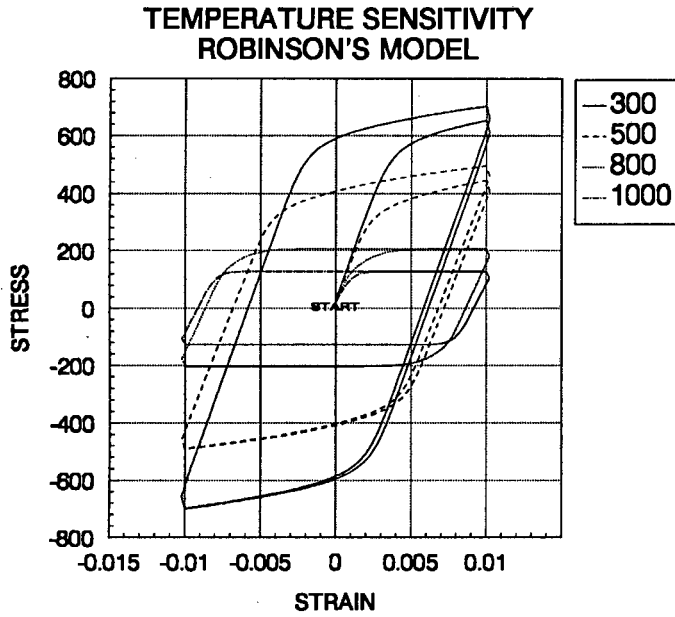


Figure 7.16: Stress ( $T_{11}$ )-strain ( $L_{11}$ ) showing thermal sensitivity over the range 300° to 1000° for Robinson's model

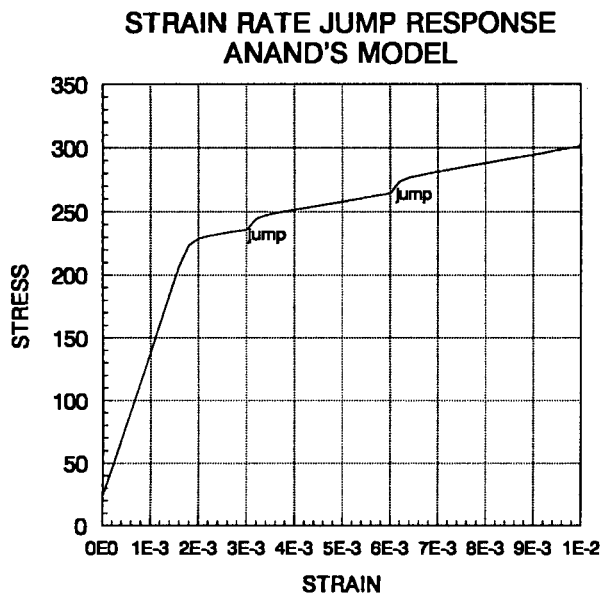


Figure 7.17: Stress ( $T_{11}$ )-strain ( $L_{11}$ ) showing the response to jumps in strain rate for Anand's model

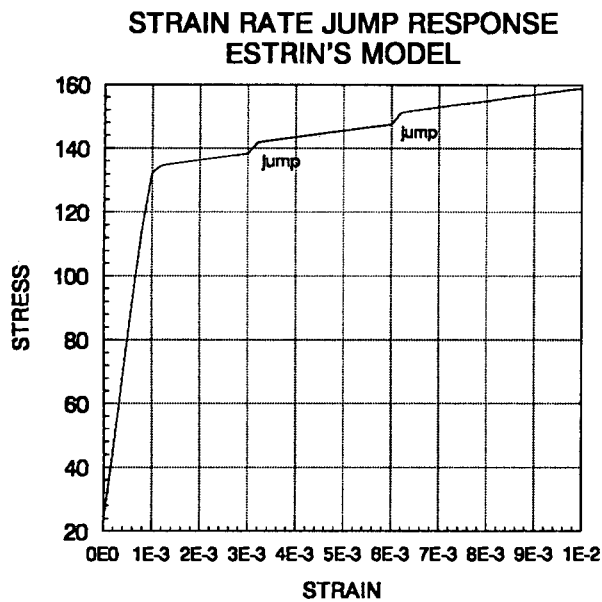


Figure 7.18: Stress ( $T_{11}$ )-strain ( $L_{11}$ ) showing the response to jumps in strain rate for Estrin's model

Fig.(7.18) for Estrin's model is qualitatively similar to the one for Anand's model with only the magnitudes being different. Further these differences could be attributed to the difference between the steels for which parameters were identified.

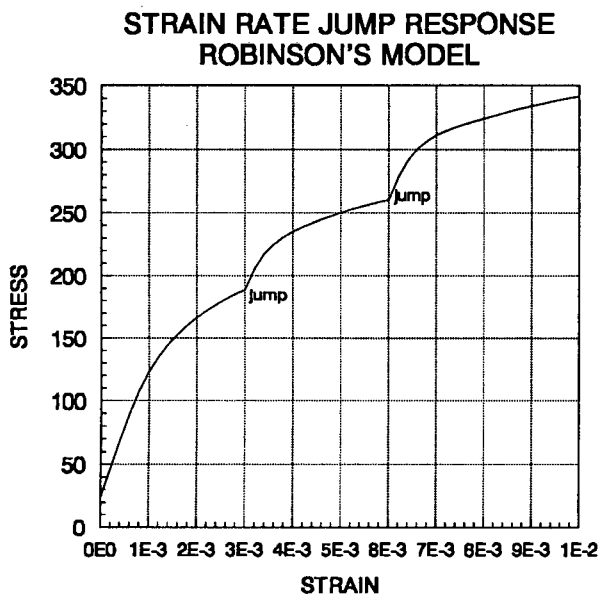


Figure 7.19: Stress ( $T_{11}$ )-strain ( $L_{11}$ ) showing the response to jumps in strain rate for Robinson's model

## 7.6 Results for the Thermo-Mechanical BVP

The boundary value problem which serves as the benchmark problem in assessing the affect of using different models with the characteristics as highlighted in the time integration studies consists of using one of the previously attained temperature field shown in Fig(7.6), and then solving the coupled thermo-mechanical problem as the plate is cooled. The residual stresses and strains which can be evaluated at the end of cooling are then compared for the different models. This is something of a simplification since ideally one would solve the coupled thermo-mechanical problem throughout to simulate real welding conditions. This work is, however, of a more theoretical nature and all the aspects which can be incorporated during welding are included in this formulation of the problem without too large a cost in terms of CPU time.

Results in the form of: displacement, graphs of stress and strain components along the weld line (  $X=0\text{mm}, Z=12\text{mm}$  ) and contour plots of stress, strain and internal variables are presented for Anand's, Estrin's and Robinson's models. The presentation and analysis of results for Leblond's model is reserved for future work. The deformation of the half plate as depicted in Fig(7.20) shows a depressing of the top surface in the z-direction (the direction labelled 3 on the axis) as the main source of deformation. The half plate is also depressed inward at the center of the weld line, this deformation results in less strain than the aforementioned one as can be seen in the graphs of curves of strain components which follow. The deformed mesh is shown as a solid line while the original mesh is dashed. The deformation has been magnified 30 times in relation to the original mesh measurements. The deformation is most pronounced in the figure for Robinson's model (c) in terms of the region deformed and smallest in Estrin's (b) . The residual strain components are shown along the weld line in Figs. (7.21), (7.22), and (7.23) . The legend components are labelled according to ABAQUS format with the total strain components labelled with an E and the total stress components being labelled with a S as apposed to the  $L$  and  $T$  used throughout the text of this paper.

The  $L_{33}$ ,  $L_{13}$  and  $L_{23}$  dominate the solution. This is in keeping with the deformation shown previously where the deformation is primarily in the z-direction to account for the dominance of  $L_{33}$  strain and this combined with the rotation inwards accounts for the dominance of the  $L_{13}$  and  $L_{23}$  over part of the range. The  $L_{11}$  and  $L_{22}$  are approximately equal so that the  $L_{12}$  component is approximately zero along the weld line. This would indicate symmetry in the thermal strains imposed along the weld line in the x and y-directions. This symmetry does not extend through the z-direction. The graphs of stress along the weld line are shown in Figs. (7.21), (7.22), and (7.23). An interesting comparison between the dislocation density models (Anand and Estrin ) and the flow potential model (Robinson) is that of the relative size of the  $T_{11}$  and  $T_{22}$  components. As we have seen the  $L_{11}$  and  $L_{22}$  are relatively small for all the models. The corresponding stress components are, however, of the same magnitude as the  $T_{13}$  component for the Anand and Estrin models but remain relatively small for Robinson's

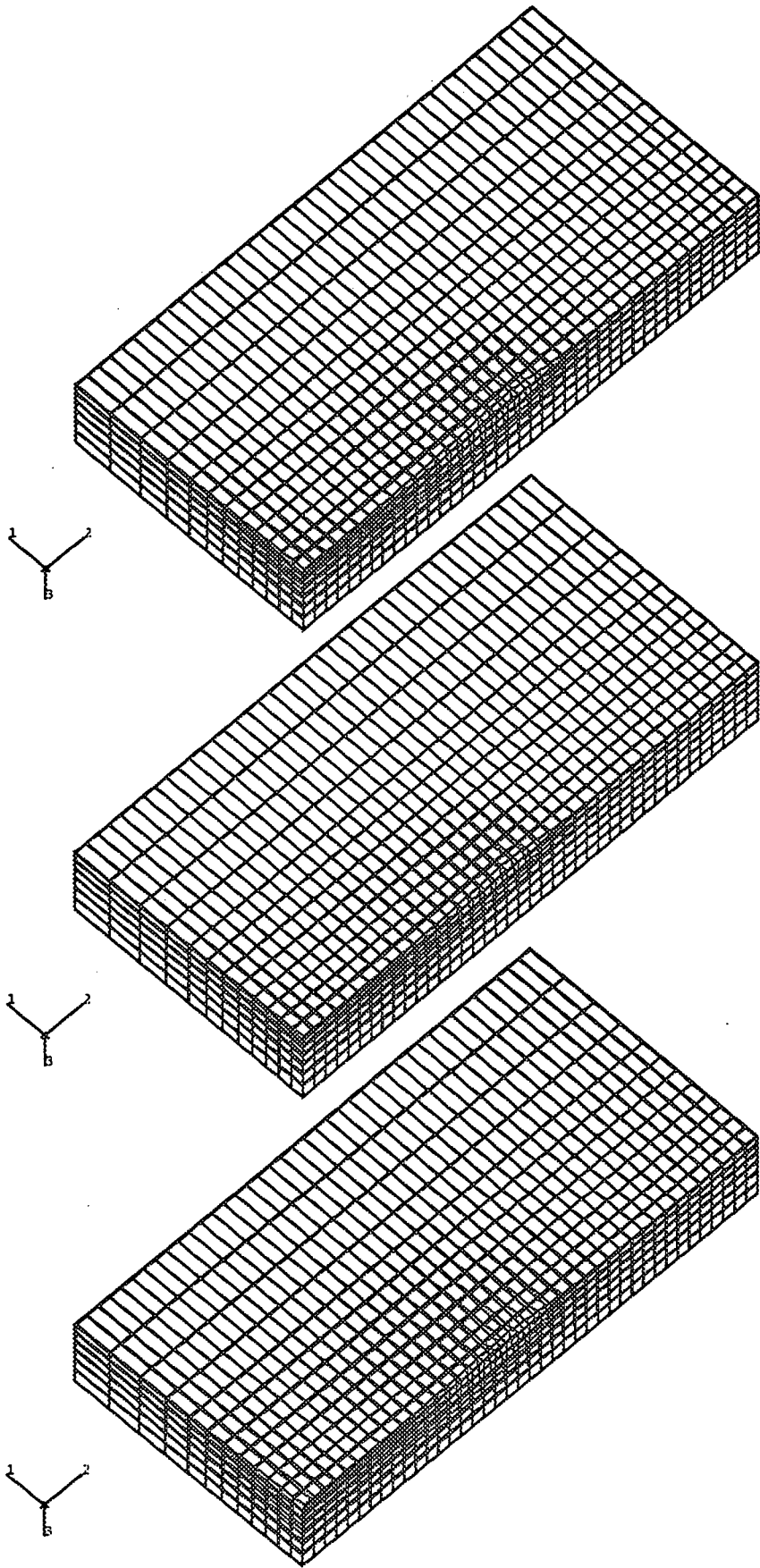


Figure 7.20: Permanent deformation for (a) Anand's, (b) Estrin's and (c) Robinson's model

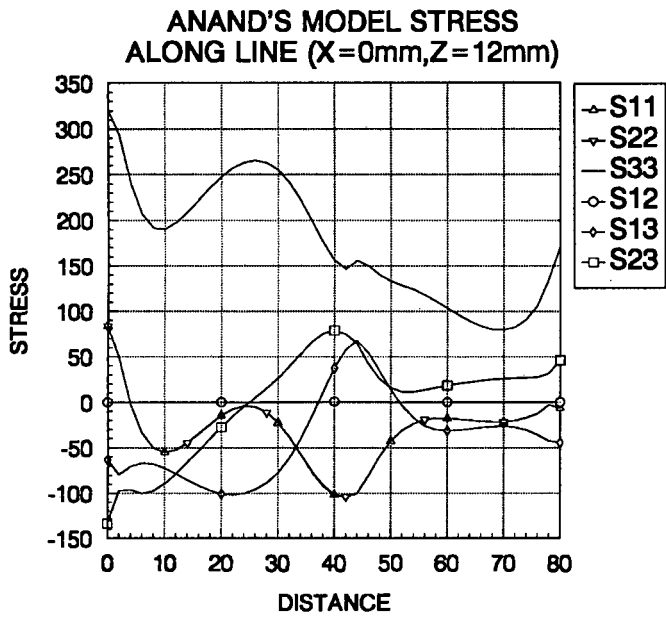
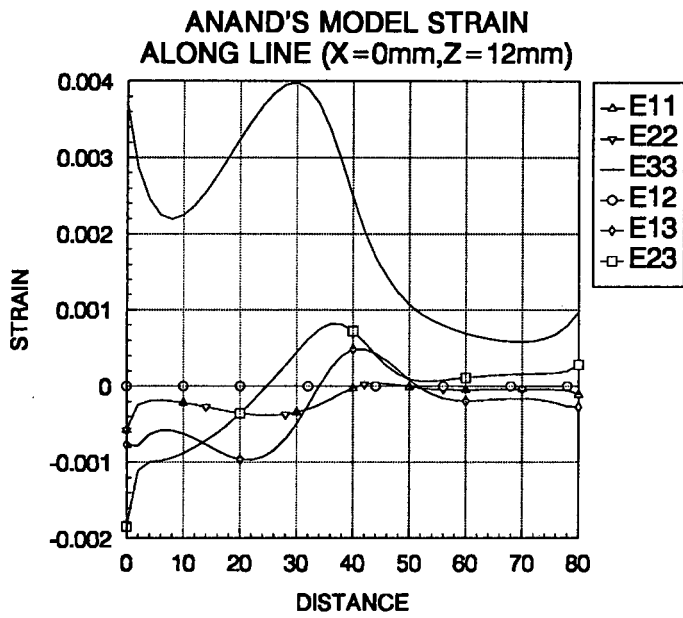


Figure 7.21: Graph of residual a) strain b) stress components for Anand's model along weld line

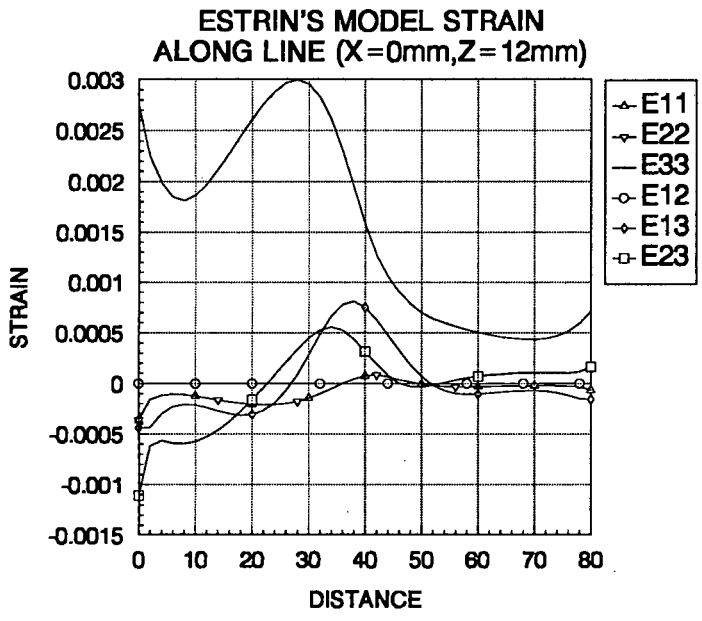
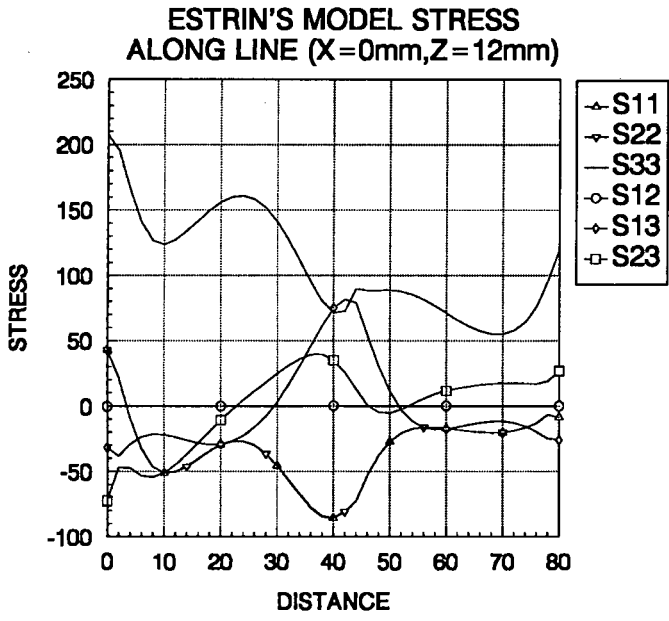


Figure 7.22: Graph of residual a) strain b) stress components for Estrin's model along weld line

model. It is further interesting to note that the dominant stress components in Robinson's model are translated at approximately  $y=28\text{mm}$  on the weld line in the direction of negative stress in comparison with the other models. As was noted previously the grades of steel for which the parameters for Anand's and Robinson's model were calculated are comparable but this is not true for Estrin's model. We chose to use the available parameters so that all the mechanisms should function as they were intended to rather than use statistical methods to change parameters to produce stresses of the same order of magnitude. We have thus avoid making any comments on the relative magnitudes of the stresses although we would like to do so in future work.

Comparison of stress components on the surface of the half plate can be made with the use of contour plots. These are presented as grayscale pictures but they should really be in colour for clarity.

The maximum Von Mises equivalent stress measure which is the norm used for calculating the onset of inelastic behaviour in conventional elastic-plastic analysis and which gives a measure of stress which combines all the deviatoric components is shown in Fig.(7.39). The maximum value of Von Mises stress is 934.4 MPa. for Robinson's model as compared to 411.9 MPa. for Anand's and only 265.9 for Estrin's model. This can be attributed to the differences in the grades of steel for which parameters were identified, as mentioned previously, but also to the differences between kinematic hardening in Robinson's model and isotropic hardening in the other models. The the maximum value for Robinson's model is attained at  $x=0\text{mm.}$ ,  $y=44\text{mm.}$  and  $z=0\text{mm.}$  which is on the base of the plate close to the middle of the line which runs parrallel to the weld line. The maximum value for Anand's model is attained on the same line with  $y=38\text{mm.}$  while that for Estrin is slightly closer to the upper surface and further from the center at  $x=0\text{mm.}$ ,  $y=48\text{mm.}$ ,  $z=3.47\text{mm.}$  The combined stress is thus greatest close to where the restraint is applied in terms of the ( $z=0\text{mm}$ ), close to the center of the HAZ ( $y=40\text{mm}$ ) and parrallel to the weld line ( $x=0\text{mm}$ ).

When we look at the maximum magnitudes of strain components we see that this is  $L_{33}$  (corresponding to E33) on the contour plot in Fig.(7.32), as was seen earlier on the graphs of components on the weld line, with the maximal magnitudes being negative. The minimum value then for Robinson's model is  $-1.598 \times 10^{-2}$  , for Anand's is  $-1.87 \times 10^{-2}$  and for Estrin's is  $-1.79 \times 10^{-2}$ . These values are attained at  $(x=0,y=36,z=0)$ ,  $(x=2.02,y=38,z=0)$  and  $(x=2.02,y=38,z=0)$  respectively. Referring to the components  $T_{22}$ ,  $T_{33}$  labelled S33 and S22 on their respective contour plots Fig.(7.25) and Fig.(7.26) we see that these are the largest stress components. The highest values are obtained for the positive stress components. The maximum value of  $T_{22}$  for Robinson's model is 840.0 MPa. , for Anand's is 368 MPa. and for Estrin's is 224 MPa. These are respectively obtained at  $(x=2.02\text{mm.},y=42\text{mm.},z=0\text{mm.})$ ,  $(x=4.16\text{mm.},42\text{mm.},0\text{mm.})$  and  $(x=4.16\text{mm.},42\text{mm.},0\text{mm.})$ . The maximum values of  $T_{33}$  are for Robinson's model 509.2 MPa., for Anand's 321.3 MPa, for Estrin's 207 MPa. It can further be seen from the contour plots Figs.(7.27), (7.28), and (7.29) that the shear components are relatively small in comparison.

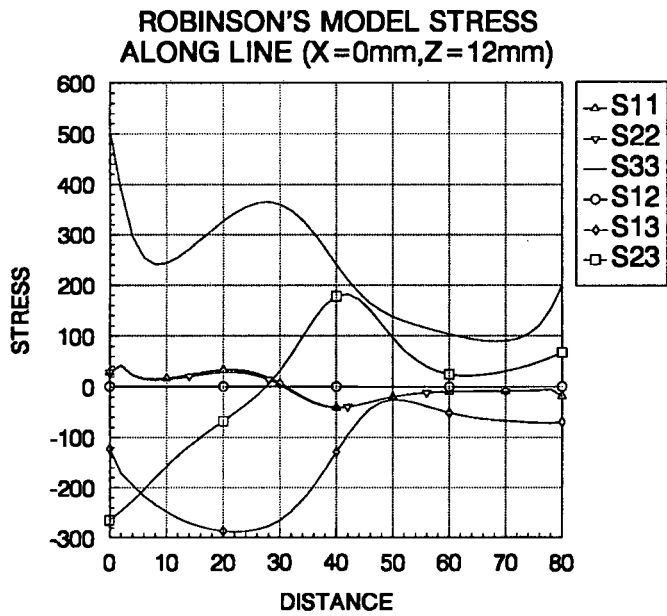
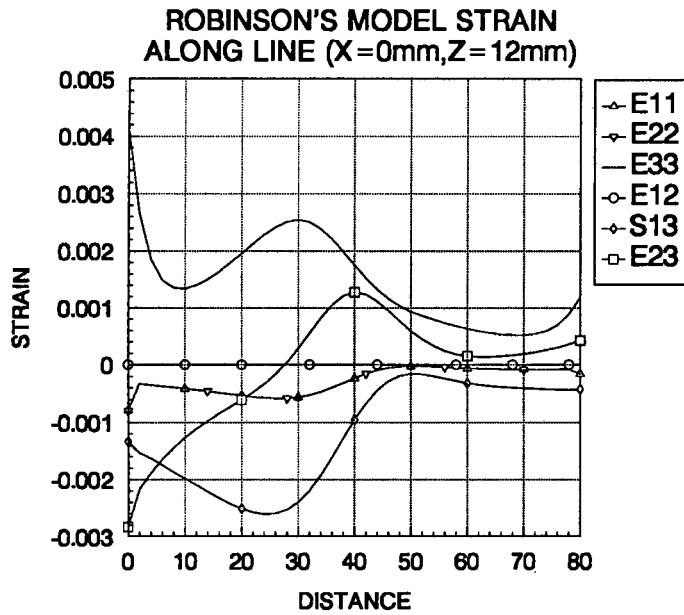


Figure 7.23: Graph of residual a) strain b) stress components for Robinson's model along weld line

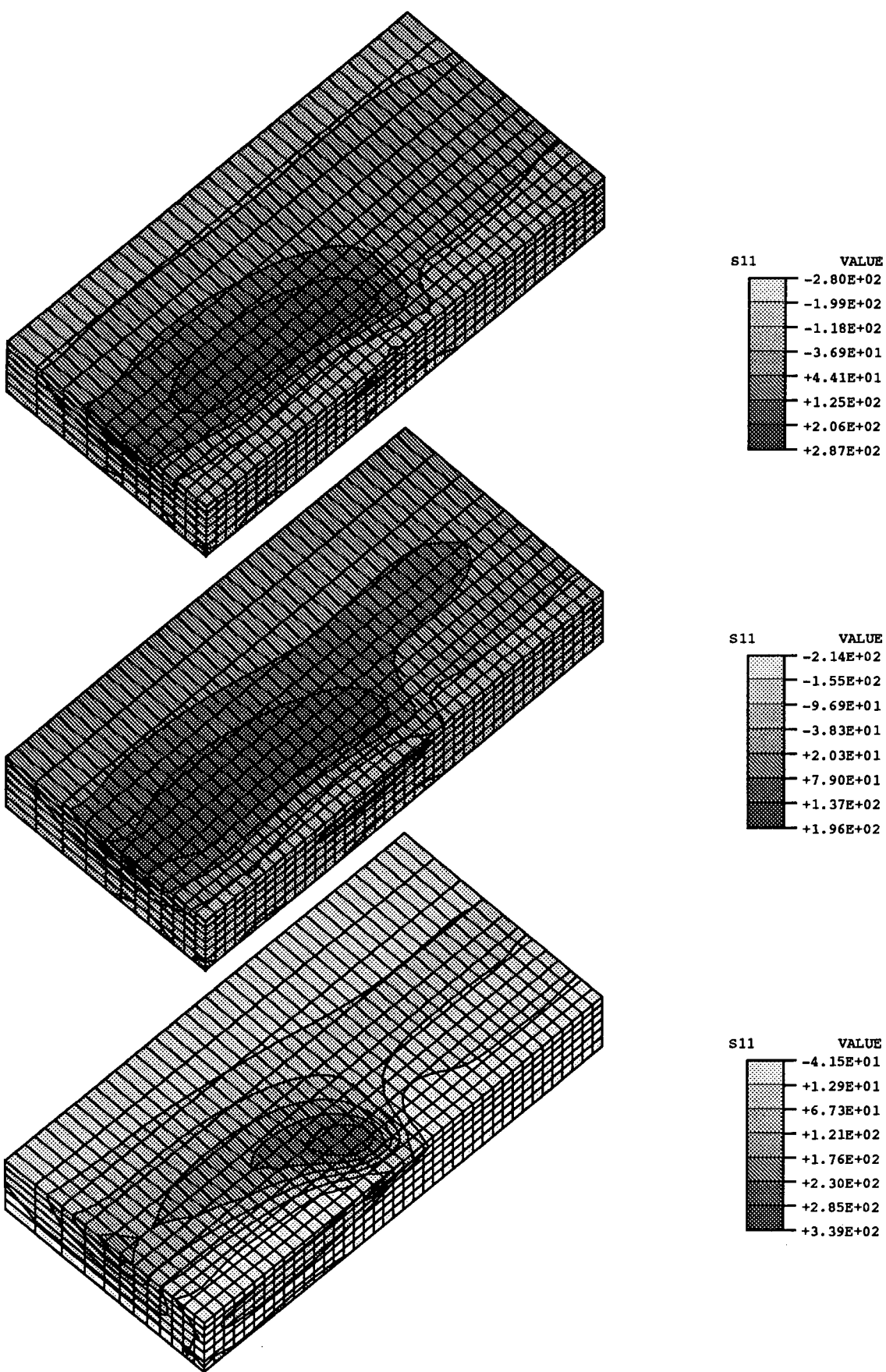


Figure 7.24: Residual stress contour plot for stress component  $T_{11}$  for (a) Anand's , (b) Estrin's, (c) Robinson's model

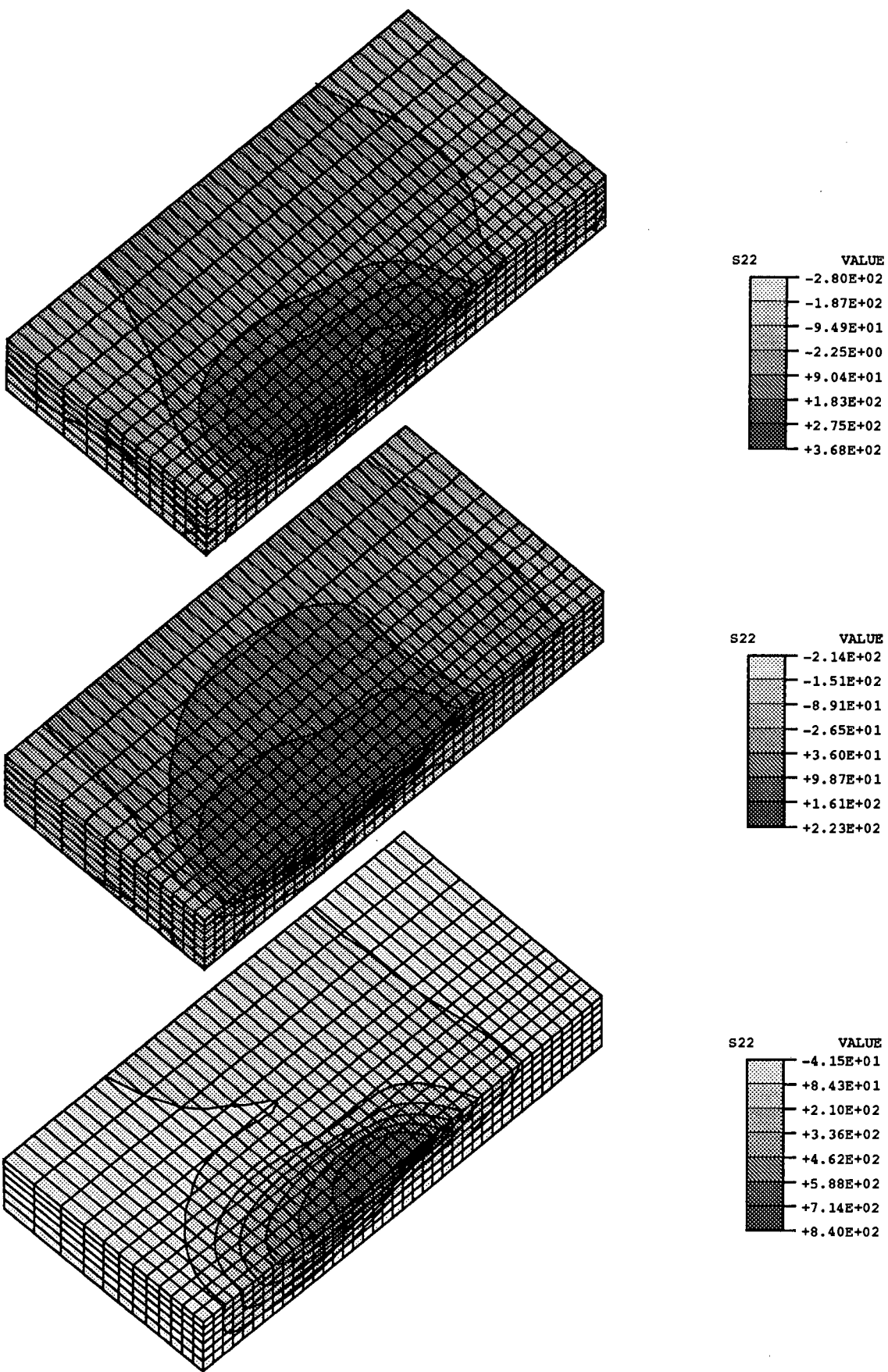


Figure 7.25: Residual stress contour plot for stress component  $T_{22}$  for (a) Anand's , (b) Estrin's, (c) Robinson's model

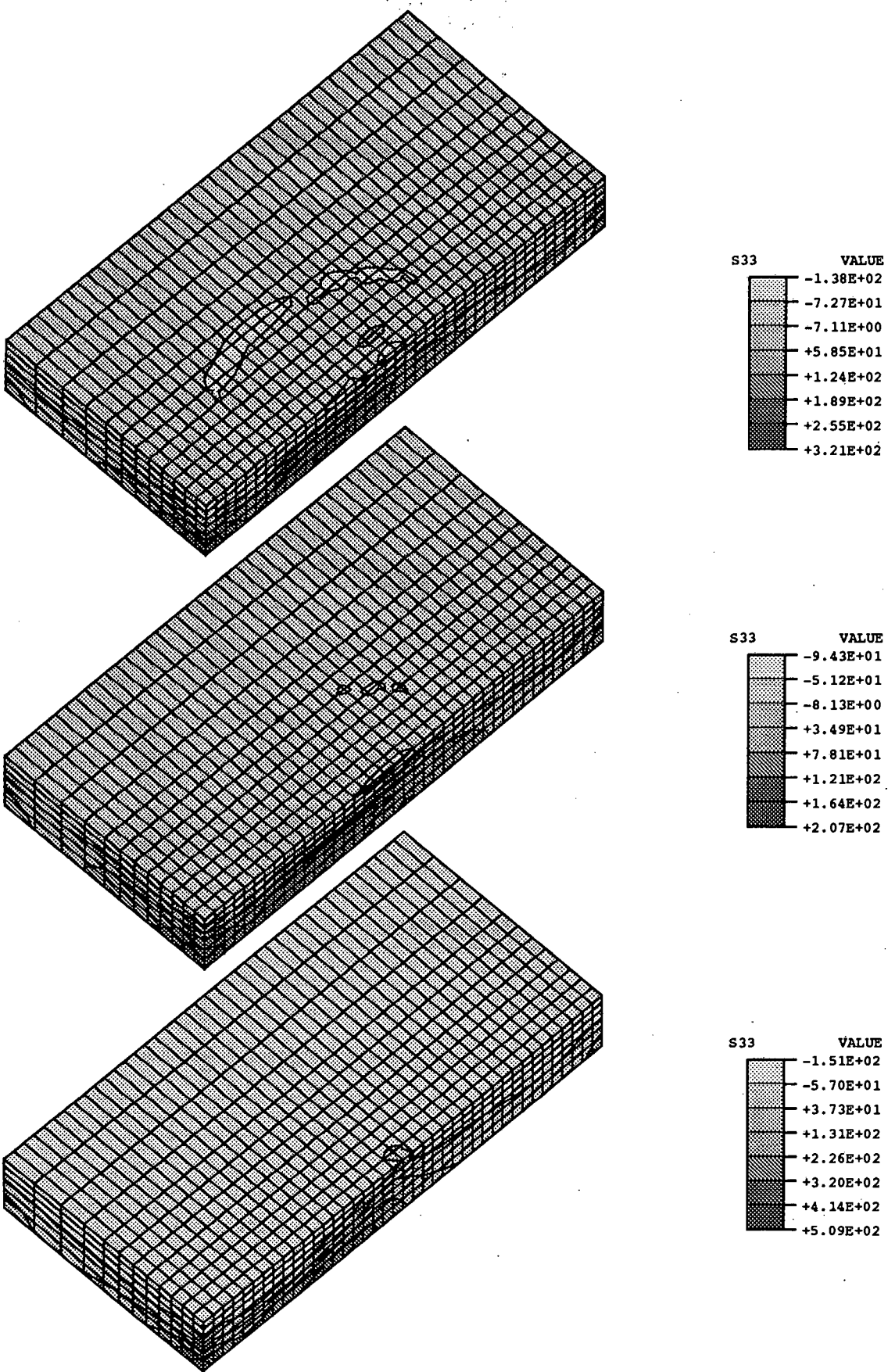


Figure 7.26: Residual stress contour plot for stress component  $T_{33}$  for (a) Anand's , (b) Estrin's, (c) Robinson's model

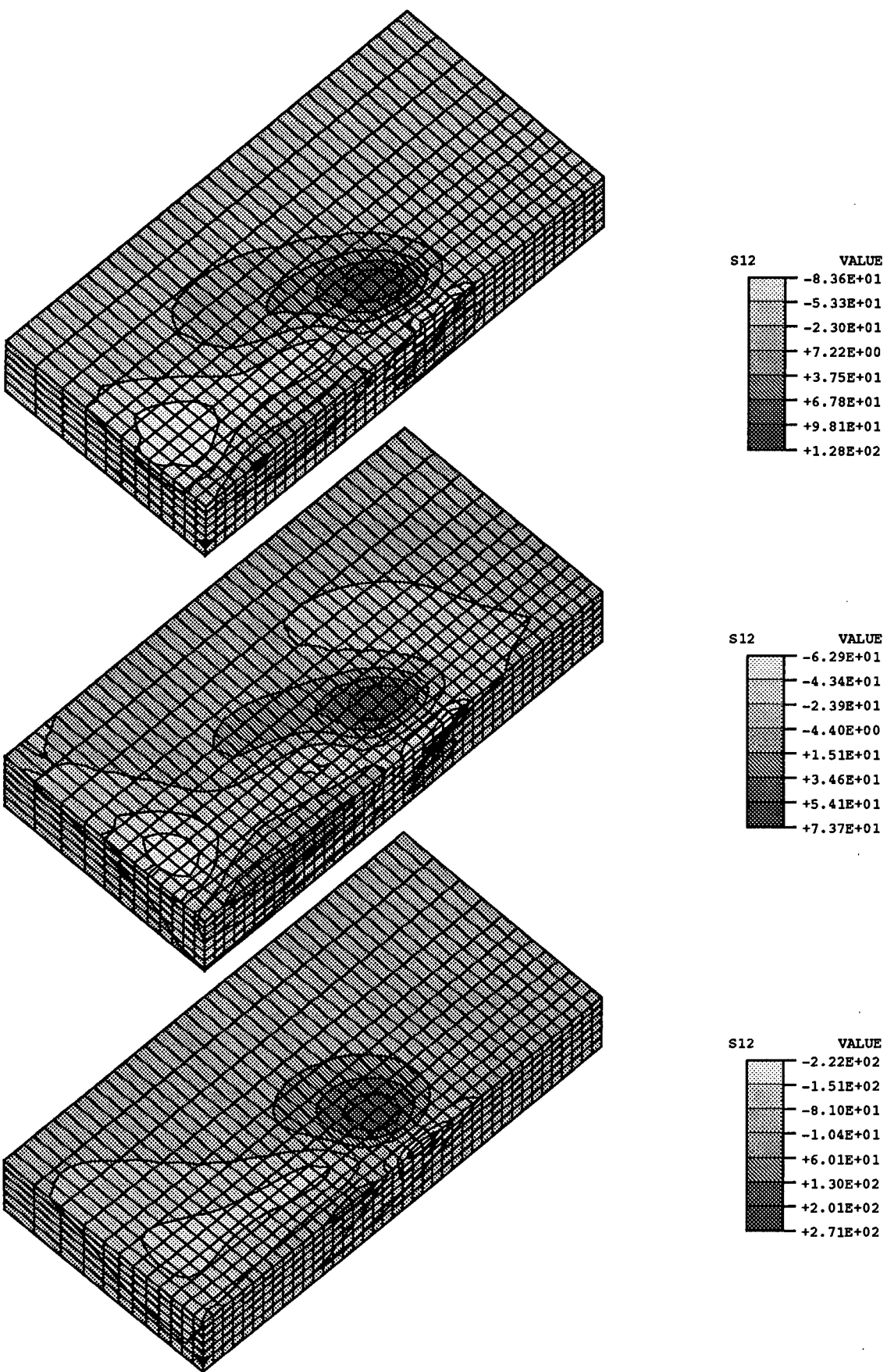


Figure 7.27: Residual stress contour plot for stress component  $T_{12}$  for (a) Anand's , (b) Estrin's, (c) Robinson's model

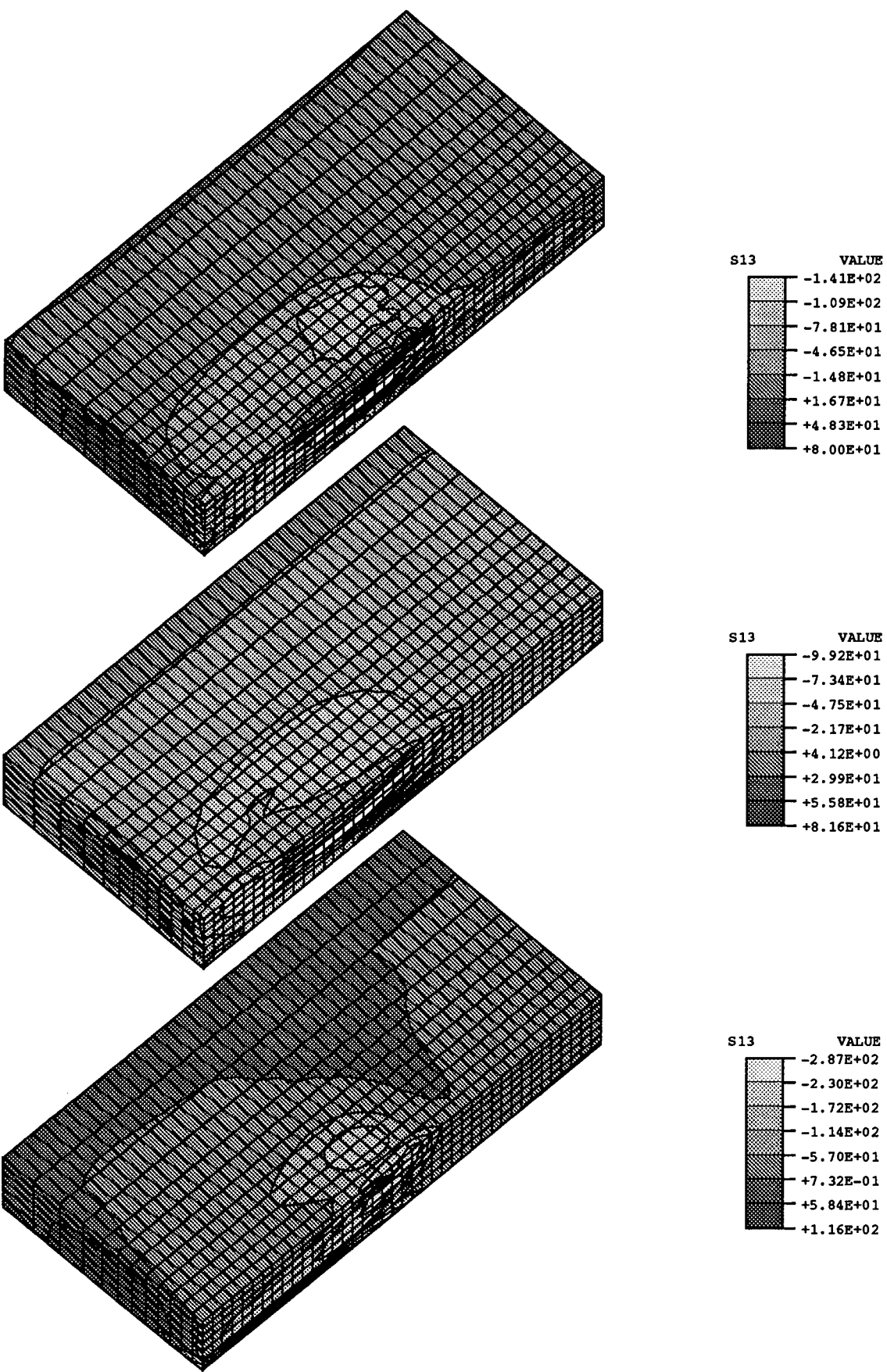


Figure 7.28: Residual stress contour plot for stress component  $T_{13}$  for (a) Anand's , (b) Estrin's, (c) Robinson's model

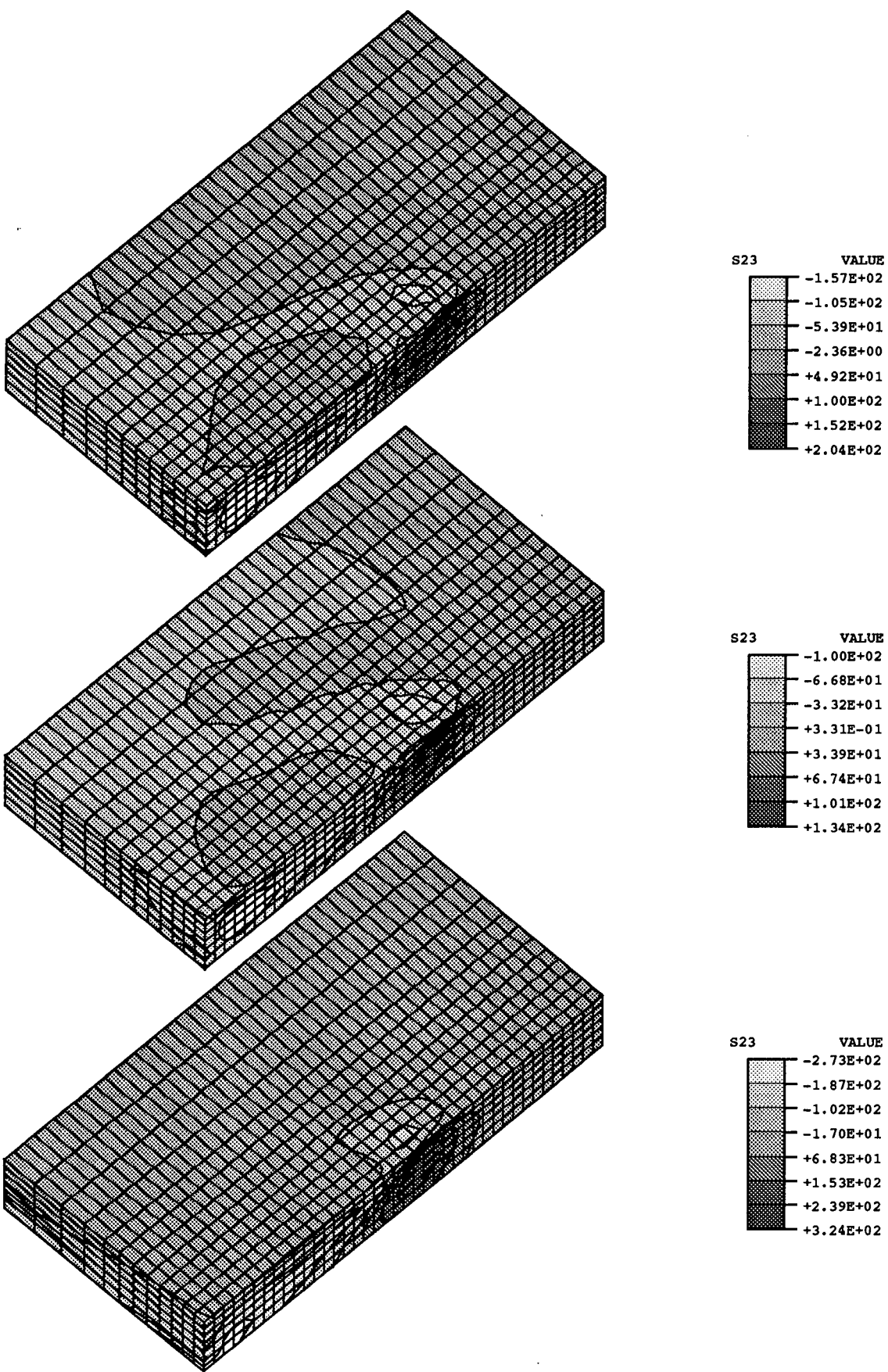


Figure 7.29: Residual stress contour plot for stress component  $T_{23}$  for (a) Anand's , (b) Estrin's, (c) Robinson's model

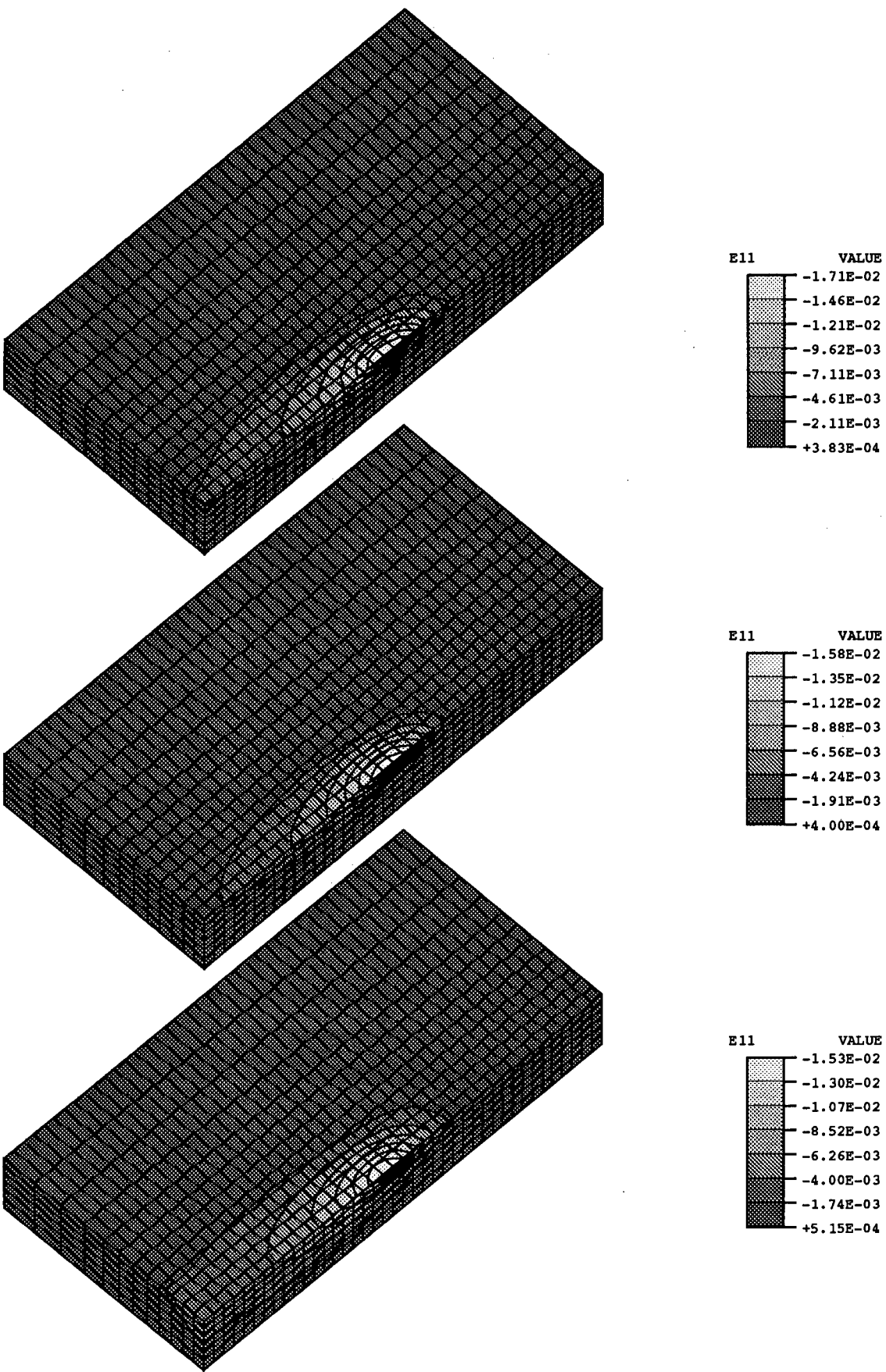


Figure 7.30: Residual strain contour plot for strain component  $L_{11}$  for (a) Anand's , (b) Estrin's, (c) Robinson's model

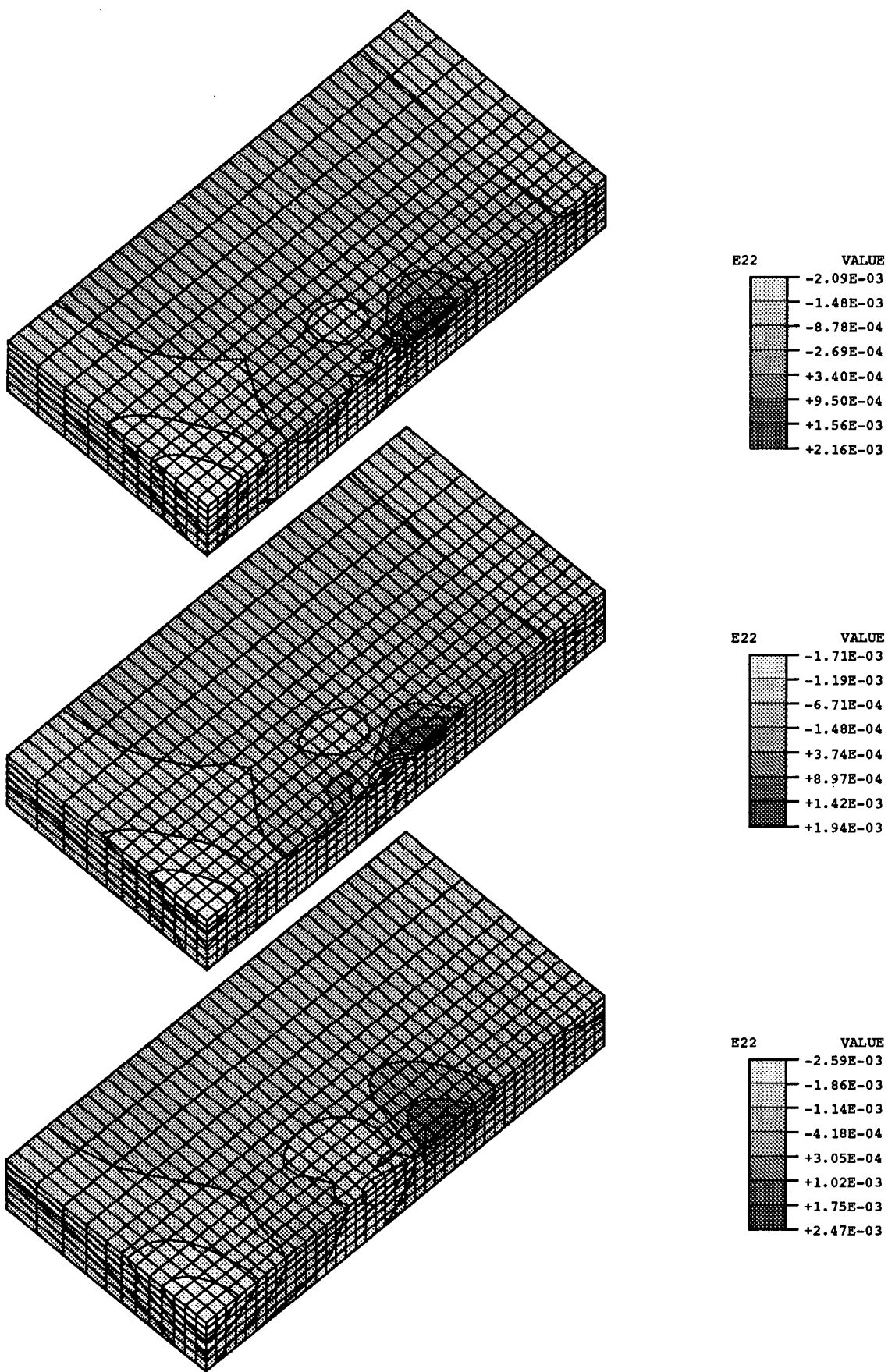


Figure 7.31: Residual strain contour plot for strain component  $L_{22}$  for (a) Anand's , (b) Estrin's, (c) Robinson's model

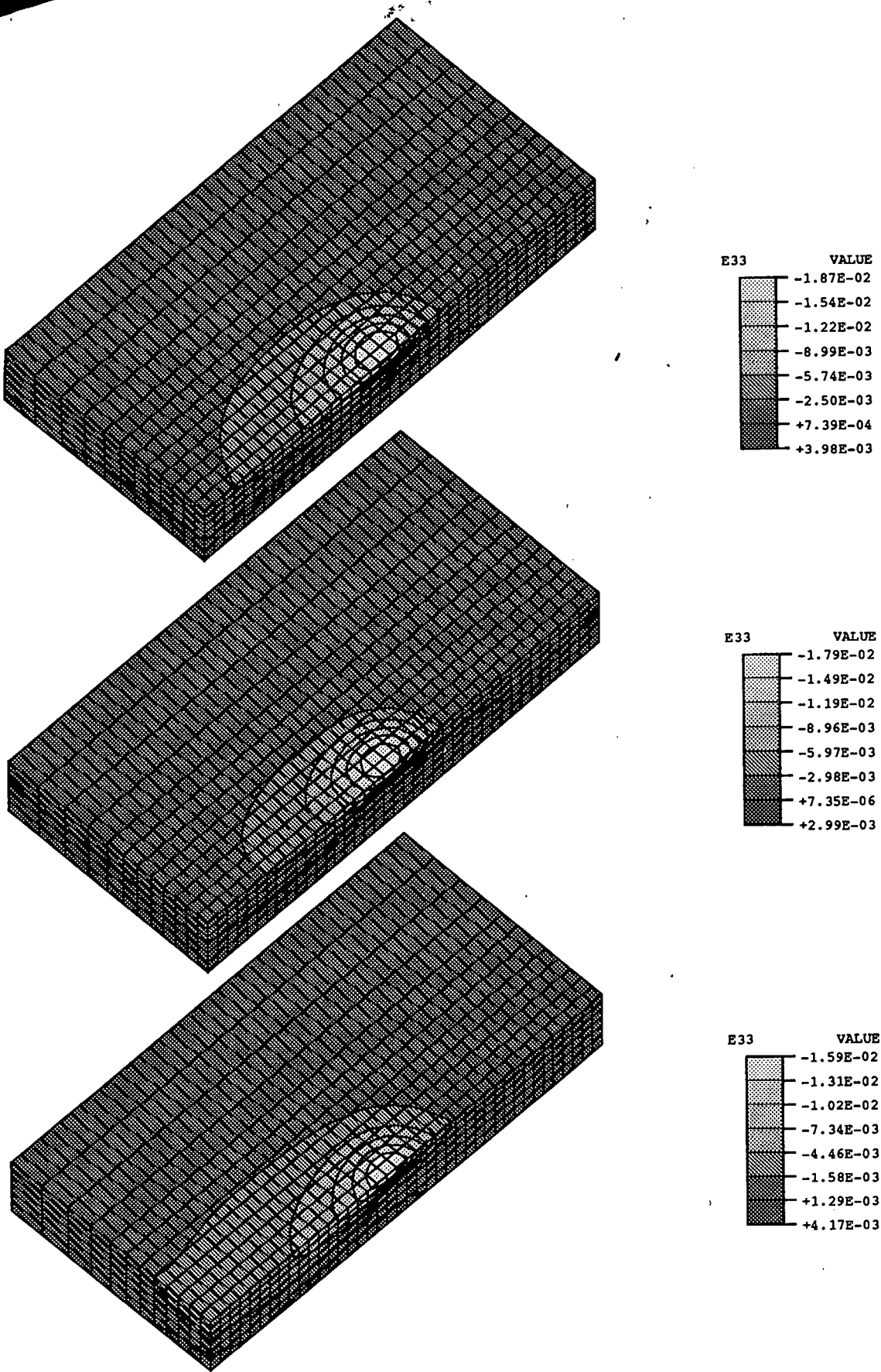


Figure 7.32: Residual strain contour plot for strain component  $L_{33}$  for (a) Anand's , (b) Estrin's, (c) Robinson's model

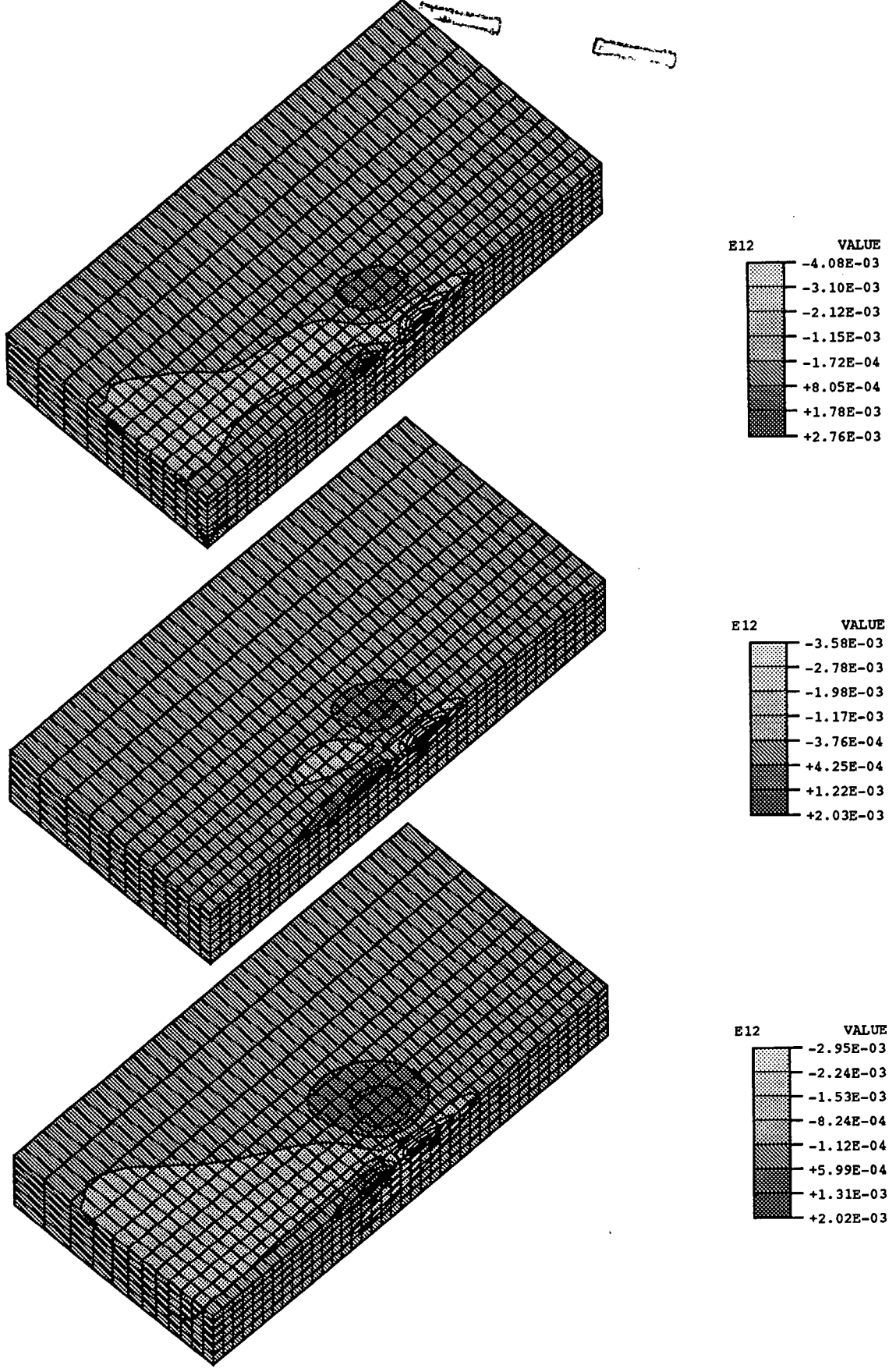


Figure 7.33: Residual strain contour plot for strain component  $L_{12}$  for (a) Anand's , (b) Estrin's, (c) Robinson's model

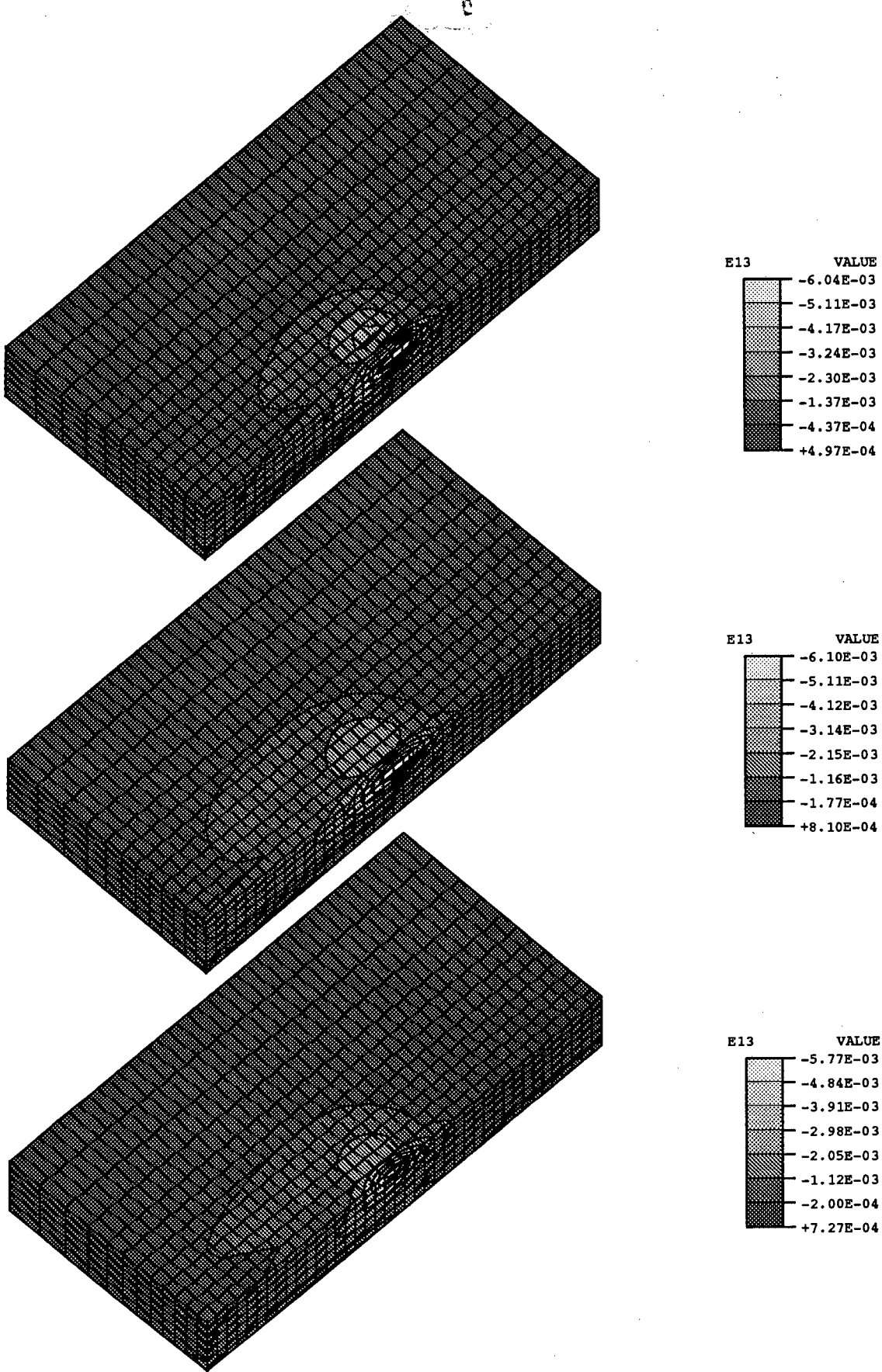


Figure 7.34: Residual strain contour plot for strain component  $L_{13}$  for (a) Anand's , (b) Estrin's, (c) Robinson's model

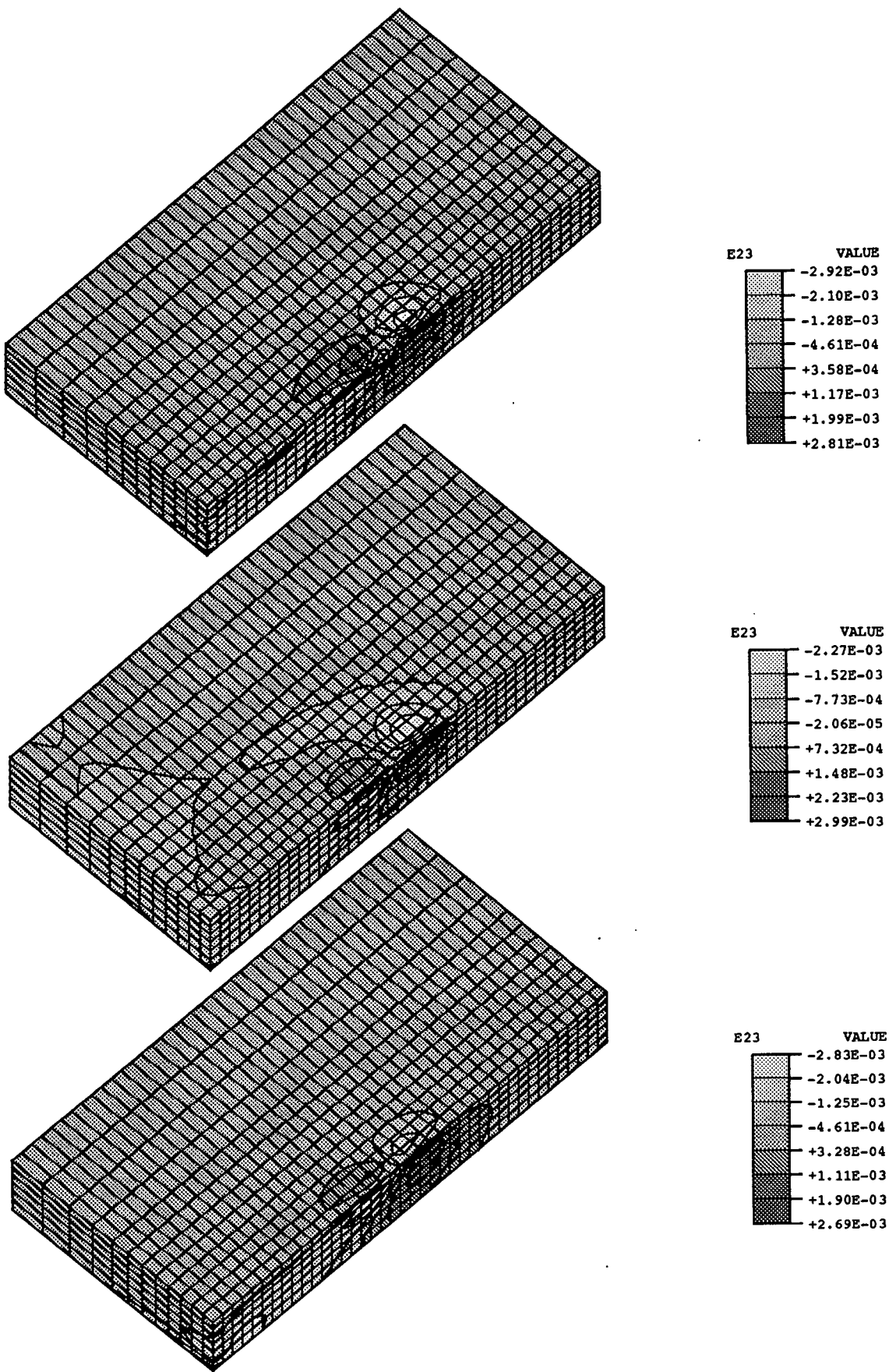


Figure 7.35: Residual strain contour plot for strain component  $L_{23}$  for (a) Anand's , (b) Estrin's, (c) Robinson's model

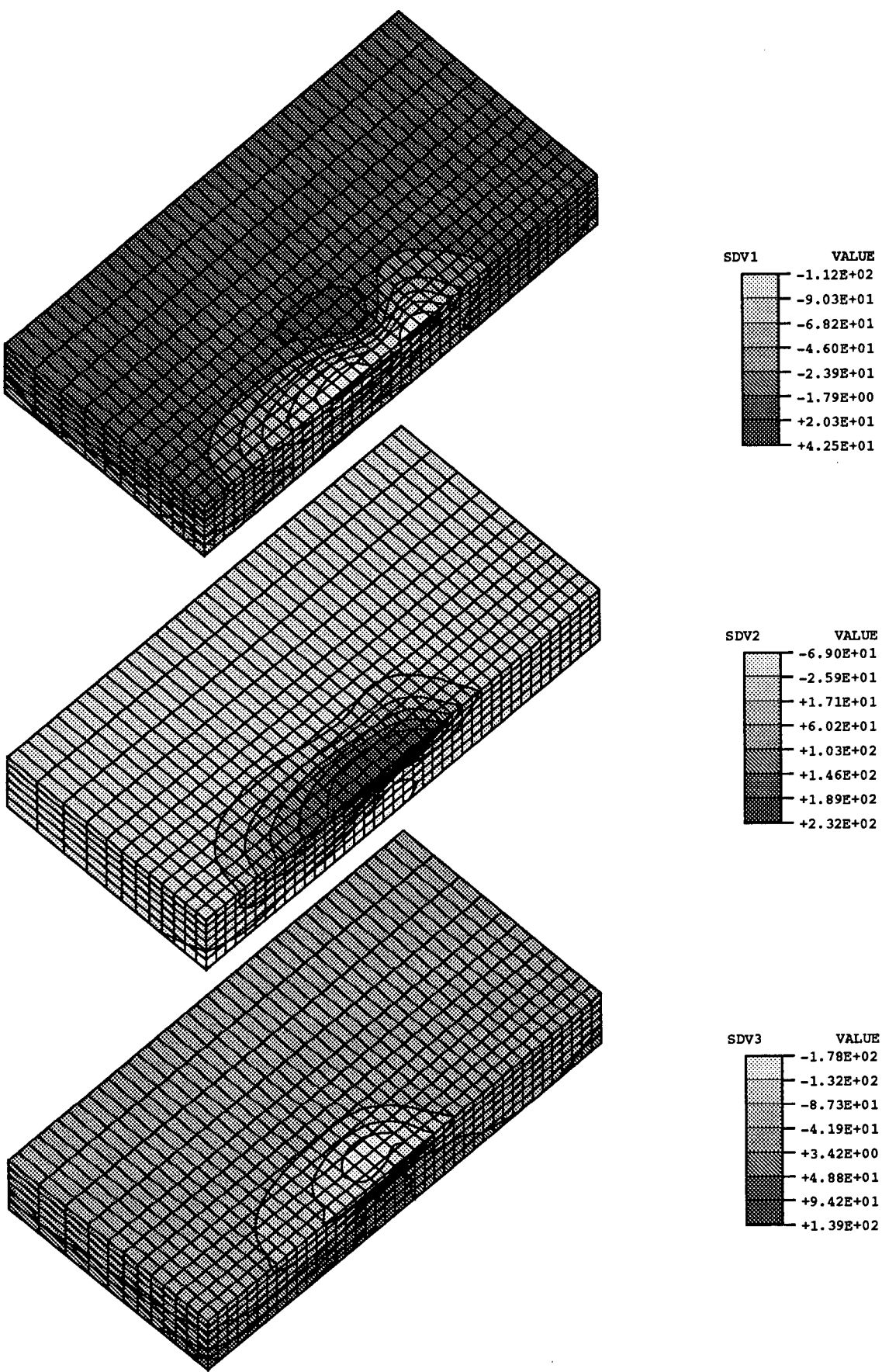


Figure 7.36: Residual value of Robinson's model backstress component (a)  $Z_{11}$ , (b)  $Z_{22}$  and (c)  $Z_{33}$

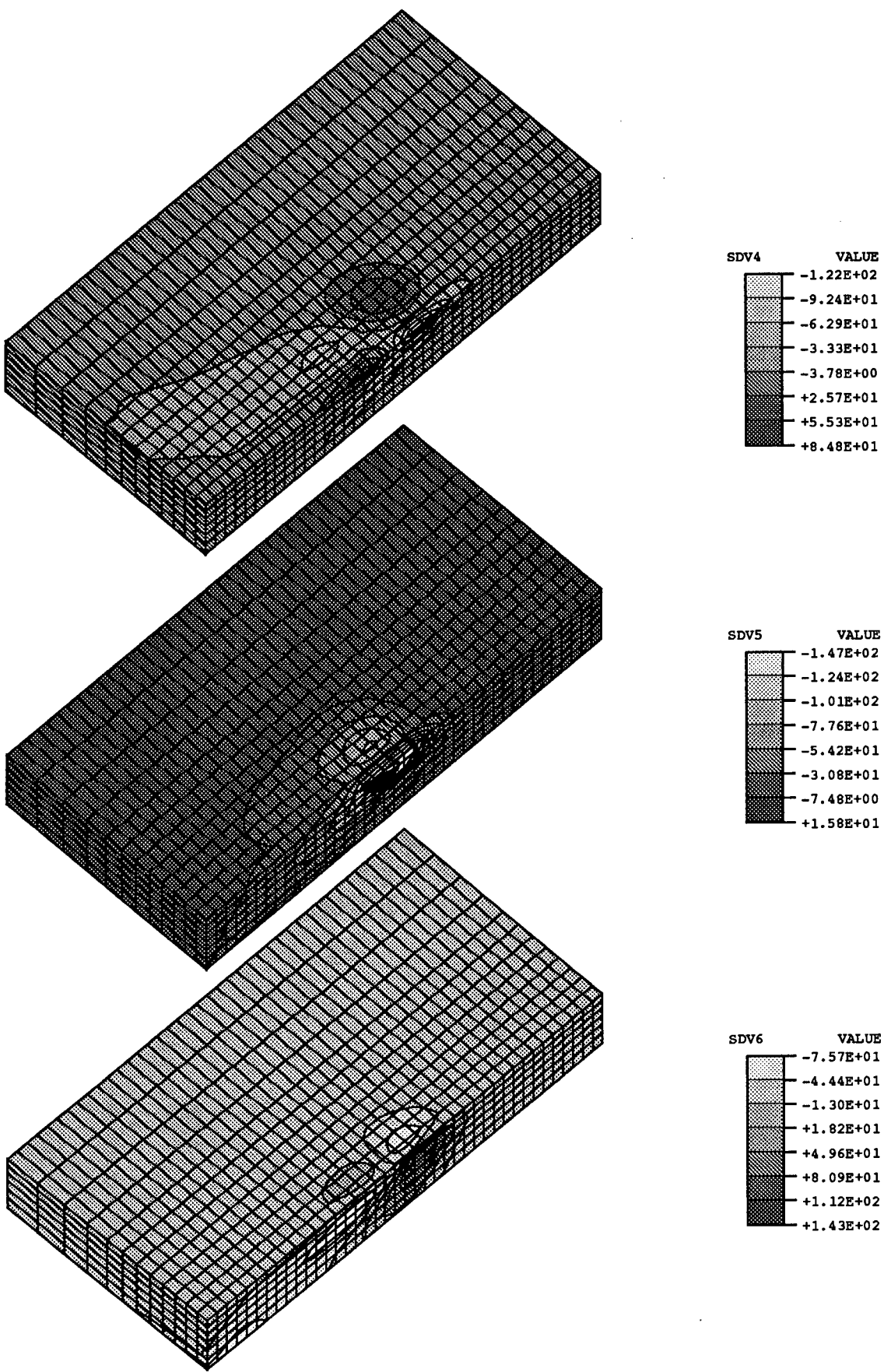


Figure 7.37: Residual value of Robinson's model backstress component (d)  $Z_{12}$ , (e)  $Z_{13}$  and (f)  $Z_{23}$

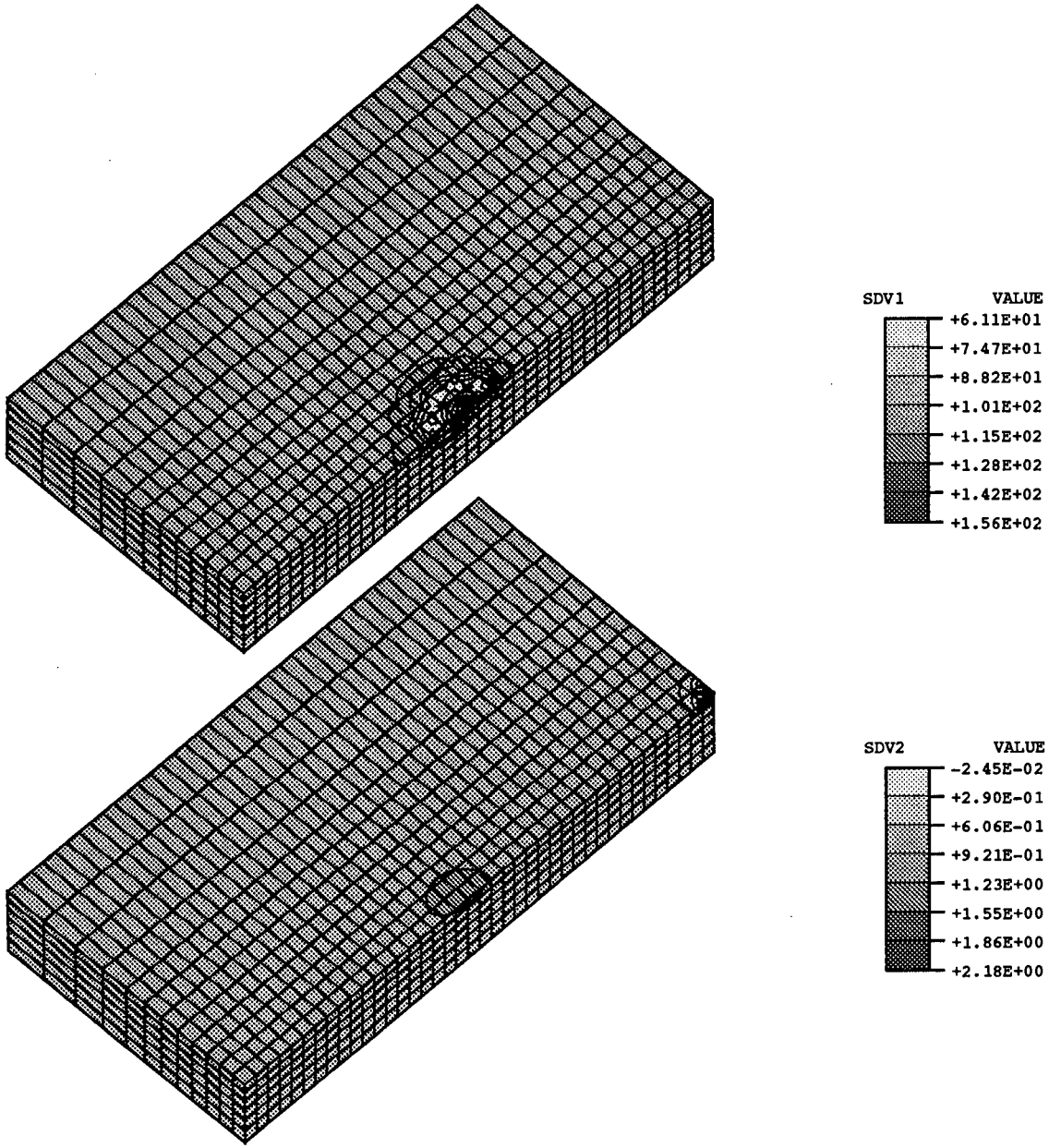


Figure 7.38: Residual value of (a) Anand's model internal variable (b) Estrin's model internal variable

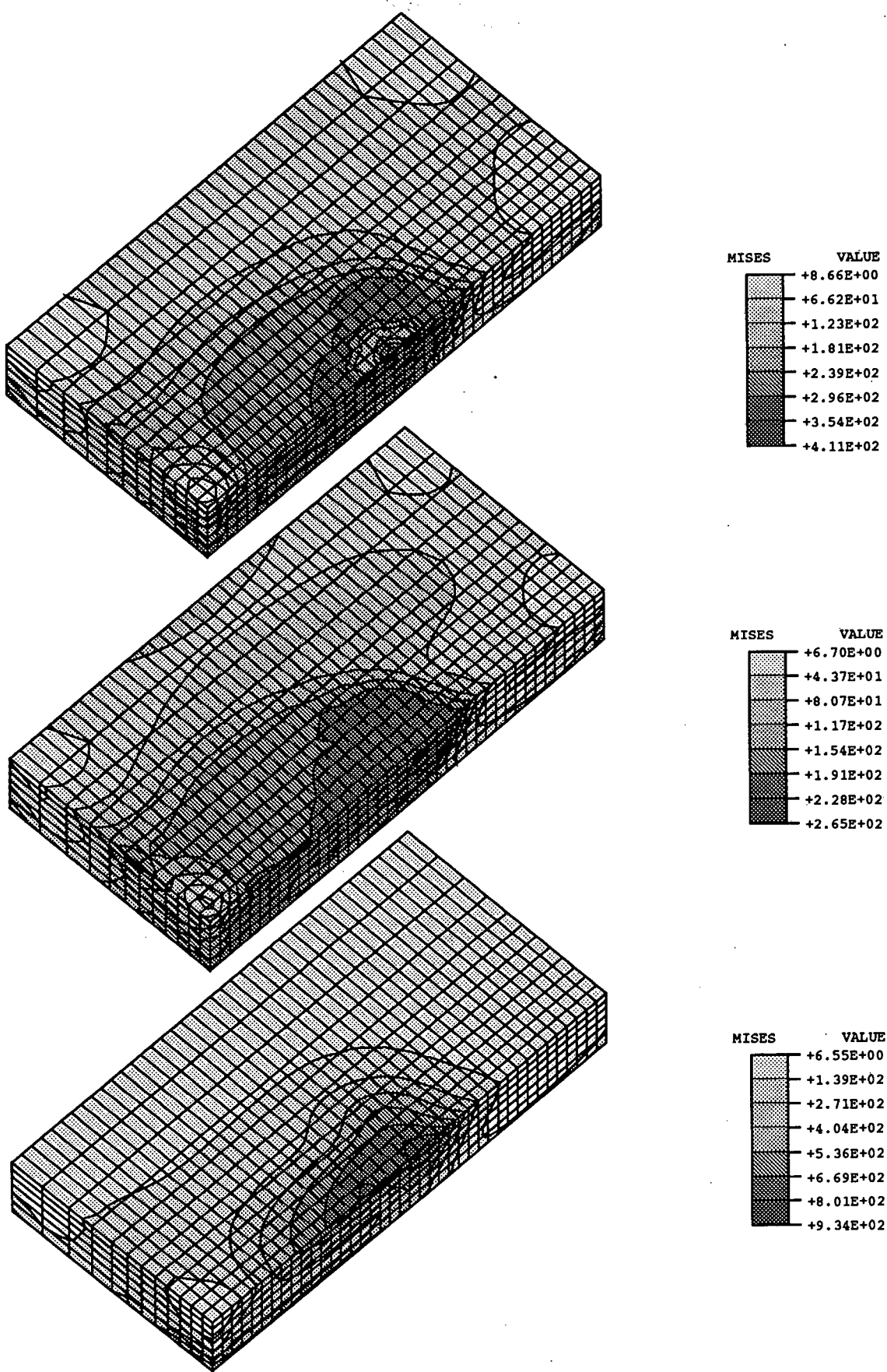


Figure 7.39: Von Mises equivalent stress contour plot for stress for (a) Anand's , (b) Estrin's, (c) Robinson's model

# Chapter 8

## Conclusions

We have set out to develop procedures to model processes in welding using a number of material models suitable for describing the mechanical behaviour of steel subjected to the thermal loads produced by the welding arc. We have presented results obtained using the Finite Element Package ABAQUS incorporating our own procedures for the material models and heat fluxes. We have highlighted some of the differences obtained for the various models in terms of the mechanisms active in the models and in residual stresses obtained for our benchmark boundary value problem.

Comparison with experimental measurements for a suitable benchmark problem is still required to evaluate the effectiveness of each model although clearly Anand's model provides a better result as far as the modelling the 'mushiness' in the HAZ and Robinson's model is more sensitive to work hardening. The results obtained for Estrin's model suffer from the deficiency of parameters not specifically identified for a steel of the right grade and data which did not incorporate the thermal sensitivity. In spite of this the result showed much similarity with Anand's model in the graphs obtained for the stresses and strains along the weld line in a qualitative comparison. While models which incorporate transformation induced plasticity offer theoretical promise in obtaining accurate results they place a very large burden on the analyst in terms of accurately modelling the transformations themselves together with the identification of sometimes obscure parameters.

Identification of parameters for specific materials will play an important role in the solution of welding problems arising from industry. The magnitudes of residual stresses obtained and the assessment of the deflection of the weld piece is very much dependent on the parameters identified for each model. One should remember that the temperature dependent functions for Young's modulus and the Poisson ratio were identical for all the results shown. These were shown to play a smaller role in terms of thermal sensitivity and the magnitudes of stresses obtained than the other parameters.

In order to obtain information which be useful to analysts one would also like to present results for a range of material parameters and also thermal loads since these are only approximations and in real problems will vary. We should thus also be able to do various analysis of sensitivity for the models and the loading conditions when we solve such problems. Sens-

itivity analysis will thus be the subject of future work.

This BVP incorporated all the procedures necessary to simulate the welding processes which would be of interest to analysts working in this field. It was, however, a simplification in that a real weld consists of many passes of welding in which stresses are created and relieved. The BVP problem considered took three to four actual days to solve (for each problem) on an IBM RISC 6000/370 compared with one and a half days for a conventional elastic-plastic analysis.

The importance of using rate dependent models which incorporate thermal effects over conventional inviscid elastic plastic analysis for welding problems does warrant the additional cost in CPU time.

# Appendix A

## Values of Parameters Used in Models

- Young's Modulus,  $E$ :

$$E = 214857 - 78.5714\theta \quad (\text{A.1})$$

- Poisson's ratio,  $\nu$ :

$$\nu = 0.2815 + 4.7957 \times 10^{-5}\theta \quad (\text{A.2})$$

- Shear modulus,  $\mu$ :

$$\mu = \frac{E}{2(1 + \nu)} \quad (\text{A.3})$$

- Bulk modulus,  $\kappa$ :

$$\kappa = \frac{E}{3(1 - 2\nu)} \quad (\text{A.4})$$

- Anand's Model parameters

- $A = 6.346 \times 10^{11}$
- $\xi = 3.25$
- $m = 0.1956$
- $a = 1.5$
- $\bar{z} = 125.1$
- $n = 0.06869$
- $Q = 312.35 \times 10^3$
- $R = 8.314471$
- $z_0 = 0.00035\theta^2 - 0.8\theta + 520.561$

- Estrin's Model

- $\sigma_0 = 200$
- $\xi = 9.999$
- $Q = 0$
- $m = 100$
- $n = 12.096$
- $C = 7.7092 \times 10^{-5}$
- $C_1 = 1.934$
- $C_{20} = 1$
- $C_3 = 30.549$
- $C_4 = 0$
- $\epsilon_0 = 1.841 \times 10^3$

• Robinson's Model

- $\mu_R = 129.96 \times 10^9$
- $K_R = 5.6514$
- $n = 4.0$
- $G_0 = 0.14$
- $\beta = 1.5$
- $m = 7.73$
- $H = 4.75 \times 10^{-6}$

# Appendix B

## Mathematical Derivations

Certain mathematical relations which have been used in the text which are easily derivable and well known in the field are presented here for completeness.

### B.1 Relation between Deviatoric stress and Strain

The summation notation is assumed throughout and  $\mu, \kappa, \lambda$  are the shear and bulk moduli and the Lamé constant respectively and  $S_{ij}, e_{ij}$  are the deviatoric stress and strain respectively. The Kronecker delta is represented as  $\delta_{ij}$  where there is no lowering or raising of indices since Cartesian tensors are used exclusively. Generalized Hooke's law gives the relation between the stress,  $\sigma_{ij}$  and strain,  $\epsilon_{ij}$

$$\sigma_{ij} = (\lambda \delta_{ij} \delta_{rs} + \mu (\delta_{ir} \delta_{js} + \delta_{is} \delta_{jr})) \epsilon_{rs} \quad (\text{B.1})$$

$s_{ij} = \sigma_{ij} - \frac{1}{3} \sigma_{kk}$  also  $\sigma_{kk} = (3\lambda + 2\mu) \epsilon_{kk}$  therefore

$$\begin{aligned} S_{ij} &= (\lambda \delta_{ij} \epsilon_{kk} + 2\mu \epsilon_{ij}) - \frac{1}{3} (3\lambda + 2\mu) \epsilon_{kk} \delta_{ij} \\ &= 2\mu \left( \epsilon_{ij} - \frac{1}{3} \epsilon_{kk} \delta_{ij} \right) \end{aligned} \quad (\text{B.2})$$

the deviatoric strain is given by  $e_{ij} = \epsilon_{ij} - \frac{1}{3} \epsilon_{kk} \delta_{ij}$  therefore

$$S_{ij} = 2\mu e_{ij} \quad (\text{B.3})$$

and also

$$\begin{aligned} \sigma_{ij} &= S_{ij} + \left( \frac{3\lambda + 2\mu}{3} \right) \epsilon_{kk} \delta_{ij} \\ &= S_{ij} + \kappa \epsilon_{kk} \delta_{ij} \end{aligned} \quad (\text{B.4})$$

## B.2 Relation between Equivalent Strain and Equivalent Stress

The equivalent or Von Mises stress is given by

$$\bar{\sigma} = \sqrt{\frac{3}{2} s_{ij} s_{ij}} \quad (\text{B.5})$$

The equivalent strain:

$$\bar{\epsilon} = \sqrt{\frac{2}{3} e_{ij} e_{ij}} \quad (\text{B.6})$$

Substitution of Eq.(B.3) into Eq.(B.5) gives

$$\begin{aligned} \bar{\sigma} &= \sqrt{\frac{3}{2} 2\mu e_{ij} 2\mu e_{ij}} \\ &= \sqrt{6\mu} \sqrt{e_{ij} e_{ij}} \end{aligned} \quad (\text{B.7})$$

$$\begin{aligned} &= \sqrt{6\mu} \sqrt{\frac{3}{2}} \sqrt{\frac{2}{3} e_{ij} e_{ij}} \\ &= 3\mu\bar{\epsilon} \end{aligned} \quad (\text{B.8})$$

The intermediate step Eq.(B.7) also gives the relation between  $\bar{\sigma}$  and  $\|e\| \equiv \sqrt{e_{ij} e_{ij}}$

# Appendix C

## Matrix and Vector Representation of Tensors

Fourth order tensors are represented by matrices:

$$C_{ijkl} = \begin{bmatrix} C_{1111} & C_{1122} & C_{1133} & C_{1112} & C_{1113} & C_{1123} \\ C_{2211} & C_{2222} & C_{2233} & C_{2212} & C_{2213} & C_{2223} \\ C_{3311} & C_{3322} & C_{3333} & C_{3312} & C_{3313} & C_{3323} \\ C_{1211} & C_{1222} & C_{1233} & C_{1212} & C_{1213} & C_{1223} \\ C_{1311} & C_{1322} & C_{1333} & C_{1312} & C_{1313} & C_{1323} \\ C_{2311} & C_{2322} & C_{2333} & C_{2312} & C_{2313} & C_{2323} \end{bmatrix} \quad (C.1)$$

hence we can represent second order tensors as:

$$S_{ij} = \begin{bmatrix} S_{11} \\ S_{22} \\ S_{33} \\ S_{12} \\ S_{13} \\ S_{23} \end{bmatrix} \quad (C.2)$$

where the usual assumptions of symmetry which reduce the nine components to six have been made.

$$\hat{\mathbf{I}}_{dev} = \hat{\mathbf{I}} - \frac{1}{3} \mathbf{1} \otimes \mathbf{1} \quad (C.3)$$

is the 4-th order deviatoric 'identity' ( which arises out of differentiating a deviatoric tensor by its full counterpart) and  $\hat{\mathbf{I}}_{dev} \hat{\mathbf{I}}_{dev} = \hat{\mathbf{I}}_{dev}$  the matrix representation of this tensor is singular as one would expect since

$$\ker \hat{\mathbf{I}}_{dev}(\mathbf{T}) = \left\{ \frac{1}{3} \text{tr}(\mathbf{T}) \mathbf{1}; \mathbf{0} \right\} \quad (C.4)$$

Considering this deviatoric so-called identity as an operator which maps a tensor to its deviatoric counterpart, it should be noted that it is not one-to-one or injective and further

that the order in which this operator is applied to a fourth order tensor is important. Care should also be taken in that  $\frac{\partial \mathbf{T}}{\partial \mathbf{S}}$  cannot be uniquely determined if  $\mathbf{S}$  is the deviator of  $\mathbf{T}$ .

# Bibliography

- [1] Andersson, B.A.B., Thermal stresses in a submerged-arc welded joint considering phase transformations, *J. Eng. and Tech., Trans. ASME*, Vol. 100, pp. 356-362, 1978.
- [2] Anand, L., Constitutive equations for the rate-dependent deformation of metals at elevated temperatures, *Journal of Engineering Materials and Technology*, Vol.104, pp. 12-17, 1982.
- [3] Argyris, J.H., Szimmat, J., Willam, K.J., Computational aspects of welding stress analysis, *Comp. Meth. Appl. Mech. Eng.*, Vol. 33, pp. 635-666, 1982.
- [4] Arya, V.K. and Kaufman, A. Finite element implementation of Robinson's unified viscoplastic model and its application to some uniaxial and multiaxial problems, *Eng. Comput.*, Vol. 6, 1989.
- [5] Bathe, K-J., *Finite Element Procedures in Engineering Analysis*, Prentice Hall, Englewood Cliffs, 1982.
- [6] Bedford, A., *Hamilton's principle in continuum mechanics*, 1985.
- [7] Boley, B.A. and Weiner, J.H.; *Theory of Thermal Stresses*, Wiley, New York, 1960
- [8] Boo, K. S. and Boo H. S., Transient temperature distribution in arc welding of finite thickness plates, Part B: *Journal of Engineering manufacture, Proc Instn. Mech. Engrs.* Vol 204, 1990.
- [9] Brown, S.B., Kim K.H., and Anand L., An Internal Variable Constitutive Model for Hot Working of Metals, *International Journal of Plasticity*, 5, 95, 1989.
- [10] Caddemi, S. and Martin, J.B. Convergence of the Newton-Raphson algorithm in elastic-plastic incremental analysis, *Applied Mechanics Research Unit, Report No. 134*
- [11] Christensen, N., Davies, V.L., Gjermundsen, K., Distribution of temperatures in arc welding, *British Welding Journal*, Vol. 12, pp. 54-75, 1965.
- [12] Denis, S., Gautier, E. and Simon, A., Modelling of the mechanical behaviour of steels during phase transformations, in Beck, G. et al (eds), *Proc. ICRS 2*, Elsevier Applied Science, London, New York, 393-398, 1989.

- [13] Estrin, Y. and Mecking, H., A unified phenomenological description of work hardening and creep based on one-parameter models, *Acta Metal.*, Vol. 32, pp. 57-70, 1984.
- [14] Estrin, Y., A versatile unified constitutive model based on dislocation density evolution, in Freed, A.D. and Walker, K.P.,(eds.), *High Temperature Constitutive Modelling, Theory and Application*, ASME, pp. 65, 1991.
- [15] Fischer, F.D., A micromechanical model for transformation plasticity in steels. *Acta Metall. Mater.*, Vol. 38, pp. 1535-1546, 1990.
- [16] Freidman, E., Analysis of weld puddle distortion, *Welding Journal Research Suppl.*, pp. 161-166. 1978.
- [17] Goldak, J.A., Chakravarati, A. and Bibby, M.J., A new finite element model for welding heat sources, *Trans. AIME.*, Vol. 15B, pp. 299-305, 1984.
- [18] Goldak, J., Oddy, A., McDill, M., Bibby, M.J., House, R., and Chakravarti, A.P., Progress in computing residual stress and strain in welds, in David, S.A. (ed.) *Conf. Proc. Int. Trends in Welding Research*, Gatlinburg, U.S.A., pp 1-6, 1986.
- [19] Goldak J, Oddy A., Gu, M., Mashaie, A., Hughes, E., Coupling Heat Transfer, Microstructure Evolution and Thermal Stress Analysis in Weld Mechanics, in Karlsson, L., Lindgren, L.E., Johnsson, M., *Mechanical Effects of Welding*, pp. 1-30, Springer-Verlag, Berlin, Heidelberg, 1992.
- [20] Henwood, C., Bibby, M.J., Goldak, J.A. and Watt, D.F., Coupled transient heat transfer-microstructure weld computations, *Acta Metal.*, Vol. 36, pp. 3037-3046, 1988.
- [21] Hibbit, H.D., Marcal, P.V., A numerical thermo-mechanical model for the welding and subsequent loading of a fabricated structure, *Comp. Struct.*, Vol. 3, pp. 1145-1174, 1975.
- [22] Hibbit, Karlsson and Sorensen (Inc.), *ABAQUS, Theory Manual*, 1989.
- [23] Hibbit, Karlsson and Sorensen (Inc.), *ABAQUS, User Manual*, 1989.
- [24] Holman, J.P., *Heat transfer*, McGraw-Hill, Singapore, Auckland 1989.
- [25] Hughes, T.J.R., *The finite element method*, Prentice-Hall, Inc., Englewood Cliffs, 1987.
- [26] Inoue, T. and Raniecki, B., Determination of thermal-hardening stress in steels by use of thermoplasticity theory. *J. Mech. Phys. Solids*, Vol. 26, pp. 187-212, 1978.
- [27] Inoue, T. and Wang, Z.G., Finite element analysis of coupled thermoinelastic problem with phase transformation, in *Numerical Methods in Industrial Processes*, pp. 391-400, Pineridge Press, Swansea, 1982.
- [28] Ju, J.W., Consistent tangent moduli for a class of viscoplasticity, *Journal of Engineering Mechanics*, Vol 116, pp. 1764-1779, 1990.

- [29] Karlsson, L., Thermal stresses in welding, in Hetnarski, R.B. (ed) Thermal Stresses, Elsevier, pp. 300-389, 1986.
- [30] Karlsson, R.I. and Josefson, B.L, Three dimensional finite element analysis of temperature and stress in single-pass butt weld pipe. J. Press. V. Tech., Trans. ASME, 1987.
- [31] Kleiber, M., Computer-Assisted Sensitivity Analysis in Nonlinear Solid Mechanics, Lectures at the University of Cape Town, 1993.
- [32] Kou, S., Wang, Y.H., Computer simulation of convection in moving arc weld pools, Met. Trans. A, Vol. 17A, pp. 2271-2277, 1986.
- [33] Leblond, J.B., Mottet, G. and Devaux, J.C., A Theoretical and numerical approach to the plastic behaviour of steels during phase transformations of general relations—I derivation of general relations. Journal of the Mechanics and Physics of Solids Vol. 34, pp. 395-409, 1986.
- [34] Leblond, J.B., Mottet, G. and Devaux, J.C., A theoretical and numerical approach to the plastic behaviour of steels during phase transformations of general relations—II Study of classical plasticity for ideal-plastic phases. Journal of the Mechanics and Physics of Solids Vol. 34 No 4., pp. 411-432, 1986.
- [35] Leblond, J.B., Devaux, J. and Devaux, J.C. , Mathematical modelling of transformation plasticity in steels I: Case of ideal-plastic phases. International Journal of Plasticity, Vol 5 pp-573-591, 1989.
- [36] Leblond, J.B, Devaux, J. and Devaux, J.C. , Mathematical modelling of transformation plasticity in steels II: Coupling with strain hardening phenomena. International Journal of Plasticity, Vol 5 pp. 573-591, 1989.
- [37] Leung, C.K., Pick, R.J., Finite element analysis of multi-pass welds, WRC Bulletin 356, pp. 11-33, 1990.
- [38] Lindgren, L., Karlsson, L., Deformations and stresses in welding of shell structures, Int. J. Num. Meth. Eng., Vol. 25, pp. 635-655, 1988.
- [39] Lomakin, V.A., (in Russian) Izv. Acad. Nauk SSSR, Mekh. Mashinostr., Vol. 2, pp. 20-32, 1958.
- [40] Lomakin, V.A., (in Russian) Izv. Acad. Nauk SSSR, Mekh. Mashinostr., Vol. 1, pp. 103-112, 1959.
- [41] Lubliner, J., Plasticity Theory, Macmillan Publ. Comp., New York, 1990.
- [42] Lush, A.M., Weber, G., Anand, L., An implicit time- integration procedure for a set of internal variable constitutive equations for isotropic elasto-viscoplasticity, International Journal of Plasticity, Vol. 5, pp. 521-549, 1989

- [43] J J Marais, Welding design for mechanical and metallurgical designers Part 1 and 2, Course Notes: Welding Design for Mecanical and Metallurgical Designers, November 1992.
- [44] Masubuchi, K., Analysis of Welded Structures, Pergamon Press, New York,1980.
- [45] Matsunawa, A., Yokoya, S., Asako, Y., Convection in weld pool and its effect on penetration shape in stationary arc welds, Trans. JWRI, Vol. 16, pp. 1-8, 1987.
- [46] Okerblom, N.O., The calculations of deformations of welded metal structures, London, Her Majesty's Stationery Office, 1958.
- [47] Pardo E. and D.C. Weckman, Prediction of Weld Pool and Reinforcement Dimensions of GMA Welds Using a Finite-Element Model, Metallurgical Transactions B Vol 20B, pp. 937-946, 1989.
- [48] Ohji, T., Ohkubo, A. and Nishiguchi, K., Mathematical modelling of molten pool in arc welding, in Karlsson, L., Lindgren, L.E., Johnsson, M., Mechanical Effects of Welding, pp. 207-214, Springer-Verlag, Berlin, Heidelberg, 1992.
- [49] Overlay model for determining thermal-hardening stresses in metallic solids, Materials Science and Technology, Vol. 1, pp. 857-862, 1985.
- [50] Ronda, J. and Oliver G. J., Stresses in Weldments. Proc. 11th Symposium on Finite Element Methods in SA, University of Cape Town, pp. 469-480, 1992.
- [51] Ronda, J., Mahrenholtz O., Thermal problems of welding, in Karlsson, L., Lindgren, L.E., Johnsson, M., Mechanical Effects of Welding, pp. 75-84, Springer-Verlag, Berlin, Heidelberg, 1992.
- [52] Ronda, J., Mahrenholtz, O., Hamann, R., Thermomechanical simulation of underwater welding processes. Archive of Applied Mechanics, 62, pp 15-27, 1992.
- [53] Ronda, J., Mahrenholtz, O., Hamann, R., Quality of the TF-3D - A new FEM solver of nonlinear heat transfer problem, Numerical Heat Transfer, Part B, Vol. 22, pp. 25-48, 1992.
- [54] Ronda, J., Oliver, G.J., Meinert, N., Simulation of welding with phase transformation, Proc. Eighth Int. Conf. on Num. Meth. in Thermal Problems, in Lewis, R.W., (ed.), Pineridge Press, Swansea, 151-163, 1993.
- [55] Ronda, J., Underwater welding problem formulation and numerical solution by means of Tf-3D FEM Package, Part 1, Report for Tailiesprojektes A4 im SFB 264, Technische Universitat Hamburg-Harburg, Arbeitsbereich Meerestechnik II, 1989.
- [56] Rosenthal, D., The theory of moving sources of heat and its application to metal treatments, Trans. ASME, Vol. 68, pp. 849-865, 1946.

- [57] Rybicki, E.F., Stonisifer, R.B., Computation of residual stresses due to multipass welds in piping systems, Trans. ASME, J. Press. V. Tech., Vol. 101, pp. 149-154, 1975.
- [58] Shinoda, T., Masumoto, I., Prediction of weld geometries for  $CO_2$  butt-welded joints, Mat. Sci. and Tech., Vol. 5, pp. 293-298, 1989.
- [59] Simo, J.C., Kennedy, J.G., and Govindjee, S., Non-smooth multisurface plasticity and viscoplasticity. Loading/unloading conditions and numerical algorithms, Int. J. Numerical Methods Engrg., 26, 2161-2185, 1988.
- [60] Ueda, Y. and Yamakawa, T., Analysis of thermal elastic-plastic stress and strain during welding by finite element method, Trans. Japan Welding Soc. Vol. 2, pp. 90-100, 1971.
- [61] Ueda, Y. and Murakawa, H., Applications of computer and numerical analysis in welding research, Trans. JWRI, Vol. 13, pp. 337-346, 1984.
- [62] Wang, Z. and Inoue, T., Viscoplastic constitutive relation incorporating phase transformation - Application to welding. Material Science and Technology, Vol. 1, pp. 899-903, 1985.
- [63] Wilmanski, K., Thermodynamic foundations of thermoelasticity. In: Lebon, G.; Perzyna, P. (ed.) Recent developments in thermodynamics of solids, pp. 1-92. Wien, New York: Springer 1980.
- [64] Vinokurov V.A, Welding Stress and Distortion, The British Library Board, 1977.
- [65] Ziegler, H., An Introduction to Thermomechanics, North- Holland, Amsterdam, 1977